Bis-triazolium perylene diimides: self-aggregation of twisted organic dyes

by

Jamie Scott Hillis

Student Number [redacted]

A thesis submitted to the University of Birmingham for the degree of

Master's by Research

Contents

Acknowledgements

My greatest thanks must go to Tim for taking a chance on me and bringing me to Birmingham, and while things weren't always easy, I couldn't have done it without his constant support.

I must also thank the whole of the Barendt group, Sam, Angus, and Tom plus Denis and Atul who joined us during my stay, as well as the master's student Emily and Rob for welcoming me. Special thanks must go to Sam and Angus for their help in getting me up running both on a personal level, having moved to a new city, and on my chemistry as well as their patience considering I was a bit rusty when I started.

Finally, my thanks to the University of Birmingham and the Haworth building, and all its staff and researchers, for hosting me and making me feel so welcome. As someone that moved so far from home, I couldn't have asked for a better reception.

Glossary

Abbreviation	Definition
A0-0	0-0 vibronic band of the S0-S1 transition
A0-1	0-1 vibronic band of the S0-S1 transition
CHCl3	Chloroform
CPL	Circularly polarised luminescence
DCM	Dichloromethane
DMF	Dimethylformamide
DNA	Deoxyribonucleic acid
ESI MS	Electrospray ionisation mass spectrometry
EtOAc	Ethyl acetate
GC	Gas chromatography
HPLC	High-performance liquid chromatography
MALDI-TOF MS	Matrix Assisted Laser Desorption/Ionization Time-of-Flight mass spectrometry
MeCN	Acetonitrile
MeOH	Methanol
NMR	Nuclear magnetic resonance
PBI	Perylene bisimide
PDI	Perylene diimide
PTCDA	Perylenetetracarboxylic dianhydride
TCE	1,1,2,2-tetrachloroethane
THF	Tetrahydrofuran
TLC	Thin layer chromatography
Θ	PDI dihedral twist angle (°)

Abstract

This thesis aims to showcase the potential of perylene diimide (PDI) aggregates for anion sensing. PDIs are notable class of organic dyes that are well suited for this type of study owing to their strong absorbance and fluorescence and their ability to form aggregates. In this thesis, charge-assisted hydrogen bonding is explored as a tool to control the interactions between PDIs and with anions, thereby impacting photophysical properties for optical anion sensing. Through this work it is shown that a novel bis-triazolium PDI forms aggregates. Using UV-vis spectroscopy the dimerization constant of the bis-triazolium, with PF_6^- as the counterion was found to be 1.25 ± 0.11 x 10^5 M^{-1} with a ΔG of dimerization of -29.1 kJ mol^{-1} when measured in chloroform. This value is in line with the aggregation constants of planar PDIs. This is significant since the bis-triazolium PDI possess a twisted perylene core and so would be expected to exhibit weak aggregation through π–π interactions, which highlights the potential role of charge-assisted hydrogen bonding. Additionally, the ability of this PDI to act as an anion sensor has been shown. With colour change visible with the naked eye when the iodide counter ion was exchanged for PF_6^-.

1. Introduction to Perylene Dimides (PDIs).

Perylene-3,4,9,10-tetracarboxylic acid diimides (PDIs), sometimes referred to as perylene bisimides (PBIs), are a class of polycyclic aromatic dyes. First discovered in 1913 as *N,N'*-dimethyl PDI, Pigment Red 179, they were initially used as pigments with colours ranging from red to violet and all the way to shades of black, depending on the exact chemical structure and how the PDIs packed together in the solid state. They continue to be used as colourants in the modern era, being found in high-grade industrial paints and the car industry, where they are favoured, despite their high cost, due to the durability and high quality of the colours.[1,2]

PDIs are excellent candidates for the study of the transition of monomeric dye molecules to bulk materials. This is due to the favourable properties for fundamental studies, e.g. strong absorbance in the visible region, high (approaching unity) quantum yield of fluorescence, and (photo)-chemical stability, and the ease of tailoring the chemical structure of PDIs to study their self-assembly, *vide infra*.[3] This is owed to their excellent electronic properties and three main regions for synthetic functionalisation. PDIs are capable of π-π stacking owing to their large π surface and, can be easily functionalised with other bonding motifs, such as hydrogen bonding to control the aggregation properties of the dyes.

1.1 Electronic Properties of PDIs.

PDIs have a range of properties that make them of interest to chemists in many different fields. They absorb strongly in the visible light region, with a maximum absorption at around 525 nm, with this S_0-S_1 transition well described by a HOMO→LUMO transition. A high fluorescence quantum yield, regularly >0.9, in a range of organic solvents as well as water, and as such have been considered as a standard for measuring fluorescence quantum yields.[4] Resistance to degradation by both heat and (photo)-chemical means and established and robust synthetic methods to functionalise three distinct sites, see Figure 1, two on the perylene core and the imide group. Such properties mean that PDIs have been used in fundamental studies of conventional and single molecule fluorescent spectroscopy, photoinduced energy and electron transfer processes, as well as singlet fission and artificial photosynthesis.[3] Additionally, they have been investigated for their application in optical and optoelectronic devices such as dye lasers, optical power limiters, fluorescent solar light collectors, optical sensors, and probes for biomacromolecules, e.g., DNA, RNA, and proteins.[1]

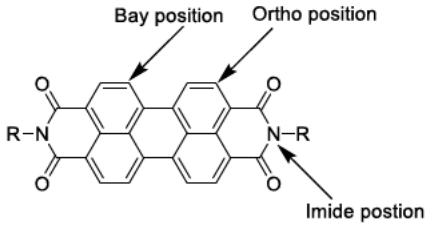

Figure 1: PDIs contain three distinct sites for functionalisation. The R group is typically a solubilising group.

PDIs are electron poor, owing to the two electron-withdrawing imide substituents, shifting the absorbance of perylene from ~440 to ~525 nm.[3] The HOMO and LUMO of PDIs are localised on the perylene core, with nodes at the imide nitrogen's, therefore the imide substituent has only a small inductive effect on the position of the lowest energy transition, typically causing a < 5 nm shift.[5] Core substitution has a far more significant effect as the bay-, and ortho-, positions have significant HOMO and LUMO coefficients, as a result, it would be expected that π-acceptor substituents would stabilise the LUMO, while π-donors destabilise the HOMO, both of which lead to a red-shift of the lowest energy transition. Although, as a result of core-twisting brought about by bay substitution, a blue-shift can occur, although the former effect often dominates the latter.[2]

1.2 H- And J-Type Aggregates and Their Spectral Features.

The self-assembly of dye aggregates results in optical properties that differ from the dye monomer. This is most readily seen in the UV-vis absorption spectra, where the wavelength of maximum absorption shifts to either the red (longer wavelength, lower energy) or blue (shorter wavelength, higher energy). Depending on this shift in the spectra the aggregates are assigned as J-aggregates (J for Jelly, who discovered J-type aggregates) for the former and H-aggregates (H for hypsochromic) for the latter.[6]

H-type aggregates form when molecules align in a face-to-face alignment of the transition dipoles, lying along the long axis of a PDI, forming π-stacks, e.g., rod-like structures.[7,8] In addition to showing a blue-shifted maximum absorption, H-type aggregation also results in decreased fluorescence emission due to aggregation-caused quenching (ACQ). This is described by the two exciton states that arise from aggregated species, as seen in Figure 2. For H-aggregates only excitation to the higher exciton state allowed, resulting in the blue-shift in the UV-vis spectra. This then rapidly undergoes internal conversion to the lower, forbidden, exciton state, from which fluorescence is forbidden.[9] For

unaggregated species the strongest absorption is at 0-0 vibronic band of the lowest energy transition (the absorption labelled as $A_{0\text{-}0}$), followed by the 0-1 vibronic band (the absorption labelled as $A_{0\text{-}1}$), therefore $A_{0\text{-}0}/A_{0\text{-}1} > 1$. As H-type aggregation occurs, this ratio $A_{0\text{-}0}/A_{0\text{-}1}$, inverts and the 0-1 vibronic band becomes greater in intensity that the 0-0 vibronic band, therefore $A_{0\text{-}0}/A_{0\text{-}1} < 1$.[6,10]

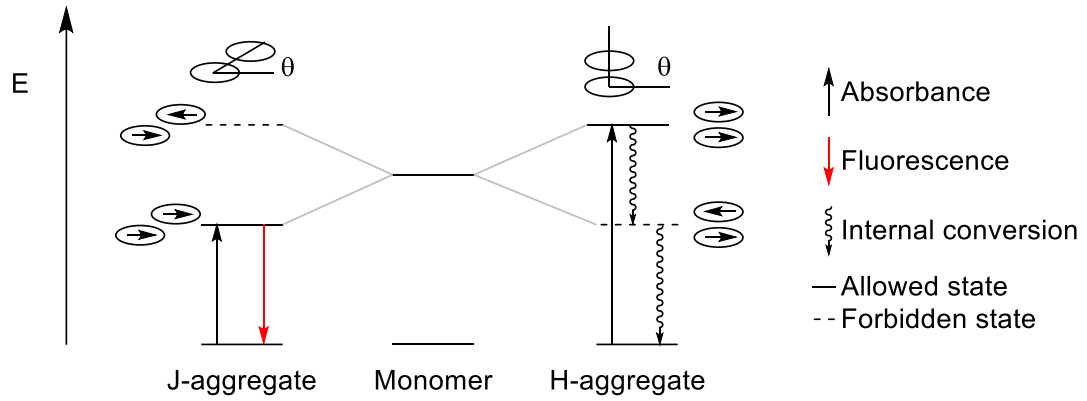

Figure 2: Energy diagram showing the splitting that arises from the aggregation of two molecules and showing forbidden and allowed excited states.

J-type aggregates form in a staggered, head-to-tail, arrangement of transition dipoles, adopting a brickwork, ladder, or staircase structure.[11] For J-aggregates, red-shifting of the maximum absorption is accompanied by no decrease in the fluorescence emission, meaning they are often described as superradient.[12] J-aggregates are favoured when the aim is to retain fluorescent properties of the dye molecules while also having a high exciton mobility which is seen as being key to light harvesting devices as observed in chlorophyll dyes as well as similar synthetic porphyrin systems. [11]

The rational design of such aggregates is of key importance. The most common type of interaction π-π stacking, has limited directionality and as a result, can lead to many different polymorphs, for example, copper phthalocyanine, one of the most common blue colourants, has ten known polymorphs.[13] Additionally, all planar aromatic molecule have two π surfaces which can both form π-π stacking interactions and therefore can give rise to a wide range of one-dimensional aggregates of varying lengths and with a low degree of order. Such aggregates are of little use as it is not possible to derive an unambiguous relationship between the overarching supramolecular structure and any functional properties. Well defined aggregates, e.g. dimers, may be preferred as the monomer to dimer (and/or vice-versa) process can be well defined in terms of a binding constant and response, e.g. UV-Vis or fluorescence, with the addition of a stimuli. A good example of this is the single-strand helix of RNA, which adopts a poorly ordered structure in the absence of the complementary antiparallel oligonucleotide strand.[14] Therefore, careful attention must be taken to instal other

functionality to control the organisation of molecules e.g., hydrogen-bonding motifs or introducing steric bulk to block the growth of the aggregate in a certain direction.

There are several models for quantifying aggregation. These models can be used to study the self-assembly process by fitting the data from changes in the spectroscopic data gathered from concentration- or temperature-dependence studies, either from UV-vis or NMR spectroscopy. The simplest is the monomer-dimer model which only considers two monomers coming together to form a dimer, with only one association constant, e.g., pathway 1 in Figure 3. Obviously, this is not suitable for larger degrees of aggregation and risks oversimplifying the behaviour and should be avoided if there is a potential for larger aggregates to form, especially at higher concentrations. The isodesmic model can be used to assess larger aggregates and takes one of two forms, the isodesmic (or equal-*K* model) and the unequal-*K* model. The equal-*K* model assumes that the strength of monomer-monomer binding (pathway 3 in Figure 3) can be used as the strength of a monomer binding an extended aggregate of any size. The second form of the isodesmic model treats the binding of two monomers as a distinct process from that of forming longer aggregates, pathway 2 in Figure 3, where $K_1 \neq K_2$. If this initial nucleation step (dimer formation) is less favoured than the elongation step (i.e., $K_1 < K_2$), then this is referred to as a cooperative process. Conversely, if the formation of dimers is more favoured than the elongation process then this is referred to as an anti-cooperative model.[15]

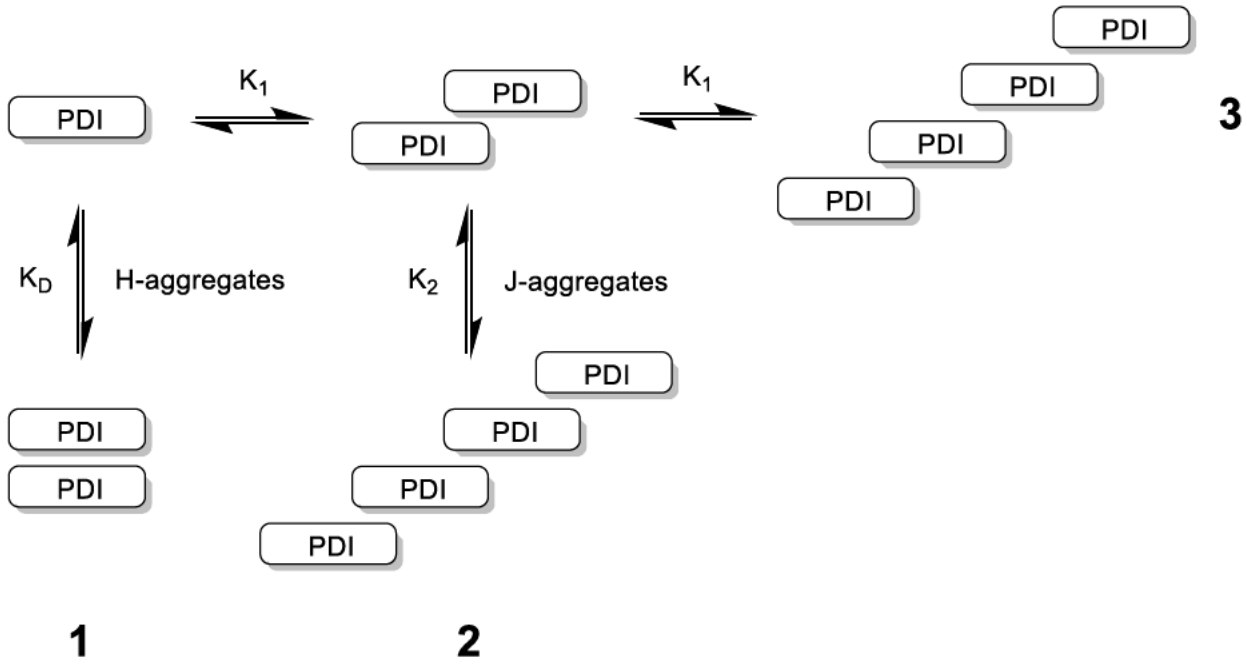

Figure 3: Pathway 1 - monomer-dimer model. Pathway 2 - cooperative ($K_1 < K_2$) and anti-cooperative ($K_1 > K_2$) model. Pathway 3 – Isodesmic (equal-K) model. Both H- and J-aggregates can undergo all three pathways.

1.3 PDI Synthesis and Aggregation Properties.

Fundamentals of PDI Synthesis.

The starting point for PDI synthesis is 3,4,9,10-Perylenetetracarboxylic 3,4:9,10-dianhydride (PTCDA), which is largely insoluble in common solvents.[16] To improve solubility the dianhydride groups are replaced with imide groups, through imidisation, with the most common route being the reaction of PTCDA with zinc diacetate in imidazole with a range of primary amines. The scope of the amine that can be used is vast, with straight and branched chain aliphatic amines tolerated, as well as a range of electron rich or electron poor, and sterically hindered or unhindered aniline derivatives.[2] Bulky imide groups, such as swallow-tail C_{11} chains or 2,6-diisopropyl aniline derivatives, see Figure 4, are typically used to improve solubility and improve aggregation as these groups point perpendicular to the perylene core as a result of the steric clash between the imide groups and the carbonyl oxygens.[17]

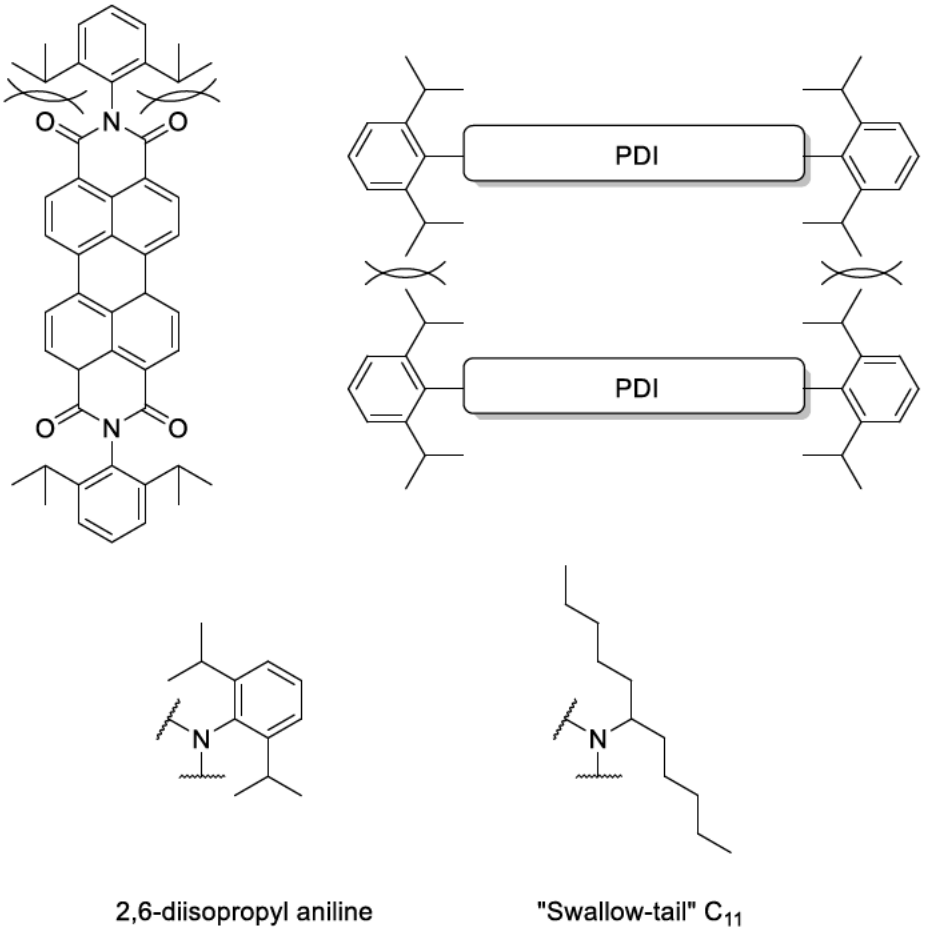

Figure 4: Steric clash between bulky imide groups and the neighbouring carbonyls forces them to sit perpendicular to the PDI plane, hindering aggregation.

One of the most commonly encountered synthetic routes for functionalising PDI is by bromination of the perylene core at the bay positions.[16] Bromination by refluxing the PDI in dichloromethane (DCM) with Br_2, this reaction produces a mixture of two dibromo regioisomers, Figure 5, the 1,7 (major) and the 1,6 (minor) isomer, then following repeated crystallisations from DCM/hexane or DCM/MeOH, the 1,7 isomer can be obtained in pure form.[16,18]

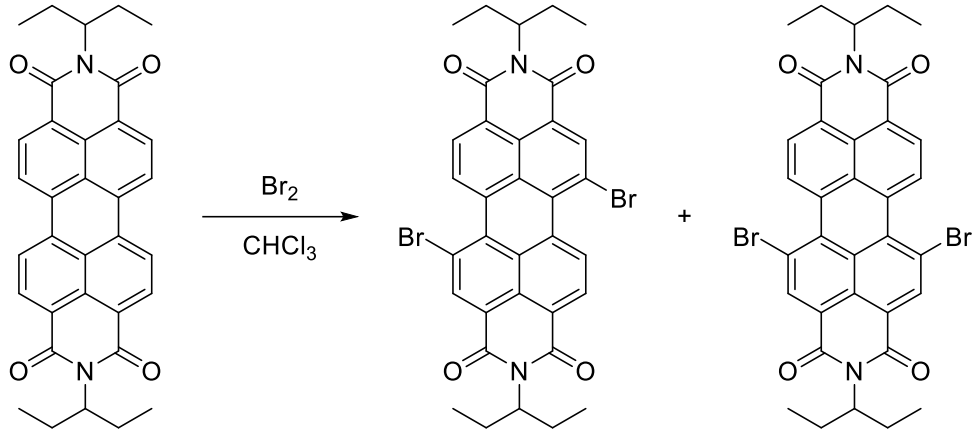

Isomer	1,7	1,6
Typical ratio	4	1

Figure 5: Bromination using Br_2 results in two regioisomers which are produced in a 4:1 ratio.

Formation of H-Type Aggregates.

Perhaps the simplest method of promoting H-type aggregation is by using core-unsubstituted PDIs. By leaving the core unsubstituted the perylene unit remains planar, and the large π surface is capable of π-π stacking which promotes H-type aggregation.

Würthner and co-workers have developed a number of bay-unsubstituted PDIs, such as those shown in Figure 6. Due to the steric bulk provided by the alkyl chains the growth of the aggregate is limited to one dimension and therefore form small (up to eleven molecules), well-defined, columnar structures, with an aggregation constant of $1.2 \times 10^5\ M^{-1}$ at 25°C using the isodesmic equal-K model.[19,20]

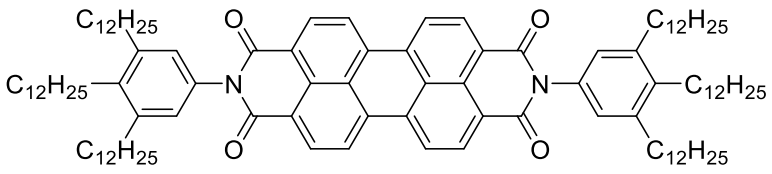

Figure 6: Bay-substituted PDIs are planar and therefore can stack face-to-face and therefore form extended aggregates.

This was expanded upon by introducing amide groups at the imide position, see Figure 7, to allow for hydrogen bonding. By using linear alkyl chains H-type aggregation was favoured, forming gels, as a result of the increased strength of the intermolecular interactions, in which the PDIs stack in a helical structure. The UV-vis spectra show a blue-shifted absorption maximum. For bulkier alkyl chains that have branching methyl groups, J-type aggregation is observed as the branched group cause steric clashing between the stacked PDIs and so they slip out of the axis of the helix to alleviate the strain. This is seen through the appearance of a new absorption band that appears 93 nm red-shifted compared to the monomeric form of the dye and the loss of the vibronic pattern seen in the monomeric spectrum. Finally, by increasing the length of the branched chains to an ethyl group, no evidence for aggregation was seen at the same concentration as in the previous examples. In this case, the organogels seen in the previous two examples is not observed as the increased steric bulk is enough to disrupt the hydrogen bonding required to form the gels.[21]

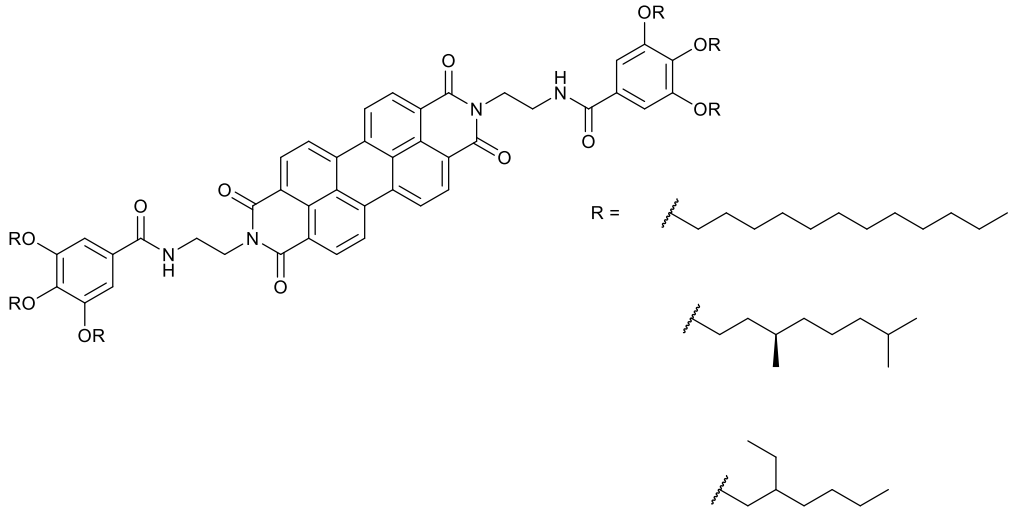

Figure 7: Hydrogen bonding motifs increase the strength of aggregation and allow for the formation of gels. Introducing steric bulk of the phenyl groups causes the PDIs rotate within the columnar stack.

Formation of J-Type Aggregates.

J-type aggregates arise from the slip-stacked arrangement of PDI molecules that have a longitudinal displacement of between 6.5 and 9 Å. Such an arrangement is not typically favoured by larger π-systems which tend to seek to maximise interactions through co-facial, i.e. H-type, stacking.[22] The simplest way to achieve this slip-stacked arrangement needed is to distort the π-scaffold of the PDI by introducing four bulky substituents at the bay position which introduces a large core-twist of ~ 25°.[3] The large core-twist limits co-facial π-π interactions and thereby hinders the formation of H-type aggregates and instead favours the formation of heterochiral polymer arrangements through the interaction of naphthalene imide subunits of neighbouring PDIs. This can be enhanced by the

introduction of binding motifs at the imide position. With simple NH imide groups this can promote the formation of polymer cable-like structures over columnar stacks. A good example of this is the compound shown in Figure 8. The large alkoxy substitutes, shown by the cones, induce a large core-twist that prevents H-type aggregation, naphthalene subunits are free to π-π stack in a slipped arrangement, and H-bonding encourages the formation of 1D ribbons.[23]

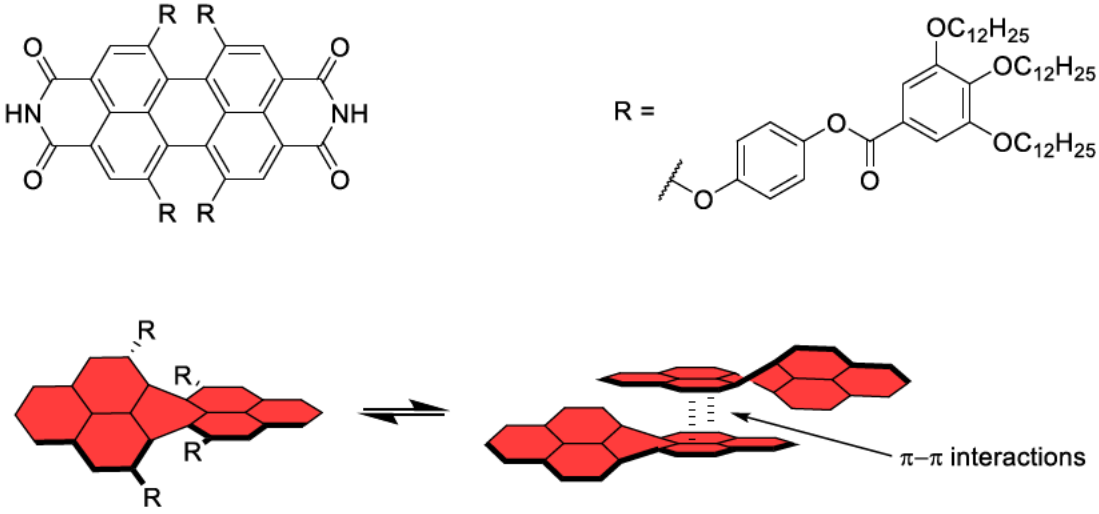

Figure 8: Top - tetra bay-substituted PDI investigated by Würthner. Bottom – typical stacking arrangement leading to the formation of J-aggregates in PDIs.

Effects of Bay-Position Substitution on Aggregation – Twisted Vs. Planar PDIs.

A pronounced difference in aggregation behaviour can be seen when PDIs are substituted at the bay position. This was investigated in a paper by Würthner and co-workers by comparing a range of bay-substituted PDIs with a reference PDI that was not bay-substituted but otherwise had the same imide groups, with the bay-substituted PDIs forming dimers in methylcyclohexane in millimolar concentrations, while the bay-unsubstituted PDIs form larger π-π stacked oligomers at the same concentrations. This is rationalised by the core-twisting effect seen in bay-substituted PDIs. When planar PDIs aggregate, their π surfaces are equal with respect to another PDI molecule approaching either the top or bottom face, and so extended aggregates are often formed. By comparison, for bis bay-substituted PDIs, the bay-substituents point such that they are on the same side of the molecular plane and so the most sterically unhindered faces of two PDIs can come together to form an energetically-minimised dimeric aggregate. Conversely, the other face is sterically hindered and therefore disfavouring π-π interactions and the formation of higher aggregates. Furthermore, this study found a good correlation between the twist angle of the PDI and the Gibbs free energy of π

stacking. As the twist angle, Θ, increases from 0 ° to 37 ° a large decrease in the aggregation constant is observed. The effects of bay substitution are summarised in Figure 9.[24]

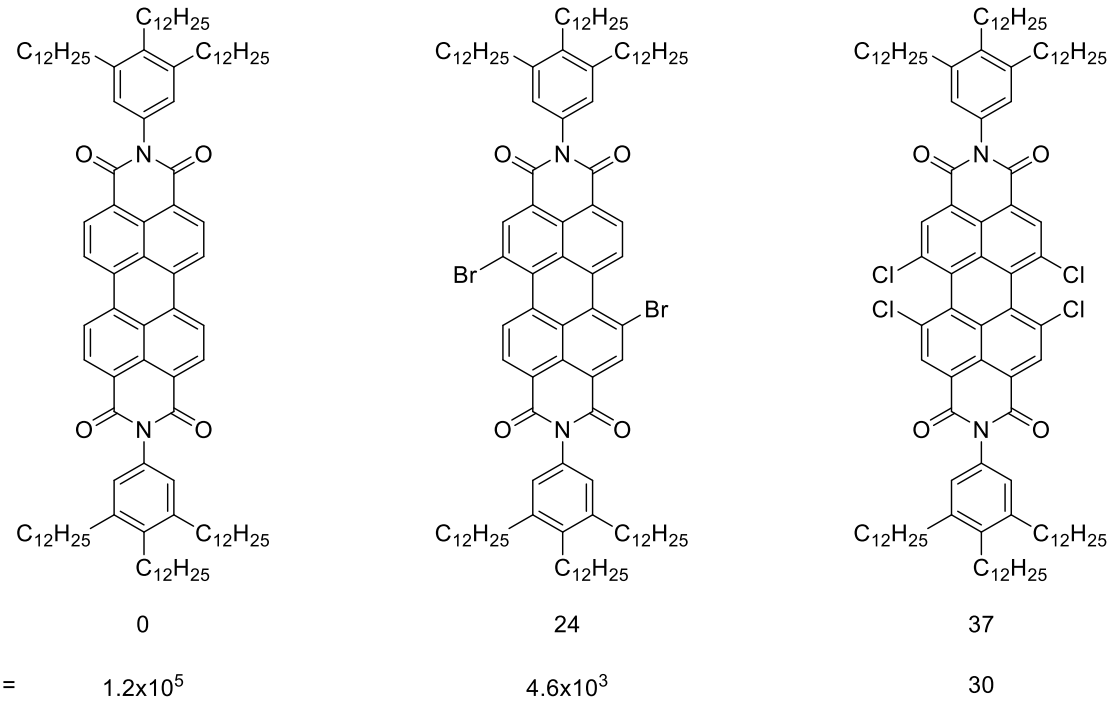

Figure 9: Comparison of PDIs with various degrees of core twisting and its effect on their aggregation. Left example is fitted according to the isodesmic model, while the middle and right examples are fitted according to the monomer-dimer model.

1.4 Optical Anion Sensing and Supramolecular Chemistry.

With the ever-increasing role the chemical industry has been playing in our lives an increasing focus has been placed on the presence of toxic pollutants, e.g., heavy metals and their ions, organic compounds, and pesticides etc, in the air, water, or earth. With this, the need for quick, selective, and sensitive sensing methods has greatly increased. Of those pollutants, anions are of key importance, with the misregulation of chloride being linked to cystic fibrosis[25] and nitrate and sulfate being linked to acid rain[26] amongst many other problematic anions.[27] The sensing of anions is particularly difficult given the synthetic difficulty in designing water-soluble organic molecules, anions have a tendency to become protonated at low pH and the fact that anions are highly solvated, more so than cations of similar size and charge resulting in weaker electrostatic interacions.[28]

Of the current approaches to sensing analytes, i.e., high-performance liquid chromatography (HPLC), capillary electrophoresis, and gas chromatography (GC) all are time-consuming and expensive due to the equipment or training required or electrochemical sensors that can suffer from poor selectivity

when exposed to similar analytes.[29] As a result, less expensive and quicker to perform methods are required. Optical sensors that utilise UV-vis or fluorescence spectroscopy have seen a substantial amount of interest due to them being comparatively cheap, easy to perform, highly sensitive, and have the potential to automate the process to perform high-throughput screening e.g., chiral sensors for chiral catalyst activity.[30] To create good fluorescent probes several factors must be considered, such as the absorbance of the molecule, quantum yield of fluorescence (what proportion of the light that is absorbed gets emitted), and fluorescence lifetime (the decay of the emission intensity). PDIs, therefore, make excellent candidates for study due to their strong absorption in the visible region and high fluorescence quantum yield.[31]

The complexation of anions is one of the fundamental pillars of supramolecular chemistry, with research into its applications in anion sensing, anion-responsive materials, organocatalysts that utilise anion complexation, and the removal of anions from mixtures of compounds. Supramolecular sensors rely on non-covalent interactions, Figure 10, with responses to stimuli such as affecting the conformation or aggregation state of the sensor which triggers changes in the absorption and/or the fluorescence spectra.[32] Supramolecular sensors have the benefit over more traditional small molecule sensors that rely on irreversible binding or reactions as they may be recoverable and/or may be more tailorable owing to the different factors that can be exploited by supramolecular systems, e.g. preorganisation or incorporating a range of binding motifs.

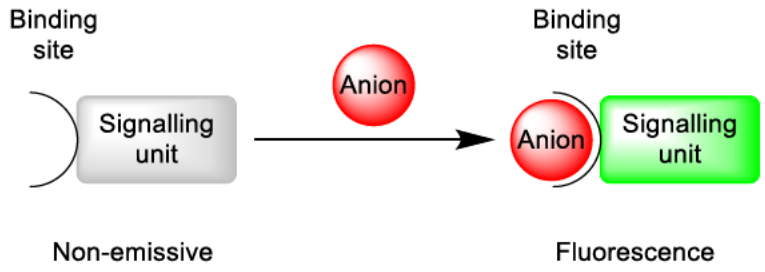

Figure 10:Basic principle of a supramolecular sensors.

At the most fundamental level sensing relies on molecular recognition, which is the consequence of intermolecular interactions, the most important of which will be discussed in the following section. These range from the strongest, Lewis acid-base donor-acceptor complexes, through to π-π interactions and hydrogen bonding, and finally the weakest forces, dipole-dipole interactions and van der Waals forces.[33] Stronger interactions should be preferred as they should fundamentally lead to greater sensitivity and greater ability, when tuned to the analyte of choice, to differentiate among mixtures or similar analytes.[34]

1.5 Relevant Non-Covalent Interactions.

The following sections will outline the non-covalent interactions that are of greatest importance to this thesis.

Hydrogen Bonding.

Hydrogen bonding is one of the most important building blocks to life as it is these interactions, between DNA base pairs, which give rise to the double helix structure of DNA,[35] as well as giving Kevlar its strength.[36] Hydrogen bonds are formed between a hydrogen covalently bonded to an electronegative atom, e.g., oxygen or nitrogen, which polarises the X-H bond (X =O or N) and an atom with accessible lone pairs, e.g. oxygen or nitrogen. These bonds vary greatly in terms of strength form as weak as < 4 kJ mol^{-1}, indistinguishable from van der Waals forces, to around 160 kJ mol^{-1} (for $[F_2H]^-$), or half as strong as a C-C single bond.[35] Additionally, hydrogen bonds are very directional and are at their strongest when the angle between the donor and acceptor, D-H···A, is 180°.[37]

The hydrogen bond donor behaviour of the triazole ring is a relatively recent addition to the toolkit of anion recognition. The hydrogen bonding ability of this ring comes from the polarisation of the C-H bond as a result of the three N atoms that generate a large 5-debye dipole almost co-linear with the C-H bond. Furthermore, the carbon bearing the hydrogen is made even more electron deficient by the removal of electron density by conjugation to the three electron-withdrawing nitrogens. These effects combine to make a hydrogen bond donor that is similar in strength to traditional hydrogen bond donors such as N-H bonds of pyrrole and amide groups.[38] The strength of this hydrogen bond can be further enhanced by quaternisation of the nitrogen, Figure 11. The introduction of a formal positive charge increases the degree of polarisation and therefore the now charge-assisted hydrogen bond donor ability becomes stronger.[39,40]

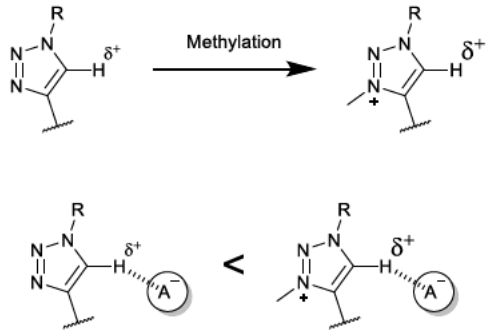

Figure 11: Triazoles have an acidic C-H bond meaning it can act as a hydrogen bond donor, which can be enhanced by methylation.

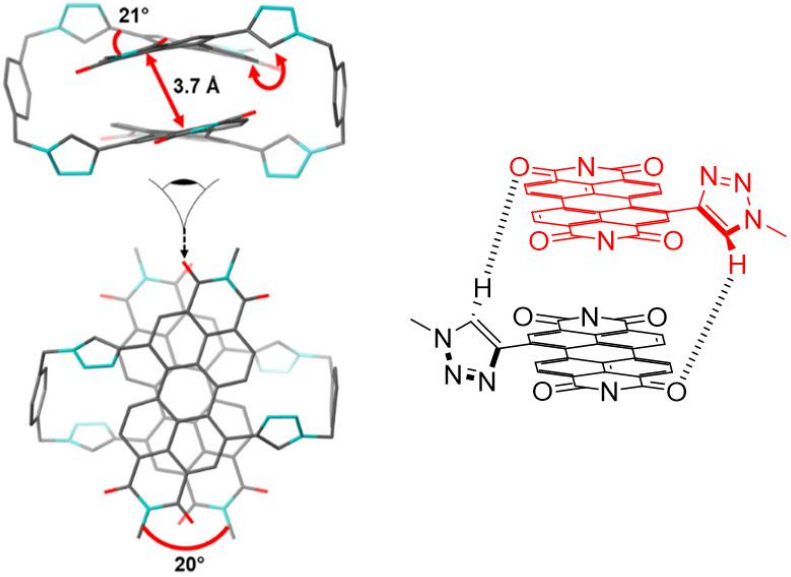

Figure 12: (Left) Pink box adapted from reference 44. (Right) simplified diagram shown intramolecular hydrogen bonding.

Hydrogen bonding has been observed between PDIs functionalised with two triazole heterocycles at their bay positions. In the PDI macrocycle in Figure 12, it can be seen in the crystal structure the four triazole rings point towards the opposing carbonyls, providing evidence for hydrogen bonding. A favourable face-to-face arrangement is also observed that promotes π-π stacking (see next section) and H-type aggregation.[41] Hydrogen bonding has also been applied in the H-type aggregation of imidazolium PDIs, see Figure 13. In $CHCl_3$ significant aggregation was observed, while aggregation was hindered in polar solvents e.g., MeCN, while in the protic solvent MeOH the aggregates were broken up, which points to the substantial contribution of hydrogen bonding to the aggregation of this PDI. The length of the alkyl chain also has a significant effect on aggregation as longer chains shield the negatively charged iodide from the positive imidazolium centre, promoting disaggregation. On the other hand, these long chains also promote van der Waals interactions with neighbouring PDIs, thereby promoting aggregation. As a result of the combination of these effects, the highest aggregation constant, according to the isodesmic model, is seen with an intermediate chain length.[42]

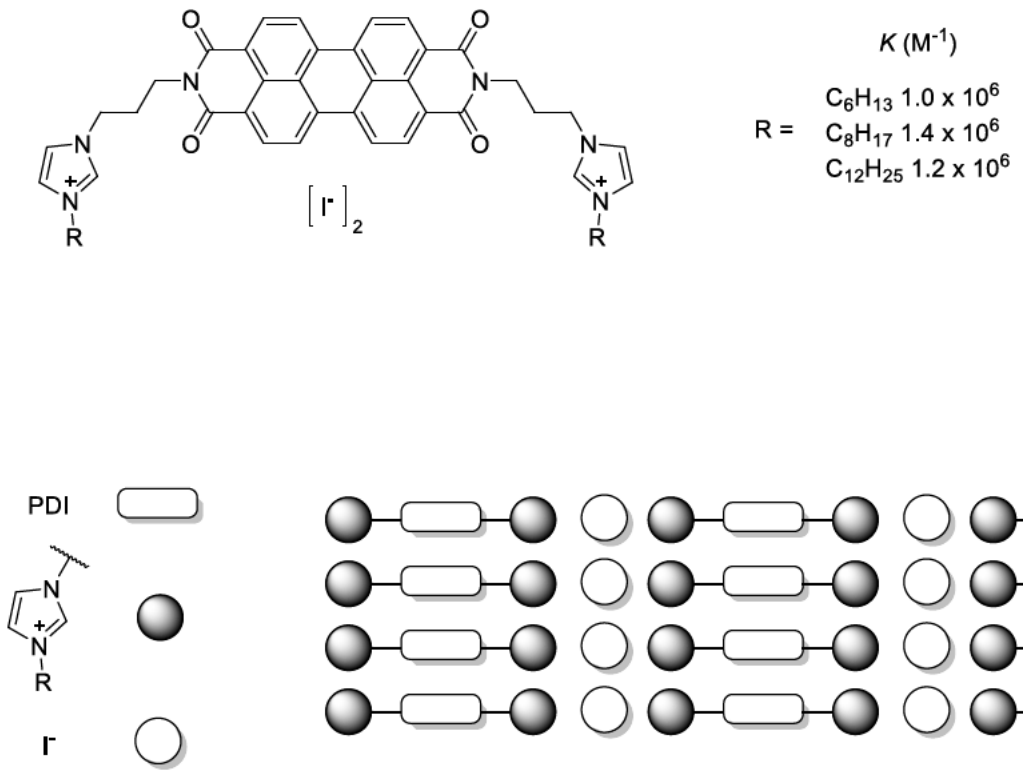

Figure 13: Charge-assisted hydrogen bonding has previously been applied to diimidazolium PDIs (top). Aggregation constants are also supported by the planar π surface and the presence of a coordinating anion (bottom).

Aromatic Stacking of Molecules.

Benzene, being the archetypal aromatic molecule, has been heavily studied in order to understand the interactions between neighbouring π systems. For π systems that are electronically identical, that is they are of equal "electron-richness", face-centred stacking is disfavoured due to the electrostatic repulsion between two faces. Instead, in the solid state, 't-shaped' edge-to-face alignment is preferred. While in the liquid phases, parallel offset dimers and the 'γ-shaped' edge-to-face configurations are favourable. In both cases this allows for the positive σ framework of one molecule to sit over the negative π system of the second molecule which leads to a favourable electrostatic

interaction. These orientations are shown in Figure 14. However, between electron-rich and electron-poor aromatic rings, so-called donor-acceptor interactions, face-to-face interactions are favoured due to the electrostatic attraction between the electron-rich π system and the neighbouring electron-poor π system.[43]

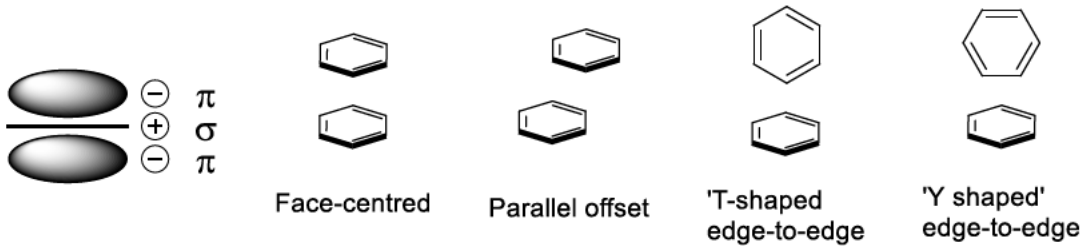

Figure 14: Electrostatic interactions between the negatively charged π cloud above and the positively charged σ framework of a neighbouring molecules promotes π-π stacking (left). The different interactions two neighbouring pi surfaces can partake in (right).

For larger π systems, such as PDIs, face-to-face arrangements are also preferred due to the significant increase in the electrostatic and/or dispersion energy arising from the increased interacting π surfaces.[44] Indeed, for PDIs, the presence of heteroatoms means there is a pronounced quadrupole moment resulting from the high electron density at the carbonyl oxygens and the low electron density at the bay area, according to calculations based on *N,N'*-dimethyl PDI.[15] For aggregates in solution this results in a rotational displacement to minimise the electrostatic interactions between these charged areas.[15] This is supported by a calculated potential energy surface, calculations based on an imide unsubstituted PDI dimer, shows that this rotationally displaced arrangement, Figure 15 right, is the global minimum, with an energy of binding of -117 kJ mol^{-1}. Two local minima exist within 20 kJ mol^{-1} of the global minima which have no rotational displacement and instead favour a transversal or longitudinal displacement, Figure 15 left and middle respectively.[45]

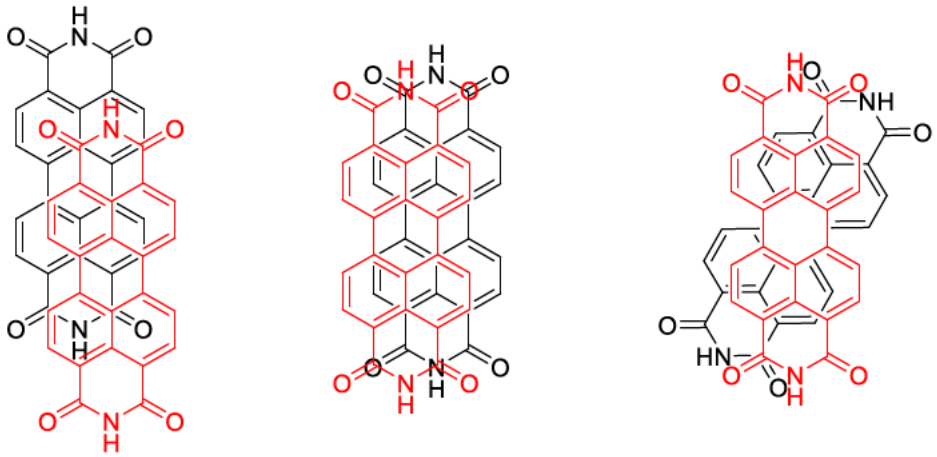

Figure 15: Left to right the three most favoured PDI-PDI stacking interactions based on a computed potential energy surface.

The π stacking behaviour of bay-unsubstituted PDIs in solution has been investigated by Würthner and co-workers. [46]They found that different contributions of intermolecular forces played a role in the π stacking of these unsubstituted PDIs. For low polarity solvents the aggregation constant decreases as the polarity is increased, e.g., from hexane to toluene, with is explained by the decrease in electrostatic interactions between the PDIs. Then, as the polarity is further increased to very dipolar and protic solvents, e.g., MeCN and MeOH, the aggregation constant increases because of solvophobic effects. Notable outliers in this trend were with solvents such as CCl_4 and $CHCl_3$, where the high polarizability of these solvents provided the best solvation for the PDIs and therefore the aggregation constant was much lower than would be expected.[46]

1.6 Aggregation-Disaggregation as a Sensing Mechanism.

As mentioned earlier, the formation of H-type aggregates leads to the quenching of fluorescence. It therefore follows that if those aggregates can be broken up by the addition of an analyte, then the dye can be used as a supramolecular sensor, with this process being referred to as "disaggregation-induced emission".

Disaggregation-induced emission has been utilised to design a PDI based probe to sense pyrophosphate in aqueous solution (Figure 16).[47] In this system the Gly-Asp (Glycyl-L-aspartic acid) imide groups bind Cu^{2+} ions which promotes the formation of aggregates with quenched fluorescence. This relies on the stronger affinity of pyrophosphate for Cu^{2+} compared with carboxylate. Therefore, as pyrophosphate is introduced to the solution the Cu^{2+} ions are sequestered from the PDI aggregates causing them to break up and restoring their fluorescence. As a result of the reliance on the pyrophosphate-Cu^{2+} this probe shows good selectivity. Whereas other anions such as halides, nitrate and nitrite, sulfate and sulfite, and even the phosphate ion, which often coexists with pyrophosphate, did not significantly increase the fluorescence response of the PDI.[47]

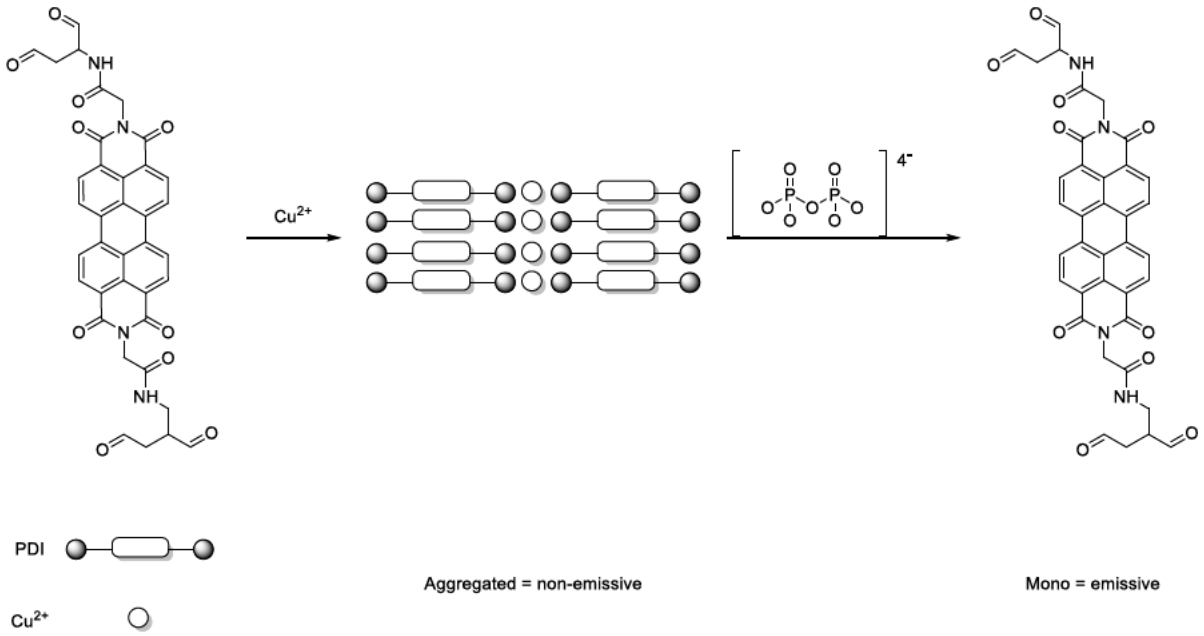

Figure 16.: Aggregation is supported by the presence of Cu^{2+} which can then function as a disaggregation-induced emission sensor for pyrophosphate.

A similar method was used by Yu and co-workers to design a fluorescent PDI with carboxylic acid groups at the imide position to act as a sensor for DNA (Figure 17).[48] The addition of a polymer polycation or polymers containing hydrogen bond donating amines was able to induce aggregation in the PDIs through electrostatic interactions between the anionic PDIs and the polycations and aided π-π interactions between the now neighbouring PDIs, thereby quenching the fluorescence of the PDIs. These aggregates could then be broken up by the addition of DNA, which is a polyanion, causing the fluorescence to be restored, thus leading to optical sensing of the DNA strand.

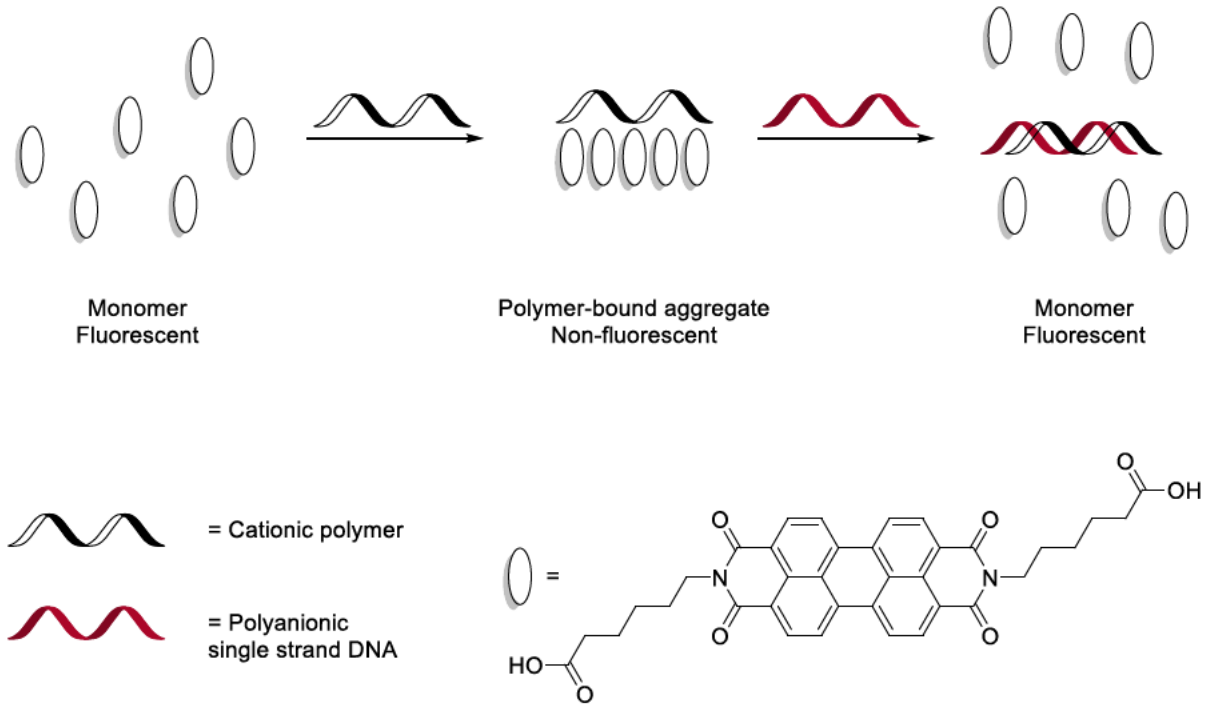

Figure 17: Anionic PDI monomer binds to the polycationic polymer, turning off the PDI fluorescence. Introduction of polyanionic single strand DNA displaces the PDI, realising to its monomer form turning the fluorescence response.

2. Motivation and Aims of the Project.

Anions play a fundamental role in our daily lives, where they form the basis of many biological and industrial processes and as such, they can be key to sustaining life or being toxic to it.[49] Therefore, the need to sense the presence of these species is clear. Of the current approaches to sensing analytes, i.e., high-performance liquid chromatography (HPLC), capillary electrophoresis, and gas chromatography (GC) all are time-consuming and expensive due to the equipment or training required or electrochemical sensors that can suffer from poor selectivity when exposed to similar analytes.[50] As a result, less expensive and quicker to perform methods are required.

Optical sensors that utilise UV-vis or fluorescence spectroscopy have seen a substantial amount of interest due to them being comparatively cheap, easy to perform, highly sensitive, and have the potential to automate the process to perform high-throughput screening.[30] To create good fluorescent probes several factors must be considered, such as the absorbance of the molecule, quantum yield of fluorescence (what proportion of the light that is absorbed gets emitted), and fluorescence lifetime (the decay of the emission intensity). Metal-based sensors have low extinction coefficients[51,52] and, due to the more complicated excited state behaviours, require very careful tuning to control their binding properties, i.e., selectivity and strength, vs the luminescence properties of the metal complex.[53,54] Furthermore, many of these are based on expensive metals such as ruthenium and iridium, limiting them from an economic point of view. By contrast, PDIs offer a high quantum yield of fluorescence (approaching unity), a S_0-S_1 absorption well described by a HOMO→LUMO (π-π*) transition that allows for simpler tuning and with the starting PTCDA being commercially available and cheap. Some current attempts at using PDIs as disaggregation-induced emission sensors for anions are themselves anionic and rely on the presence of a cation to promote aggregation, of the anionic PDIs, which is then broken up by an analyte anion that is capable of binding strongly to the cation[47,48] which may limit their use.

Previous work within the group has developed the chemistry of bis-triazole PDIs. Recently published work has shown the ability of neutral bis-triazole PDI macrocycles to undergo intramolecular hydrogen bonding and form H-type dimer aggregates in solution.[41] And while it has been shown that triazole and triazolium containing molecules are capable of binding anions,[39,40,55] this has not yet been demonstrated using a PDI-based system. Therefore, the first objective of this project will be to synthesise and characterise a novel bis-triazolium PDI. Following that, UV-vis spectroscopy will be used to quantify its aggregation by fitting the resulting data to a mono-dimer model. Additionally, the potential of the PDI to act as an anion sensor will also be explored. Figure 18 displays the principle

behind the project, to combine previous knowledge of PDI aggregation and triazolium anion binding to make a disaggregation-induced emission sensor for anions.

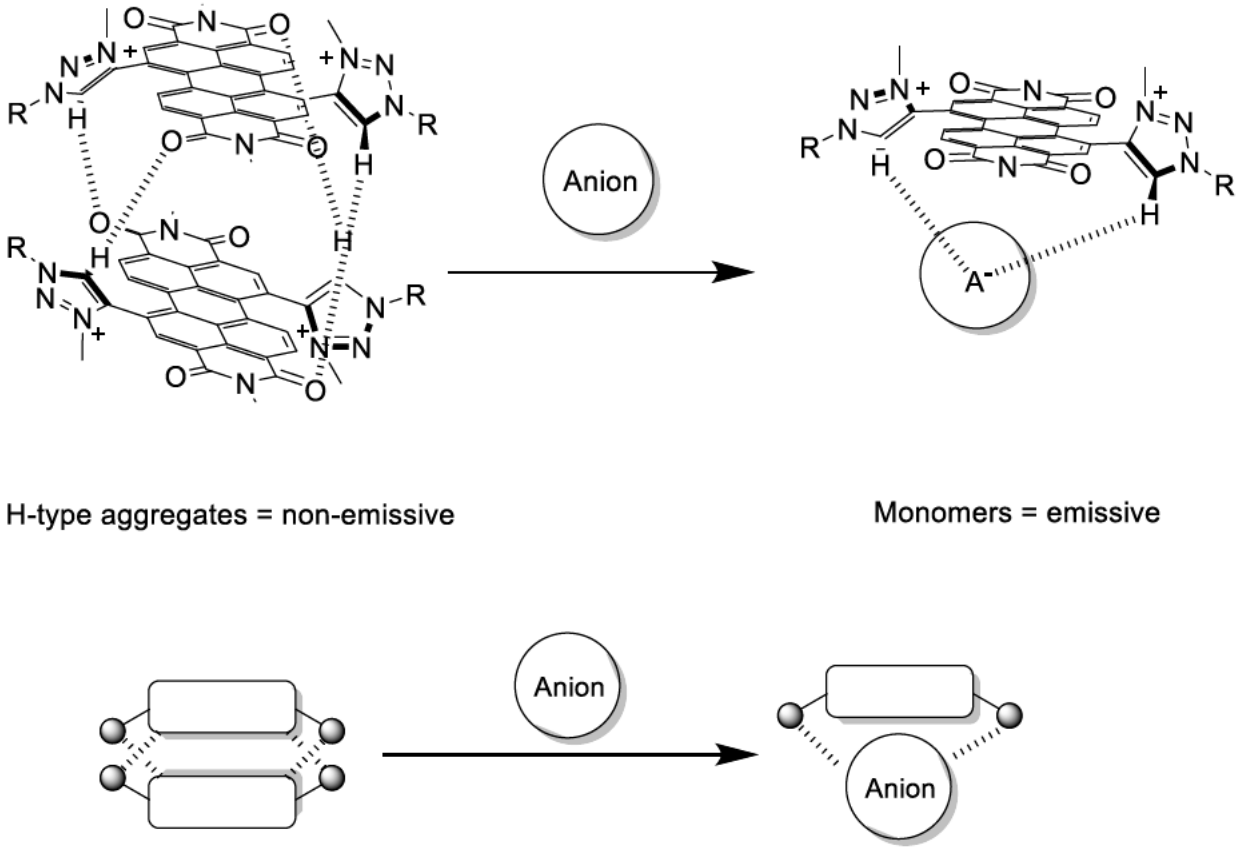

Figure 18: (Top) Design principle of a PDI sensor that relies on hydrogen bonding to form non-emissive H-aggregates that can be broken up by introduction of an anion. (Bottom) simplified cartoon very of the same principle for clarity.

3. Results and Discussion.

3.1 Synthesis of Bis-Triazole PDI 5

The synthesis of a bis-triazole PDI was carried out according to Scheme 1. 3-Amino pentane was chosen to be the imide group because swallow-tail alkyl chains are known to facilitate interactions between the PDI cores. Whereas, on the other hand, 2,6-dimethylaniline is more solubilising, preventing aggregation due to sterics by its orientation perpendicular to the PDI core.[46] Therefore, it was hoped that a swallow-tail C_5 imide group would be a good option for studying PDI-PDI interactions, while also providing good solubility. It was decided that it was beneficial to install the imide group prior to bromination, as alkyl chains are inert to such conditions (another reason to not use aniline derivatives as they may be brominated). The swallow-tail C_5 imide group was installed using standard conditions of amine and a Lewis acid, $Zn(OAc)_2{\cdot}H_2O$, in molten imidazole. Purification of PDI **1** was simple as the unreacted material was insoluble in DCM and therefore could be filtered off using a small plug of silica.

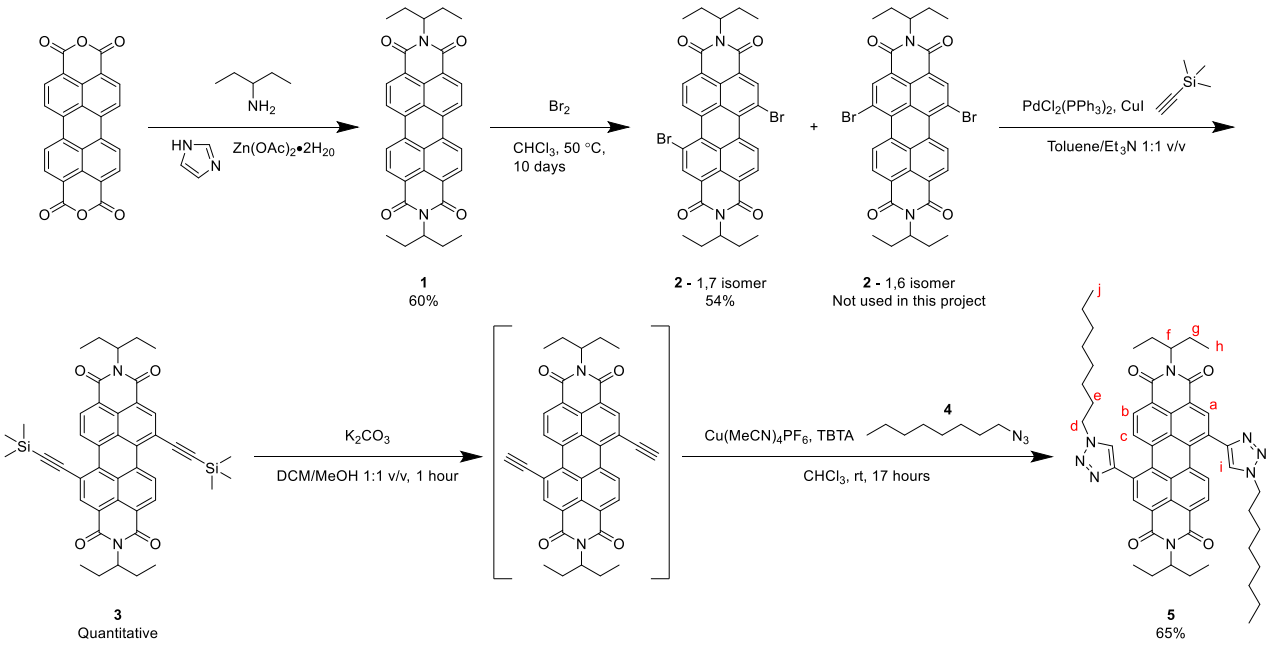

Scheme 1: Multistep synthesis of bis(octyl-triazole) PDI. The protected bis-alkyne was deprotected and used immediately and therefore was not characterised.

The synthesis of dibromo PDI **2** proceeds according to a modified literature procedure.[18] $CHCl_3$ was used as the solvent instead of DCM as the C_5 PDI **1** is more soluble in $CHCl_3$ and it allows the reaction to run at higher temperatures to drive the reaction towards completion, which after being filtered through a silica plug the desired dibromo PDI was obtained in quantitative yield. The reaction produces

a mixture of the 1,7 and 1,6 isomers of PDI **2**, in a roughly 4:1 ratio, that had to be separated before it could be used further as it becomes more difficult to separate the minor 1,6 isomer from the major 1,7 isomer at later stages of the synthesis. To achieve this the isomeric mixture was recrystallised from DCM/MeOH 1:2 v/v three times to obtain pure 1,7 dibromo PDI **2**. However, it was later found that small amounts of the 1,6 isomer could alternatively be removed by column chromatography at the triazole (PDI **5**) stage. Therefore, as each recrystallisation took two weeks, it was decided that performing only two recrystallisations and carrying through the small remaining quantity (~ 5%) of the 1,6 isomer through the following reactions was more time-efficient.

The TMS-protected alkyne was installed via a Sonogashira coupling to give PDI **3**, which after deprotection (removing the TMS group to expose the alkyne) under basic conditions, allowed for further functionalisation via a 'click' reaction to yield the corresponding bis-triazole PDI **5**. Tris(benzyltriazolylmethyl)amine (TBTA) was used as stabilising ligand. It is thought that this acts to protect the copper catalyst from oxidation.[56] The length of the octyl alkyl chains was purely a practical choice, organic azides with a low carbon/nitrogen ratio are known to be unsafe. Using the "rule of six" that is six carbons, or similarly sized, atoms per azide group should render the compound dilute enough to be safely handled and stored at a reasonable, multi-gram scale.[57] Synthesis proceeds according to Scheme 2. Extracting the product into diethyl ether, leaving any remaining sodium azide in the aqueous layer, gives the desired octyl-azide **4** without further purification in a 55% yield.

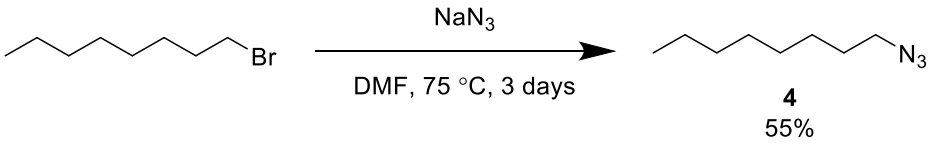

Scheme 2: Synthesis of azido-octane.

3.2 Characterisation of Bis-Triazole PDI 5.

To assign the ^{1}H NMR spectrum of PDI **5** a mixture of 2D HMBC (Heteronuclear Multiple Bond Correlation) and COSY (COrrelation SpectroscopY) NMR spectroscopy was used, with the final assignment shown on Figure 19. This characterisation was carried out in the same manner as that explained in section 3.4. See appendix Figures 40 and 41 for 2D spectra.

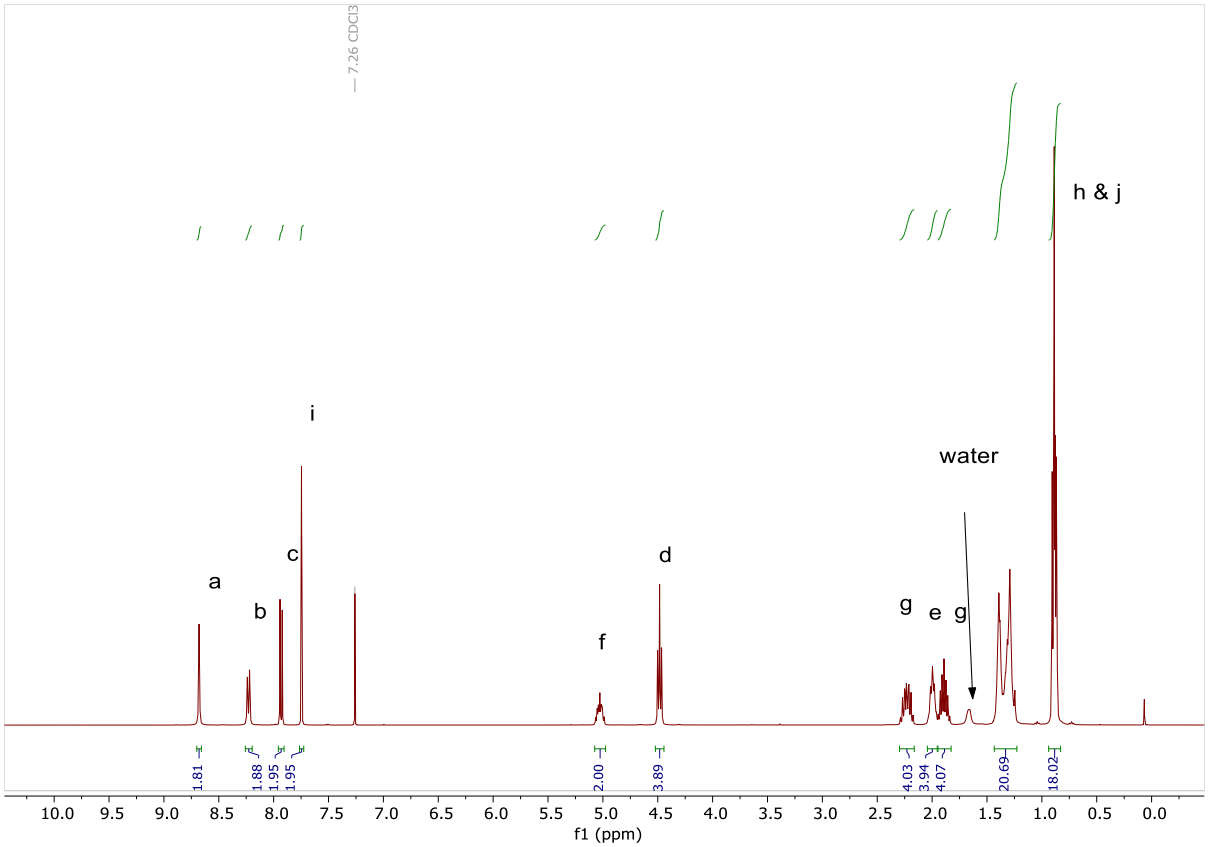

*Figure 19: ^{1}H NMR spectrum of **5** in chloroform-d, 298 K, 400 MHz.*

3.3 Methylation of Bis(Octyl-Triazole) PDI 5

The next step was to methylate the triazole heterocycles of the bis-triazole PDI **5** to increase their hydrogen bonding potential. Initial attempts to methylate PDI **5** using MeO_3BF_4 as the methylating agent were not successful, even after strict control and monitoring of reactions, i.e., by performing the reaction in a N_2 glovebox in the dark, as well as all purifications being done in the dark. This reaction led to a mixture of products visible in the ^{1}H NMR, but which could not be identified, or removed by repeated preparative TLC. As a result, it was decided an alternative methylating agent, methyl iodide (MeI), as a potential way forward. With the reasoning that even if methyl iodide did not drive the reaction to completion, it should still result in a cleaner product (as it is a weaker methylating agent and therefore less likely to cause potentially unwanted side reactions) and the desired doubly methylated product is easy to separate from the singly methylated product using preparative TLC. Initial testing in neat MeI at room temperature followed by heating to 70 °C in MeI/toluene for one day showed very little reaction by TLC, albeit with the heated reaction being slightly more effective. As heating had produced minorly better results, a method of heating the bis-

triazole PDI **5** in neat MeI was sought, but this was not straightforward given the low boiling point (42 °C) of MeI and so a pressure tube was used. By using a pressure tube the reaction could be heated well beyond the boiling point of MeI and it was found that by heating the reaction to 80 °C in neat MeI for three days, as shown in Scheme 3, that the reaction could be driven to completion. Following this, purification by preparative TLC could be carried out.

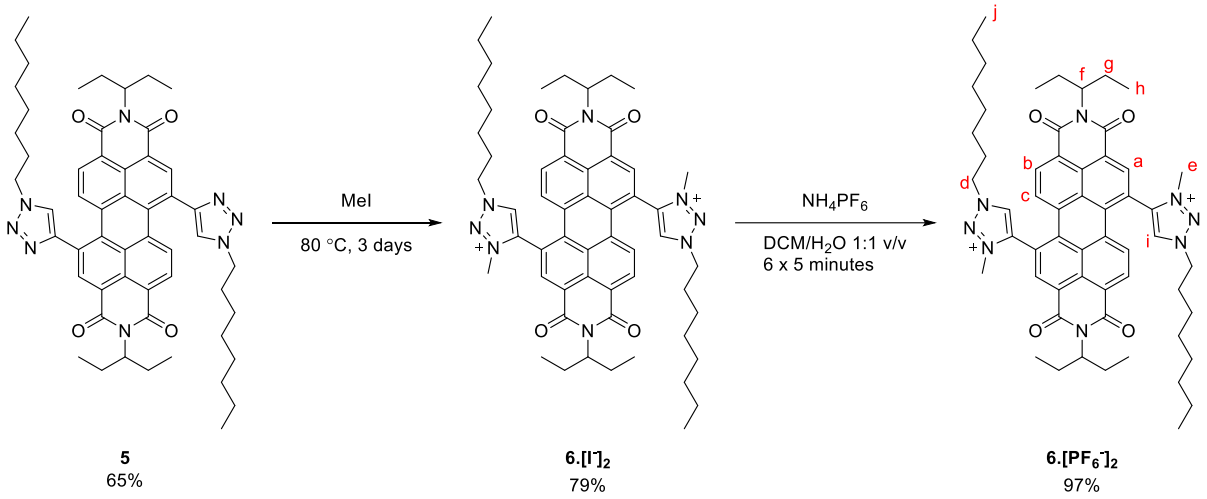

Scheme 3: Synthesis of final compound, the bis(octyl-triazolium) PDI.

However, iodide as the counter ion was less desirable for further studies as the iodide anion is potentially coordinating and may therefore impact aggregation. Therefore, iodide was exchanged for a more weakly-coordinating counter anion, hexafluorophosphate (PF_6^-). To do this a solution of the bis-triazolium PDI **6.[I^-]$_2$** in DCM was repeatedly stirred vigorously with an aqueous 0.1 M solution of ammonium hexafluorophosphate (NH_4PF_6), with a rapid colour change observed (dark to bright red), to yield the corresponding bis-triazolium PDI **6.[PF_6^-]$_2$**. A noticeable change in the ^{1}H NMR spectrum is seen indicating successful counter-ion exchange (Figure). With I^- as the counter ion the C-H of the triazolium is sharp, whereas with PF_6^- the signal is broad, indicative of a potential change in hydrogen bonding. Furthermore, colour change observed is also good evidence of this PDIs potential as an anion sensor as this point to a change in the aggregation state of the PDI.

3.4 Characterisation of Bis-Triazolium PDI 6

To assign the ^{1}H NMR spectrum of bis-triazolium PDI **6.[I^-]$_2$** and **6.[PF_6^-]$_2$** again a combination of HMBC and COSY NMR spectra were used, see Scheme 3 and Figure for full details. HMBC was used as it shows carbon-proton coupling through multiple bonds and COSY was used as those spectra show proton-proton couple over multiple bonds This was most simply done with PDI **6.[PF_6^-]$_2$** as this was

the most soluble salt and therefore was better suited to acquiring the necessary 2D NMR spectra. As in PDI **5**, the carbonyl carbon can be reasoned to be the ^{13}C peak at 164.39 ppm. The HMBC, Figure , spectrum then enables assignment of proton signals **b** and **c** as they must belong to those protons closest to the imide region. The other doublet, labelled **i** thus belongs the other PDI bay-area proton and the broad singlet, labelled **a**, is the triazolium proton.

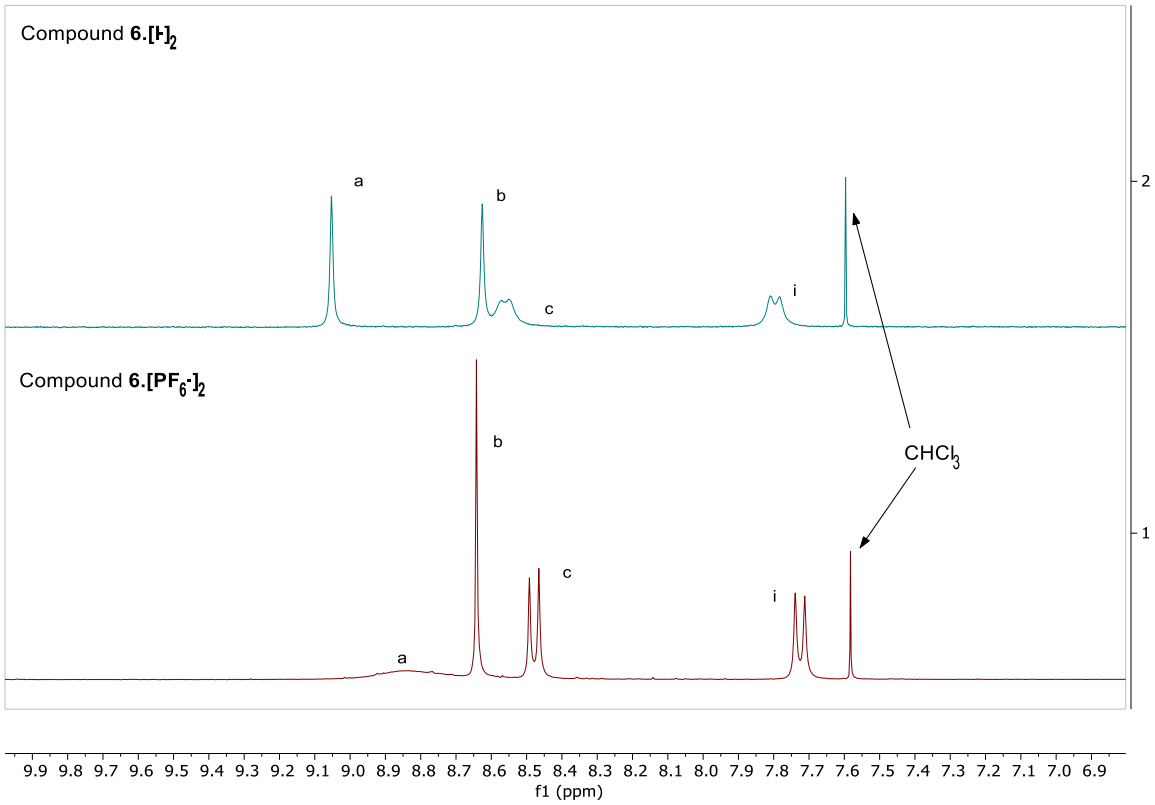

*Figure 20: ^{1}H NMR spectra comparing the aromatic region of the triazolium salts (top) bis(octyl-triazolium) PDI **6.[I^-]$_2$** (bottom) bis(octyl-triazolium) PDI **6.[PF_6^-]$_2$**.*

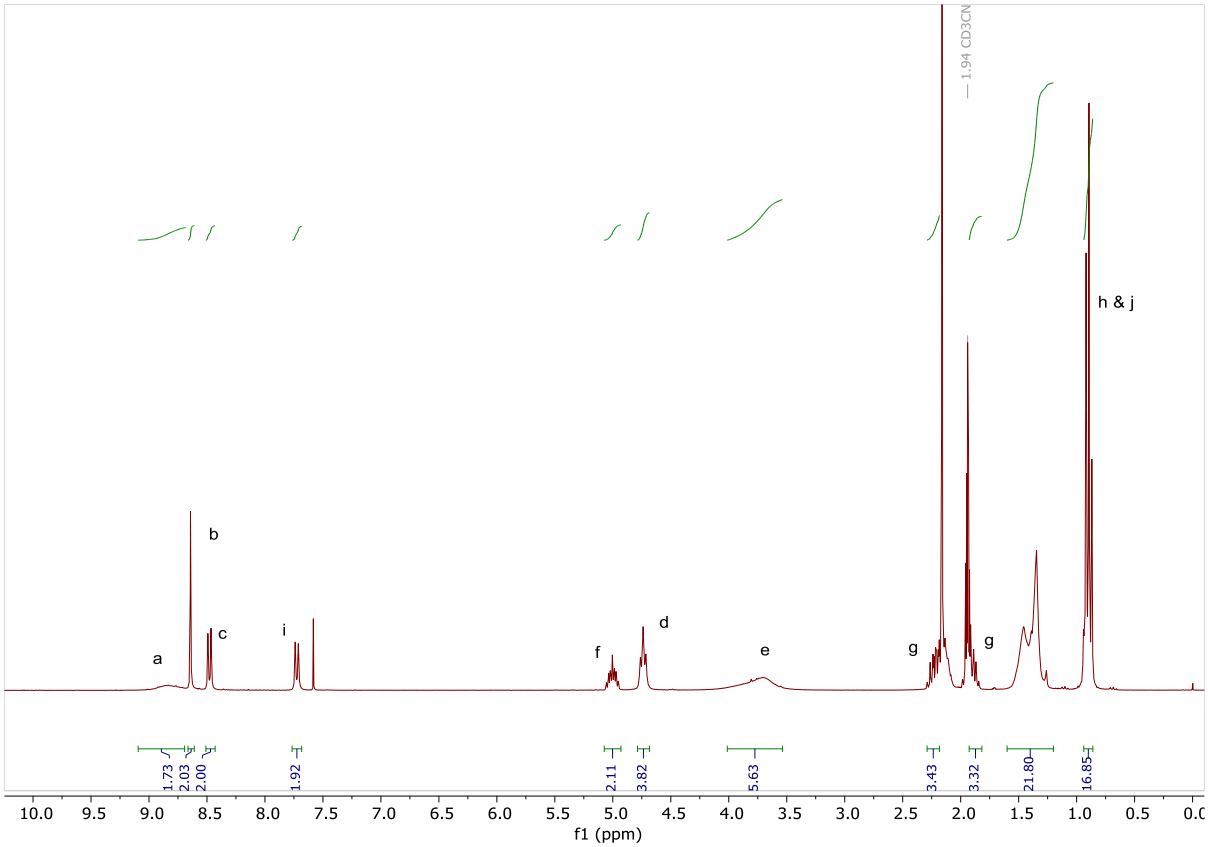

*Figure 21: ^{1}H NMR spectrum of **6.[PF_6^-]$_2$** in acetonitrile-d_3, 298 K, 400 MHz.*

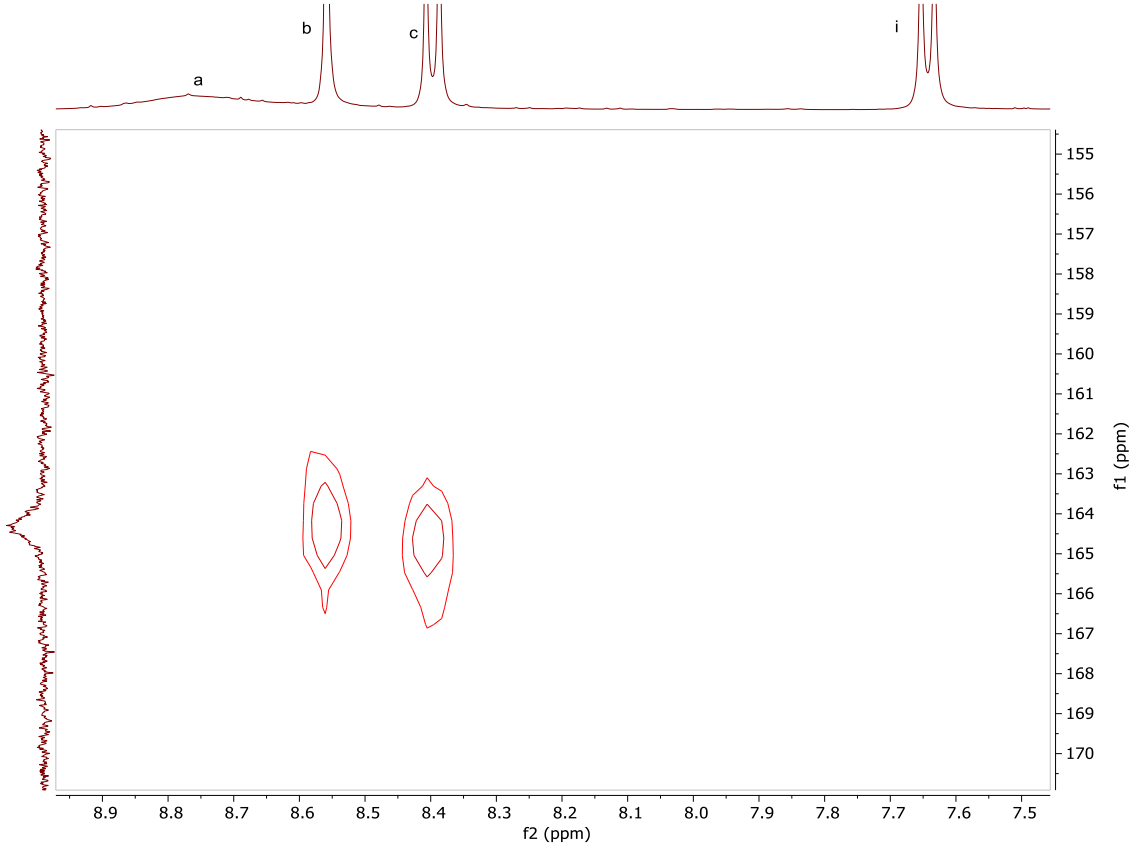

*Figure 22: HMBC NMR spectrum of **6.[PF_6^-]$_2$** in acetonitrile-d_3, 298 K, 400 MHz.*

Proton **d**, at 4.74 ppm, is easily identified because it is a downfield triplet, integrating to four protons. Further elucidation of the alkyl chain is not possible but lie in the region of 1.26 and 1.46 ppm which integrate to 20 protons. Proton **f** is easily identified as the downfield septet which integrates to four protons at 5.00 ppm. The COSY, Figure , shows cross peaks at 1.94 and 2.19 ppm that correspond to proton **g**, which integrate to eight protons. Cross peaks for proton **g** can be used to identify protons **h**, which is overlapped by the peak for proton **j**, which integrate to 18 protons, 12 from **h** and six from **j**. Proton **e** belongs to the methyl group on the triazolium and integrate to six protons.

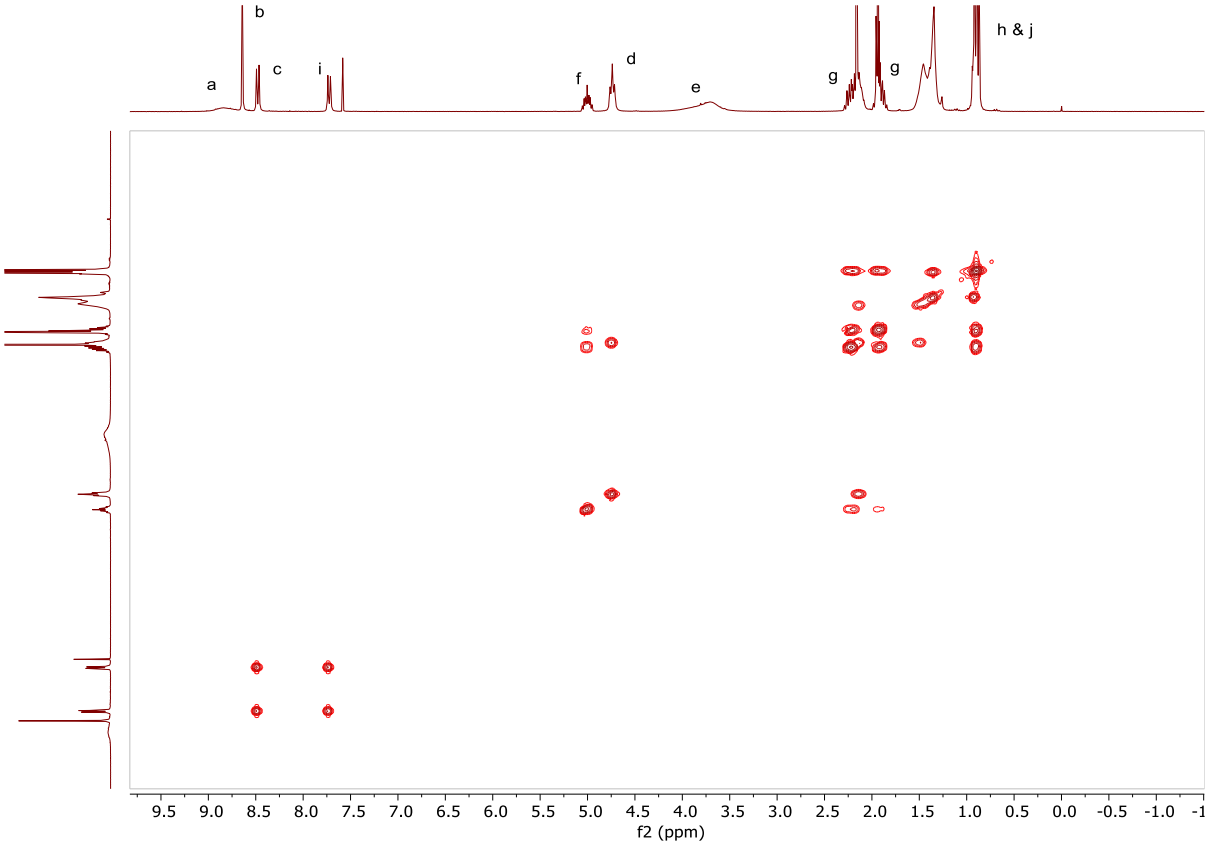

*Figure 23: COSY NMR spectrum of **6.[PF_6^-]$_2$** in acetonitrile-d_3, 298 K, 400 MHz.*

Further characterisation using ESI MS, positive mode was undertaken. The calculated and observed data is shown in Figure 2, with the calculated m/z for bis-triazolium PDI **6.[PF_6^-]$_2$** 459.2760 and the observed m/z was found to be 459.2751. These values arise as the counter anion is not visible in positive mode so therefore only the PDI itself [M-2PF_6^-] (mass 918.5509) is detectable and since the PDI is doubly charged the value for z is 2 and so the m/z expected is 459.2760. ESI MS, negative mode was also used to confirm the anion exchange, see appendix for spectra.

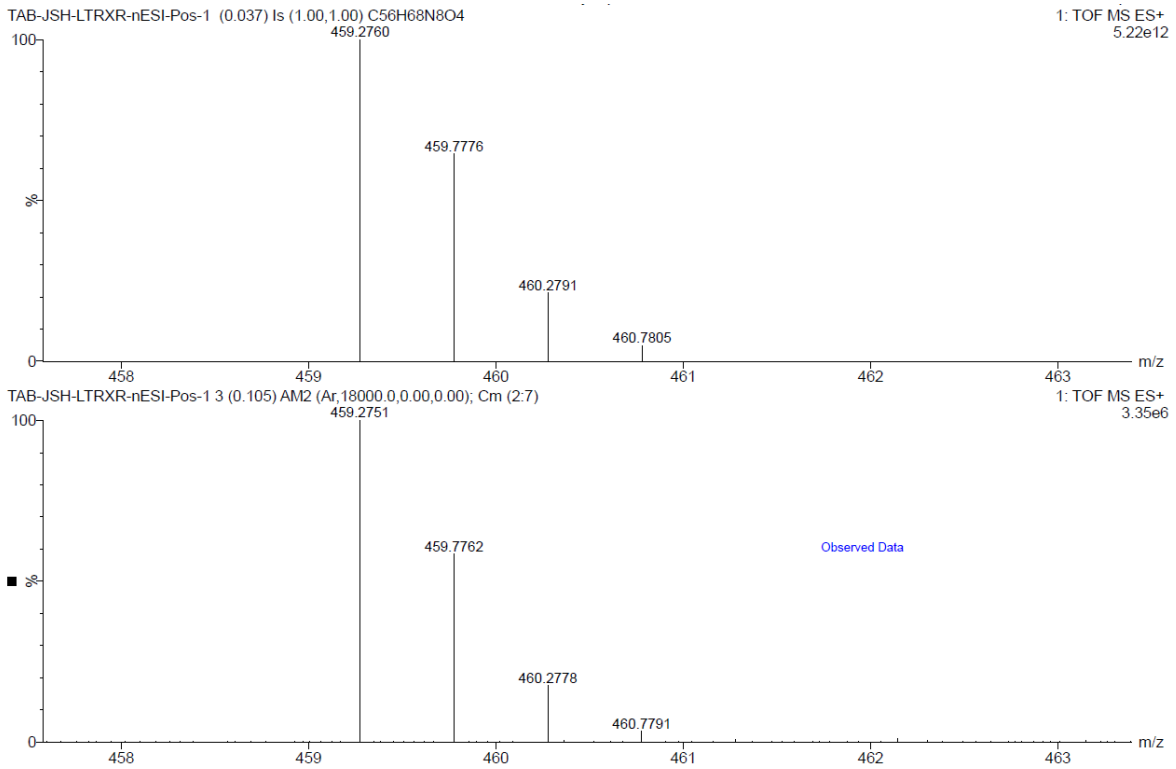

Figure 204: Calculated (top) and observed (bottom) ESI MS, positive mode, data for compound ***6.[PF$_6^-$]$_2$.***

3.5 Photophysical Properties of Triazole and Triazolium PDIs

With the target compounds isolated and characterised, it was important to establish if the PDI compounds were undergoing any significant aggregation. Here, UV-vis spectroscopy was used as it enables the assessment of the aggregation state, given by the $A_{0\text{-}0}/A_{0\text{-}1}$ ratio. As a reminder, $A_{0\text{-}0}$ and $A_{0\text{-}1}$ represent the absorbance of the 0-0 and 0-1 vibronic bands, respectively, of the lowest energy, S_0-S_1, transition (Figure 226).

The aggregation of any organic molecule via hydrogen bonding and/or aromatic stacking interactions is likely to have a solvent dependence and so it was necessary to assess PDI aggregation by measuring UV-vis spectra in a wide range of different solvents. Furthermore, these studies would allow identification of a solvent system suitable for performing aggregation experiments. Figure 21 shows the UV-vis absorption spectrum for bis-triazole PDI **5** and Figure 22 and Figure 23 show the respective UV-vis absorption spectra for bis-triazolium PDIs **6.[I$^-$]$_2$** and **6.[PF$_6^-$]$_2$**, in the same range of solvents.

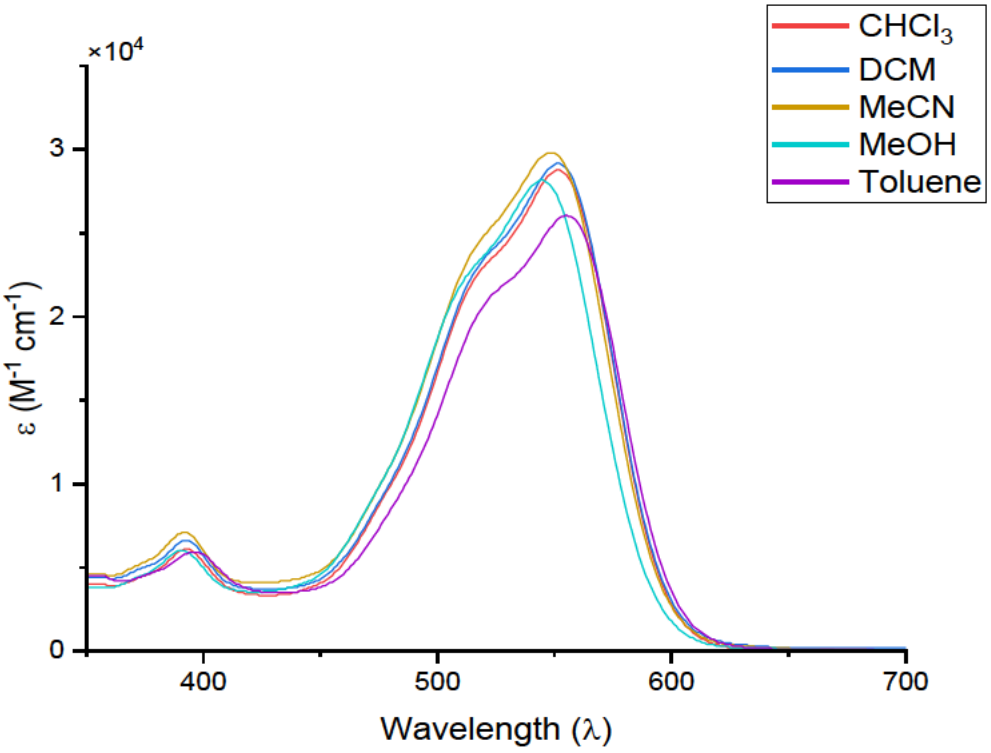

*Figure 215: Select UV-vis data of compound **5**. See appendix for further data.*

As can been seen from Figure 21 (representative data, see appendix for all spectra) solvent has little effect on the position of the $A_{0\text{-}0}$ transition of compound **5** or the extinction coefficient. It can be suggested that all these spectra represent a monomeric PDI species given the poorly defined fine structure, because of the increased ability of monomers to twist and vibrate. Furthermore, the vibronic peak ratio ($A_{0\text{-}0}/A_{0\text{-}1}$) is evidently greater than one, which is evidence for an unaggregated species. Given that lack of solvent dependent behaviour, it can also be assumed that the hydrogen bond donating ability of the triazoles, alongside π-π stacking, is not strong enough to cause significant intermolecular PDI-PDI interactions.

The solvent dependence UV-vis spectra of bis-triazolium PDI **6.[I]**$_2$ and PDI **6.[PF$_6^-$]**$_2$ are shown in Figure 226 and Figure 237 respectively (representative data, see appendix for all spectra). As a result of the cationic triazolium groups, significant changes are observed when changing the solvent. Here the fine structure is also more defined, which implies the bis-triazolium PDI is more rigid. The vibronic bands also allow for a rigorous assessment of the aggregation state in different solvents (Table 1).

Compound	**6.$[I^-]_2$**	**6.$[PF6^-]_2$**			**6.$[I^-]_2$**	**6.$[PF_6^-]_2$**		
Solvent	$\lambda A_{0\text{-}0}$ (nm)	$\lambda A_{0\text{-}0}$ (nm)	$\Delta\lambda A_{0\text{-}0}$ (nm)		$A_{0\text{-}0}/A_{0\text{-}1}$	$A_{0\text{-}0}/A_{0\text{-}1}$	$\Delta A_{0\text{-}0}/A_{0\text{-}1}$	Dielectric constant
Toluene	557	553	-4		0.85	0.84	-0.01	2.38
Chloroform	526	525	-1		1.1	0.98	-0.12	4.81
TCE	527	527	0		1.41	1.44	0.03	4.81
EtOAc	526	521	-5		0.89	1.3	0.41	6.02
THF	530	524	-6		1.09	1.41	0.32	7.58
DCM	525	523	-2		1.4	1.44	0.04	8.93
Acetone	520	519	-1		1.45	1.3	-0.15	20.7
MeOH	519	519	0		1.44	1.43	-0.01	32.7
DMF	526	526	0		1.45	1.45	0	36.7
MeCN	519	519	0		1.46	1.44	-0.02	37.5

Table 1: Comparison of UV-vis data before and after anion exchange from I^- and PF_6^-.

In analysing the data shown in Table 1 there are some broad trends that can be seen in both salts. The aggregation of bis-triazolium PDI **6** typically occurs at low solvent polarities (e.g. toluene). It would be expected that the non-polar solvent would not interact with the charged bis-triazolium PDI and therefore the solvent is not able to disrupt PDI-PDI hydrogen bonding, resulting in PDI aggregation. At higher solvent polarities (e.g. MeCN) the solvent appears to out-compete PDI-PDI and/or PDI-anion interactions, instead favouring solvent-PDI interactions, which therefore prevents the formation of aggregates.

The difference between I^- and PF_6^- salts are typically small in terms of both the $\Delta\lambda$ and $\Delta A_{0\text{-}0}/A_{0\text{-}1}$. This may be because of the low charge density of I^- which means that, like PF_6^-, it is also weakly coordinating. However, there are some exceptions, for example in acetone and chloroform where the bis-triazolium PDI is more aggregated as the PF_6^- salt, perhaps indicative that this anion is more weakly coordinating in these solvents. The opposite effect is seen in THF and EtOAc, suggesting there are additional solvent-specific factors aside from polarity that govern solvent-anion and/or solvent-PDI interactions and so impact PDI-PDI aggregation.

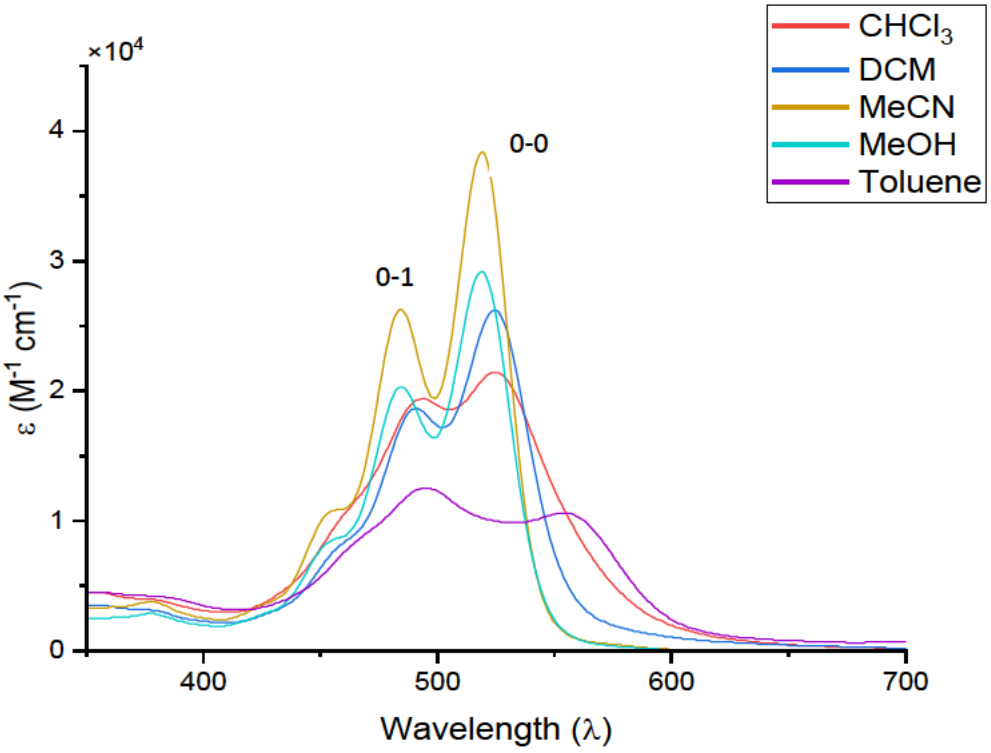

*Figure 226: Select UV-vis data of compound **6.[I⁻]₂**. See appendix for further data.*

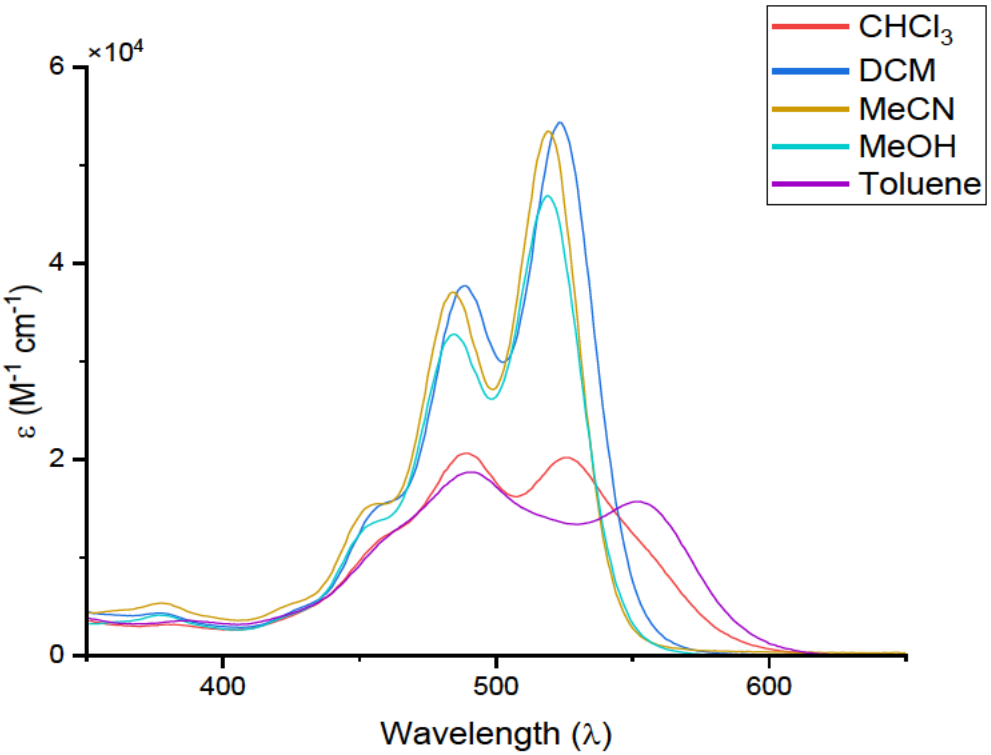

*Figure 237: Select UV-vis data of compound **6.[PF₆⁻]₂**. See appendix for further data.*

3.6 Quantitative Aggregation Study of Bis-Triazolium PDI

A quantitative aggregation study of compound **6.[PF_6^-]$_2$** was conducted by measuring the concentration dependent UV-vis spectra of this compound in chloroform (Figure). This salt was selected due to the weakly coordinating nature of the counter anion, in the hope it would best facilitate PDI-PDI interactions. Chloroform was chosen as the solvent as it can be seen from the solvent dependence study (Figure 237) that chloroform is a good intermediate in terms of how it affects the (dis)aggregation of bis-triazolium PDI **6**. Solvents that were more disruptive to aggregation, e.g., EtOAc or DCM, proved not to be suitable as aggregation could not be observed over a reasonable concentration range. Similarly, in toluene, disaggregation was not achievable even at very low concentrations. From Figure 28 the changes in the $A_{0\text{-}0}/A_{0\text{-}1}$, are indicative of H-type aggregation, i.e., at low concentrations the $A_{0\text{-}0}$ peak is greater than the $A_{0\text{-}1}$, and this ratio inverts as the concentration increases. Further evidence for reversible aggregation comes in the form of the presence of an isosbestic point, the wavelength at which the extinction coefficient remains constant regardless of the concentration, at λ = 544 nm. This indicates the PDI monomer and PDI aggregate are in thermodynamic equilibrium.[58]

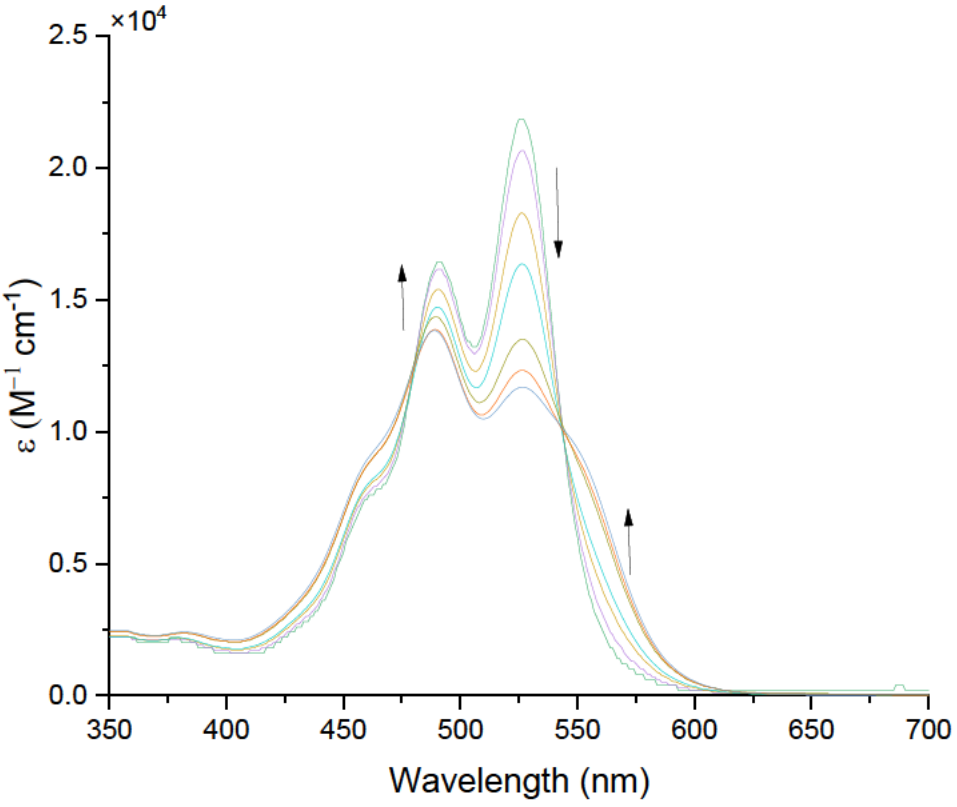

Figure 28: Representative UV-vis data that is used in determining the aggregation constant. Arrows donate the effect of increasing concentration. For full spectra see appendix.

As discussed in Section 1.2, there are two main models that can be considered to study aggregation, either the dimer model or isodesmic model. The third, the cooperative model, could be immediately ruled out as systems that undergo this type of aggregation display a shallower increase in the degree of aggregation in the beginning until a critical concentration is reached, after which the degree of aggregation rises steeply compared to the isodesmic model. The dimerization model, i.e., equation (1), was chosen given the suspected presence of PDI-PDI dimers as seen from a previously reported and related bis-PDI macrocycle,[41] as well as the general trend of core twisted, bis bay-substituted PDIs to form dimers over higher aggregates.[24] It should be noted that it is not possible to determine whether dimerization or isodesmic behaviour is being observed based purely on the fit of the data. Future methods for determining the correct model are discussed in Section 4.

$$\alpha_{agg} = \frac{4K_D C_T + 1 - \sqrt{8K_D C_T + 1}}{4K_D C_T} \qquad (1)$$

To use equation (1), the degree of aggregation α_{agg} can expressed as a function of the $A_{0\text{-}0}/A_{0\text{-}1}$ ratio as per equation (2), in which A_{obs} is the $A_{0\text{-}0}/A_{0\text{-}1}$ ratio at a given concentration and A_{agg} and A_{unagg} are the

$A_{0\text{-}0}/A_{0\text{-}1}$ ratios of the fully aggregation and fully disaggregated species respectively. To determine the aggregation constant, the data in Figure can fitted, by a nonlinear least-squares fitting method, to equation (3). Thereby, by plotting $A_{0\text{-}0}/A_{0\text{-}1}$ vs PDI concentration and then fitting this data to equation (3), the dimerisation constant, K_D, can be determined (Figure).[15,42]

$$\alpha_{agg} = \frac{A_{obs} - A_{agg}}{A_{unagg} - A_{agg}} \quad (2)$$

$$A_{obs} = \frac{4K_D C_T + 1 - \sqrt{8K_D C_T + 1}}{4K_D C_T}\left(A_{unagg} - A_{agg}\right) + A_{agg} \quad (3)$$

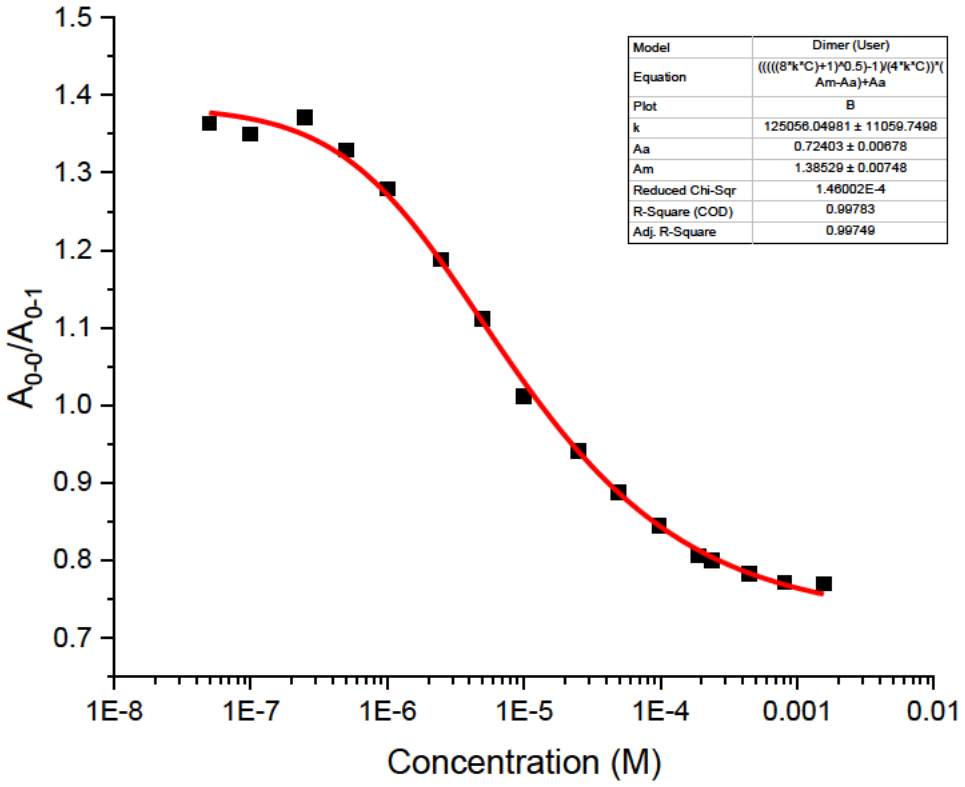

*Figure 29: Plot of the $A_{0\text{-}0}/A_{0\text{-}1}$ ratio vs concentration for compound **6.[PF$_6^-$]$_2$**. Red line is fitted according to the monomer-dimer model. C = concentration, Aa = $A_{0\text{-}0}/A_{0\text{-}1}$ of the fully aggregated species and Am = $A_{0\text{-}0}/A_{0\text{-}1}$ of the monomer, and K = dimerisation constant.*

The plot of $A_{0\text{-}0}/A_{0\text{-}1}$ vs concentration shown in Figure30 shows a clear sigmoidal trend and nonlinear fitting of this data gave a dimerisation constant of K_D = 1.25 ±0.11 x 10^5 M^{-1} (shows the full isotherm). Using K_d, the free energy of dimerisation can be calculated from equation (4), ΔG = -29.1 kJ mol^{-1}.

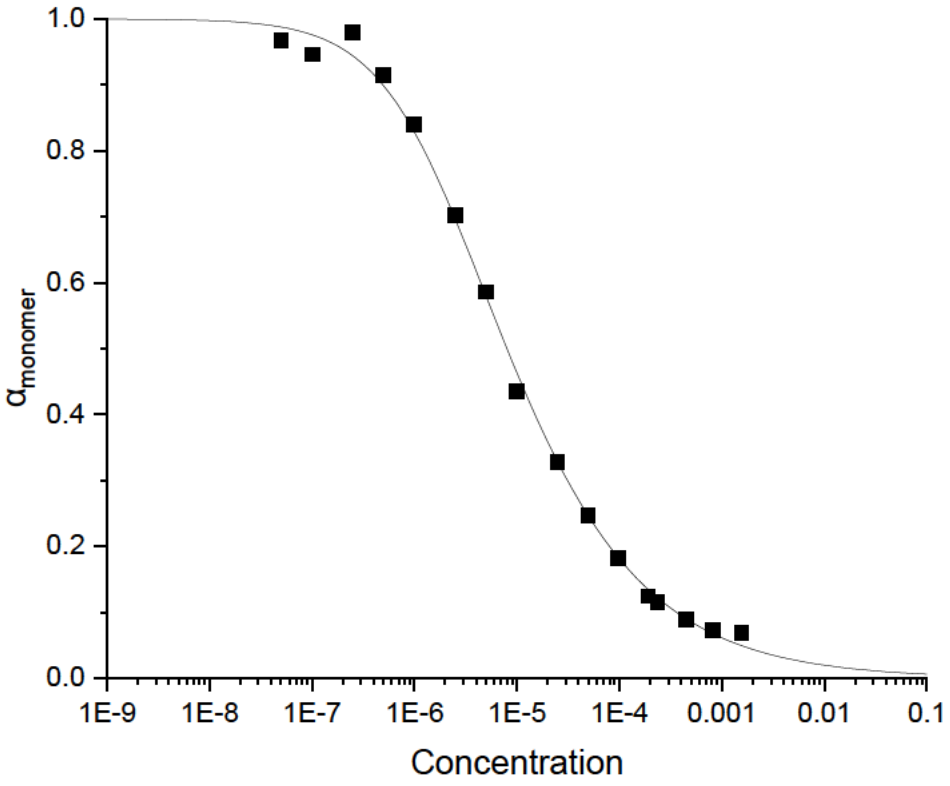

Figure 30: Plot of the fraction of monomer of compound ***6.[PF_6^-]$_2$*** *vs concentration. Black line is the simulated binding curve defined by the K and min/max $A_{0\text{-}0}/A_{0\text{-}1}$ values from the fit in Figure.*

$$\Delta G = -RTlnKd \qquad (4)$$

The dimerisation constant of **6.[PF_6^-]$_2$** is similar to in size to the aggregation constant of the core unsubstituted bis-imidazolium PDIs discussed in Section 1.5 (Figure 13)[42] as well as a range of planar PDIs synthesised by Würthner and co-workers.[19,20] In the case of the bis-imidazolium PDI (Figure 13), the aggregation is supported through hydrogen bonds to the coordinating iodide anion and π-π stacking between the planar PDI cores. However, in the case of the bis-triazolium **6.[PF_6^-]$_2$** the counter ion, PF_6^-, is weakly coordinating and therefore is expected to have little effect on the aggregation properties. Furthermore, the core-twist of this bis-triazolium PDI may represent a significant hinderance to π-π stacking. Therefore, it is expected that there is a significant contribution from

intermolecular hydrogen bonding between triazolium C-H and PDI carbonyl groups to drive dimerisation (Figure 18). The anion may also be playing a role, like the bis-imidazolium in Figure 13, where alternating cation-anion-cation stacking is seen which helps to shield some of the repulsion that would be expected from two dicationic molecules coming together.

The core-twist angle of PDIs that aggregate via π-π stacking has previously been correlated with the aggregation constant by Würthner and co-workers (Section 1.3).[15] The core-twist angle of a bis-triazole PDI is reported to be 21°,[41] meaning that one would expect the aggregation constant of bis-triazolium **6.[PF_6^-]$_2$** to be at least two orders of magnitude lower than that reported here in chloroform. This further reinforces the significant role that hydrogen bonding may be playing in facilitating bis-triazolium PDI aggregation.

4. Conclusions and Future Work.

To conclude, the novel target bis-triazolium PDI compound **6** has been successfully synthesised and characterised as its iodide and hexafluorophosphate salts, including by ^{1}H, ^{13}C and other 2D NMR spectroscopy experiments and mass spectrometry. Which has translated the insight gained in the pink box macrocycle, i.e. PDI dimerization via hydrogen bonding, into a PDI monomer, with the additional benefit of introducing a charge that should strengthen the hydrogen bonding and anion recognition. This has enabled the first aggregation studies of a bis-triazolium PDI, performed here using UV-vis spectroscopy. To quantify the strength of aggregation of **6.[PF_6^-]$_2$**, UV-vis datasets collected at different concentrations were fitted to the dimer model, giving a K_d = 1.25 ± 0.11 x 10^5 M^{-1} (ΔG = -29.1 kJ mol^{-1}). Therefore, aggregation is similar in strength to that of planar bis-imidazolium PDIs with an iodide counter anion, which has contributions from π-π stacking and hydrogen bonding with the halide anion. By contrast the aggregation of the bis-triazolium PDI reported here is likely to have a smaller contribution from π-π stacking due to the PDI core-twist, while a more weakly-coordinating PF_6^- counter ion is unlikely to disrupt intermolecular hydrogen bonding between PDI units in the dimer. Therefore, intermolecular hydrogen bonding interactions can be used to drive the aggregation of bay-functionalised PDIs such as **6.[PF_6^-]$_2$,** which may have been expected to have weak aggregation constants due to their twisted aromatic framework.[24] Additionally, the potential for the PDI to act as an anion sensor has been shown as a colour change was observed during the anion exchange, with a solution of **6.[I^-]$_2$** going from a dark red to a brighter red when the iodide counterion was exchanged for hexafluorophosphate. Which is the first example of bis-triazolium anion recognition being coupled with a PDI chromophore.

Future work should focus on determining the size of the aggregates formed by bis-triazolium PDI **6**, to confirm dimerisation. Here, single crystal x-ray diffraction crystallography would offer significant insight as well as sheading further light on the nature of the non-covalent interactions formed between the PDIs (e.g., intermolecular hydrogen bonding). As well as giving insight into the nature of PDI-anion interactions which may help to design motifs needed to give a degree of selectivity to bind specific anions and shed light on the role the anion plays in facilitating the aggregation of two dicationic molecules, as some repulsion may be expected due to the charges. One may also consider the use of DOSY (diffusion ordered spectroscopy) NMR spectroscopy to assess the size of the PDI aggregate.[59] Finally, while the changes in absorption spectra between iodide and hexafluorophosphate salts were modest (Table 1), UV-vis and fluorescence spectroscopy should be employed to probe how bis-triazolium PDI aggregation is impacted in the presence of more

coordinating and biologically or environmentally relevant anions (e.g., oxoanions), thereby establishing a successful mechanism for optical anion sensing using assemblies of aggregated PDIs. To do this it may be necessary to give the PDI a degree of water solubility as this may be crucial in detecting said more biologically or environmentally relevant anions. One method to do this may be the introduction of dendrimers which has already been applied to other PDI systems.[62]

5. Experimental.

5.1 Reagents and Solvents.

All reagents and solvents were purchased from commercial suppliers and used without further purification unless otherwise stated. $PdCl_2(PPh_3)_2$, CuI, and $Cu(MeCN)_4PF_6$ were stored in a vacuum desiccator. TBTA was prepared according to the literature procedure[56] and stored in a vacuum desiccator. Grubbs catalyst, 2nd Generation, and prepared organic azides were stored in a fridge prior to use. Water was distilled and microfiltered using an ELGA DV 35 Purelab water purification system. Chromatography was undertaken using silica gel (particle size: 40-63 μm) or preparative TLC plates (20 × 20 cm, 1 cm silica thickness).

5.2 Instrumentation.

^1H and ^{13}C NMR spectra were recorded using Bruker AVIII400 (400 MHz) or Bruker AV NEO 400 (400 MHz). Mass spectra were recorded using a Bruker UltrafleXtreme MALDI-TOF mass spectrometer or a Waters Synapt G2-S mass spectrometer. MALDI-TOF MS was conducted using trans-2-[3-(4-tert-Butylphenyl)-2-methyl-2-propenylidene]malononitrile (DCTB) as a matrix.

UV-vis spectra were recorded on a Cary 50 or Shimadzu UV3600i. All data was recorded at ambient temperature unless otherwise stated. Temperature dependence studies were performed using a Shimadzu UV3600i. All UV-Vis studies were conducted with a 3 mL cuvette with a 1 cm pathlength.

5.3 Synthetic Methods.

Synthesis of C_5 PDI 1.

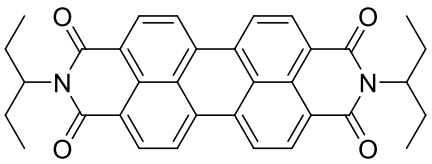

1

PDA (10.0 g, 25.5 mmol), 3-amino pentane (4.44 g, 5.94 mL, 50.9 mmol, 2 equivalents), and $Zn(OAc)_2{\cdot}2H_2O$ (11.2 g, 51.0 mmol, 2 equivalents. was dissolved in molten imidazole (90.0 g). The reaction mixture was stirred at 140 °C for 22 hours. While still warm 1 M HCl (100 mL) was added and left to stir while the mixture cooled to room temperature. The crude reaction mixture was filtered and washed with distilled water until the filtrate was clear. A red solid was collected and oven dried (at 75 °C) for 16 hours. The crude product was passed through a plug of silica using DCM as the eluant. The solvent was removed under reduced pressure to afford the final product as a red solid (8.10 g, 15.3 mmol, 60%).

^{1}H NMR (400 MHz, Chloroform-*d*) δ 8.64 (d, *J* = 8.0 Hz, 4H), 8.57 (d, *J* = 8.0 Hz, 4H), 5.07 (m, 2H), 2.34 – 2.19 (m, 4H), 2.01 – 1.89 (m, 4H), 0.93 (t, 12H).

Spectral data was consistent with previous findings.[60]

Synthesis of C_5 Dibromo PDI 2.

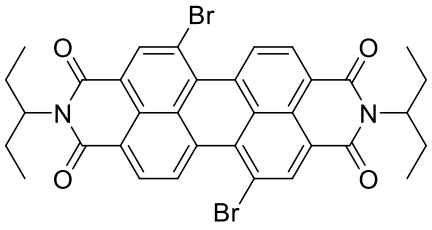

2

PDI **1** (2.00 g, 3.77 mmol) was dissolved in $CHCl_3$ (30 mL) to which Br_2 (12 mL, 37.4 g, 235 mmol, 62.5 equivalents) was added. The reaction was heated to 50 °C and stirred for 10 days. The reaction mixture was cooled to room temperature and the excess Br_2 was removed by bubbling N_2 through the solution. The reaction mixture dissolved in DCM (30 mL) which was washed with a saturated aqueous $Na_2S_2O_3$ solution until the $Na_2S_2O_3$ remained clear, followed by washing with distilled H_2O (2 x 100 mL). The organic layer was dried over $MgSO_4$ and filtered to afford the product as a red powder (2.59 g,

quantitative). The resulting product is a 4:1 mixture of the 1,7 and 1,6 isomer. The desired 1,7 was obtained by recrystallisation from DCM/MeOH 1:2 after 3 recrystallisations (1.40 g, 2 mmol, 54%).

^{1}H NMR (400 MHz, Chloroform-*d*) δ 9.54 – 9.47 (m, 2H), 8.92 (s, 2H), 8.73 – 8.66 (m, 2H), 5.05 (m, 2H), 2.33 – 2.17 (m, 4H), 2.01 – 1.86 (m, 4H), 0.97 – 0.87 (m, 12H).

Spectral data was consistent with previous findings.[18]

Synthesis of C_5 Bis-trimethylsilyl Acetylene PDI 3.

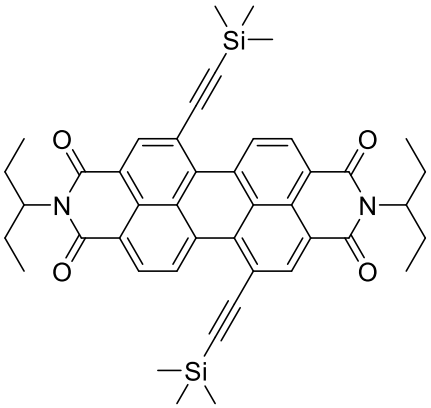

3

PDI **2** (500 mg, 0.73 mmol) was dissolved in toluene (50 mL) and Et_3N (50 mL) before being degassed, by sparging with N_2, for 10 minutes. $PdCl_2(PPh_3)_2$ (25.5 mg, 0.036 mmol, 5 mol%) and CuI (13.8 mg, 0.073 mmol, 10 mol%) was added to the mixture, followed by degassing for a further 10 minutes. TMS acetylene (357 mg, 0.5 mL, 3.63 mmol, 5 equivalents) was added to the mixture which was then heated at 60 °C for 19 hours. The reaction mixture was cooled to room temperature and the solvent was removed under reduced pressure. The crude solid was dissolved in DCM (40 mL) and the crude product was filtered over celite to afford the final product as a dark red/maroon powder (525 mg, 0.73 mmol, quantitative).

^{1}H NMR (400 MHz, Chloroform-*d*) δ 10.22 (d, *J* = 8.3 Hz, 2H), 8.82 (s, 2H), 8.65 (d, *J* = 8.3 Hz, 2H), 5.13 – 5.01 (m, 2H), 2.36 – 2.20 (m, 4H), 2.01 – 1.86 (m, 4H), 0.92 (t, *J* = 7.4 Hz, 12H), 0.39 (s, 18H).

Spectral data was consistent with previous findings.[41]

Synthesis of Octyl Azide 4.

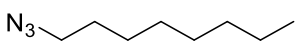

5

1-bromooctane (2.00 g, 1.68 mL, 10.4 mmol) was combined with NaN_3 (2.69 g, 41.4 mmol, 4 equivalents) in DMF (120 mL). The reaction mixture was heated at 75 °C for 3 days. The reaction mixture was cooled to room temperature and added to distilled H_2O (100 mL) and extracted with Et_2O (3 x 50 mL). The organic layer was washed with distilled H_2O (5 x 30 mL) and dried over $MgSO_4$ to afford a pale-yellow oil (0.89 g, 5.73 mmol, 55%)

^{1}H NMR (400 MHz, Chloroform-*d*) δ 3.25 (t, *J* = 7.0 Hz, 2H), 1.60 (p, *J* = 7.0 Hz, 2H), 1.40 – 1.23 (m, 10H), 0.92 – 0.84 (m, 3H).

Spectral data was consistent with the literature.[61]

Synthesis of Bis(octyl-triazole) PDI 5.

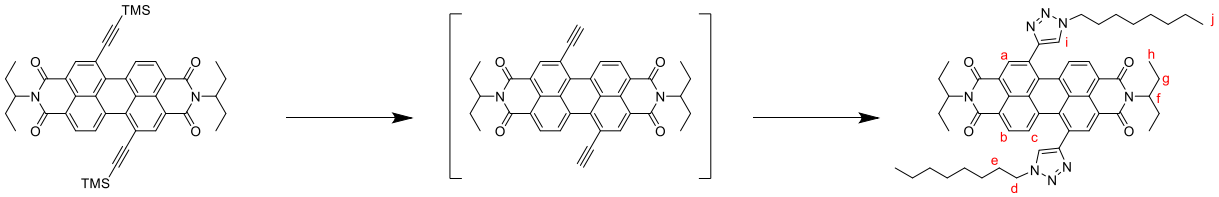

PDI **3** (420 mg, 0.581 mmol) was combined with K_2CO_3 (290 mg, 2.1 mmol, 3.61 equivalents) in $CHCl_3$ (70 mL) and MeOH (70 mL) and left to stir for 1 hour. The reaction mixture was added to distilled H_2O (100 mL) and extracted with $CHCl_3$ (3 x 50 mL) before being washed with 1 M HCl (100 mL) and washed with distilled H_2O (100 mL). The organic layer was dried over $MgSO_4$. The solvent was removed under reduced pressure. The product was carried through to the next step without further purification. Deprotected bis(alkyne) PDI (336 mg, 0.581 mmol) was dissolved in $CHCl_3$ (70 mL) and degassed. TBTA (86.7 mg, 0.23 mmol, 0.4 equivalents) and octyl azide **4** (451 mg, 2.91 mmol, 5 equivalents), and $Cu(MeCN)_4PF_6$ (86.7 mg, 0.0232 mmol, 0.4 equivalents) was added and the solution was degassed. The reaction mixture was stirred at rt for 17 hours. The solvent was removed under reduced pressure. The crude product was purified by silica gel flash column chromatography ($CHCl_3$ w/ 1% methanol) to give a purple solid (334 mg 0.375 mmol, 65%). A second column ($CHCl_3$ w/ 1.5% acetone) was performed to remove any remaining 1,6 isomer on 85 mg of a 1,6/1,7 mixture to yield 43 mg of pure 1,7 PDI.

^{1}H NMR (400 MHz, Chloroform-d) δ 8.68 (s, 2H_a), 8.23 (d, J = 8.1 Hz, 2H_b), 7.93 (d, J = 8.1 Hz, 2H_c), 7.75 (s, 2H_i), 5.03 (tt, 2H_f), 4.48 (t, J = 7.2 Hz, 4H_d), 2.23 (m, 4H_g), 2.00 (t, J = 7.2 Hz, 4H_e), 1.95 – 1.83 (m, 4H_g), 1.45 – 1.21 (m, 22H), 0.88 (m, 18$H_{h\,\&\,j}$).

^{13}C NMR (101 MHz, Chloroform-d) δ 164.0, 147.8, 135.1, 134.6, 133.4, 129.9, 129.1, 129.1, 129.1, 128.4, 122.7, 121.6, 57.6, 50.8, 31.7, 30.4, 29.7, 29.1, 28.9, 26.5, 25.0, 22.6, 14.1, 11.3.

MALDI-TOF MS m/z calculated [M-H] 887.50, found 887.58.

Bis(triazolium) PDI 2[I^-], 6.[I^-]$_2$.

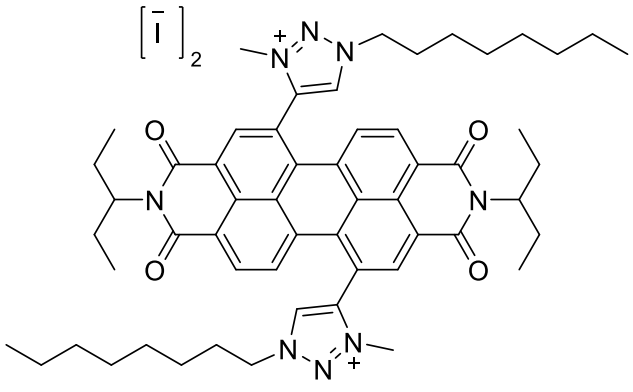

6

PDI **6** (86.5 mg, 0.097 mmol) was dissolved in neat MeI (7 mL) in an oven-dried pressure tube (rated to 10 bar). The reaction was heated at 80 °C for three days until the reaction was driven to completion as monitored by TLC (5 % MeOH in $CHCl_3$). The reaction mixture was cooled to room temperature and the MeI was removed under reduced pressure. The crude reaction was purified by preparative TLC (2 % MeOH in $CHCl_3$) over three runs to obtain a dark red solid (89.8 mg, 0.076 mmol, 79%).

^{1}H NMR (300 MHz, Acetonitrile-d_3) δ 9.05 (s, 2H), 8.63 (s, 2H), 8.55 (d, *J* = 8.1 Hz 2H), 7.80 (d, *J* = 8.1 Hz, 2H), 4.99 (m, 2H), 4.78 (s, 4H), 3.74 (s, 8H), 2.31 – 2.18 (m, 2H), 1.89 (m, 3H), 1.40 (m, 24H), 1.00 – 0.82 (m, 18H).

^{13}C NMR (101 MHz, Acetonitrile-d_3) δ 164.3, 143.5, 135.7, 133.4, 131.9, 130.6, 128.90, 124.8, 120.7, 59.0, 56.1, 55.3, 46.8, 39.7, 32.5, 29.8, 29.6, 29.5, 26.8, 25.7, 23.4, 14.4, 11.7, 8.9.

HRMS (ESI) positive mode m/z calculated for $C_{56}H_{70}N_8O_4^{2+}$ [M-2I^-]$^{2+}$ 459.2760, found 459.2746.

HRMS (ESI) negative mode m/z calculated [I^-] 126.9045, found 126.9042.

Bis(triazolium) PDI 2[PF_6^-], 6.[PF_6^-]$_2$.

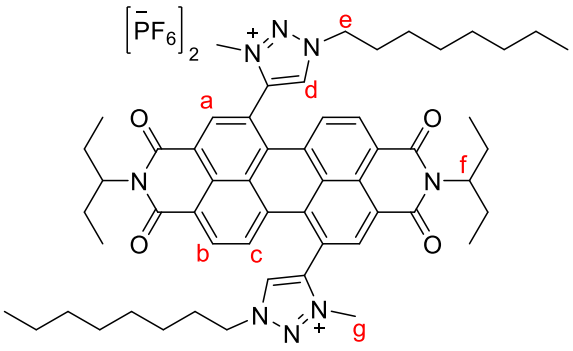

7

PDI **7** (39.9 mg, 34 µmol) was dissolved in $CHCl_3$ (5 mL). To this, a 0.1 M solution of NH_4PF_6 (5 mL) was added and the solution was stirred vigorously for 5 minutes. The organic layer was removed and added to another 0.1 M solution of NH_4PF_6 (5 mL). This process was repeated for a total of six washes. The organic layer was then removed and washed with distilled H_2O (2 x 5 mL) and dried over $MgSO_4$ to give a bright red solid (40.0 mg, 33.1 µmol, 97%)

^{1}H NMR (300 MHz, Acetonitrile-d_3) δ 8.83 (s, 2H$_d$), 8.64 (s, 2H$_a$), 8.48 (d, J = 8.0 Hz, 2H$_b$), 7.73 (d, J = 8.0 Hz, 2H$_c$), 5.00 (m, 2H$_f$), 4.74 (t, J = 7.1 Hz, 4H$_e$), 3.72 (s, 6H$_g$), 2.30 – 2.17 (m, 4H), 1.92 – 1.82 (m, 4H)*, 1.58 – 1.29 (m, 24H), 0.89 (t, J = 7.5 Hz, 18H).

^{13}C NMR (101 MHz, Acetonitrile-d_3) δ 164.4, 143.9, 135.8, 133.7, 133.2, 131.5, 130.8, 129.9, 129.1, 125.2, 120.8, 58.9, 55.7, 39.1, 32.5, 30.4, 29.8, 29.6, 26.8, 25.8, 23.4, 14.4, 11.6.

^{19}F NMR (377 MHz, Acetonitrile-d_3) δ -72.97 (d, J = 706.8 Hz).

HRMS (ESI) positive mode m/z calculated for $C_{56}H_{70}N_8O_4^{2+}$ [M-2PF_6^-]$^{2+}$ 459.2760, found 459.2751.

HRMS (ESI) negative mode m/z calculated [PF_6^-] 144.9642, found 144.9642

*Signal should read as 4 protons, but peak is obstructed by solvent and therefore cannot be accurately integrated.

6. Appendix.

6.1 Photophysical data.

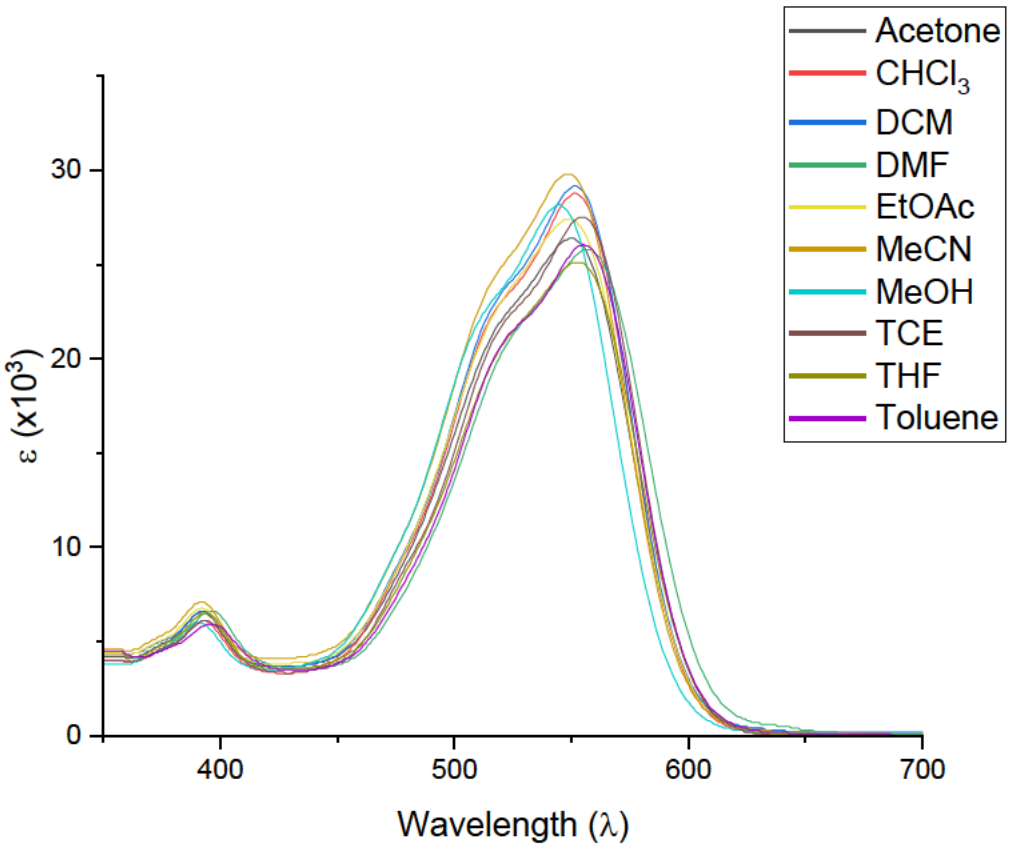

*Figure 241: Full UV-vis spectra of compound **5** at 1x10^{-5} M.*

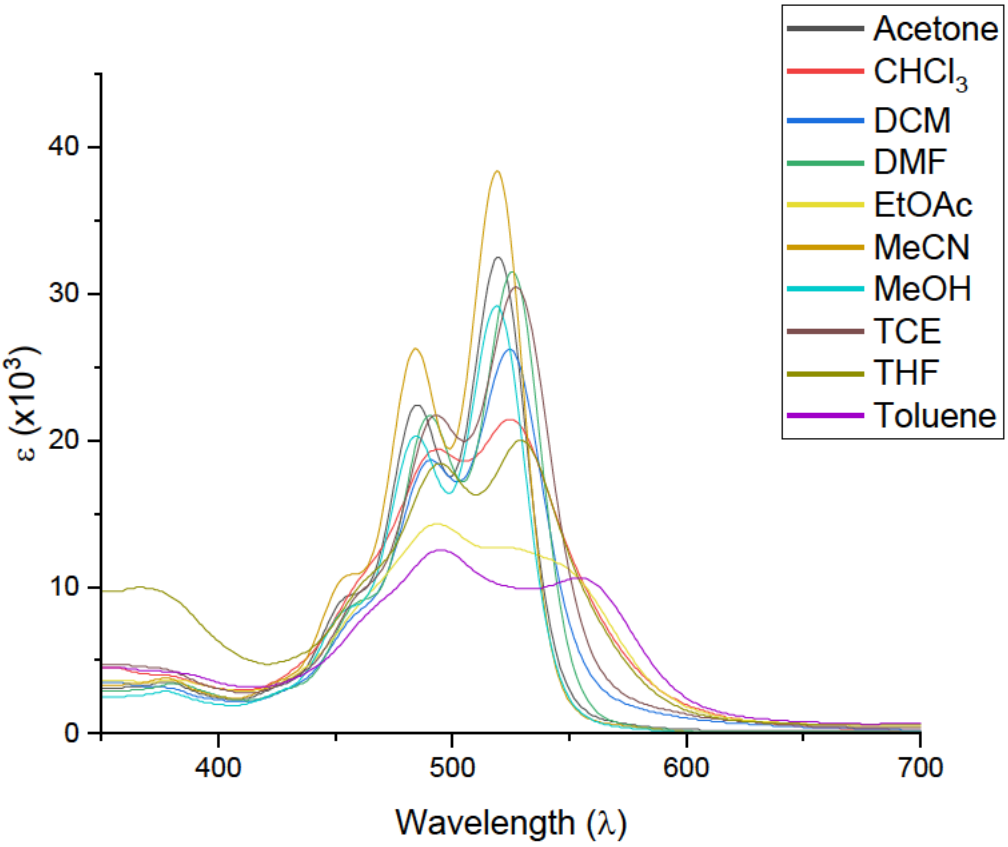

*Figure 252: Full UV-vis spectra of compound **6.[I⁻]₂** at 1x10⁻⁵ M.*

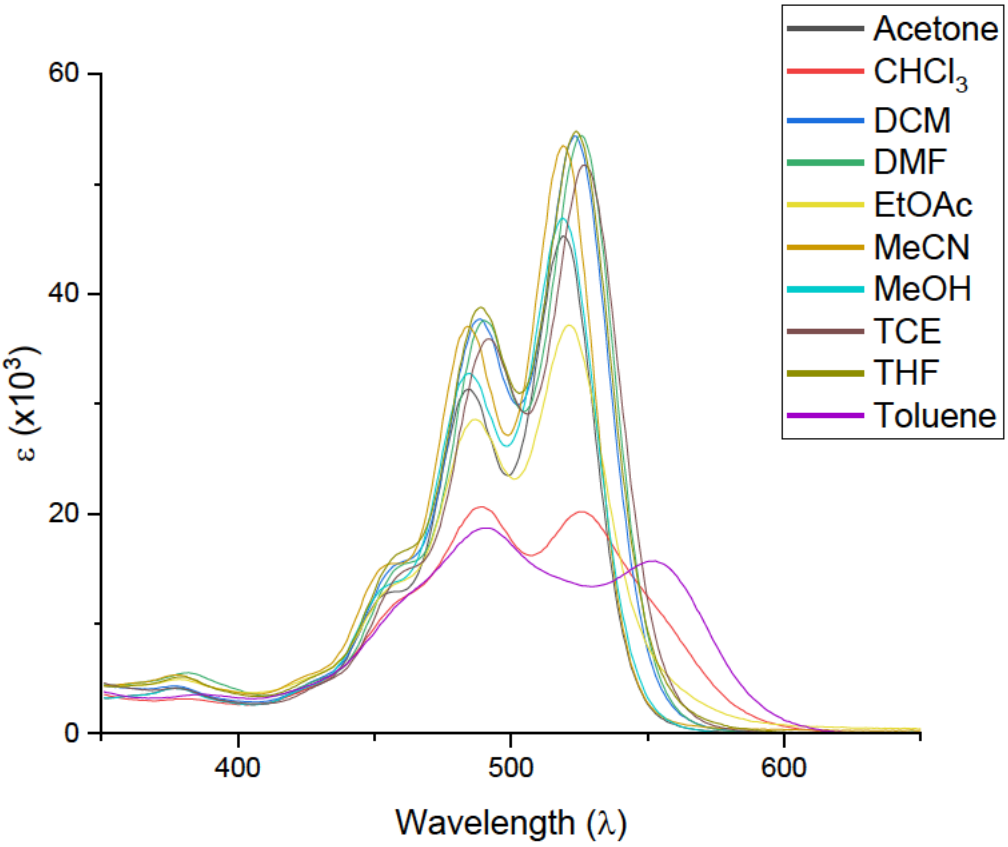

Figure 26: UV-vis spectra of compound ***6.[PF$_6^-$]$_2$*** *at 1x10^{-5} M.*

6.2 Aggregation study full spectrum.

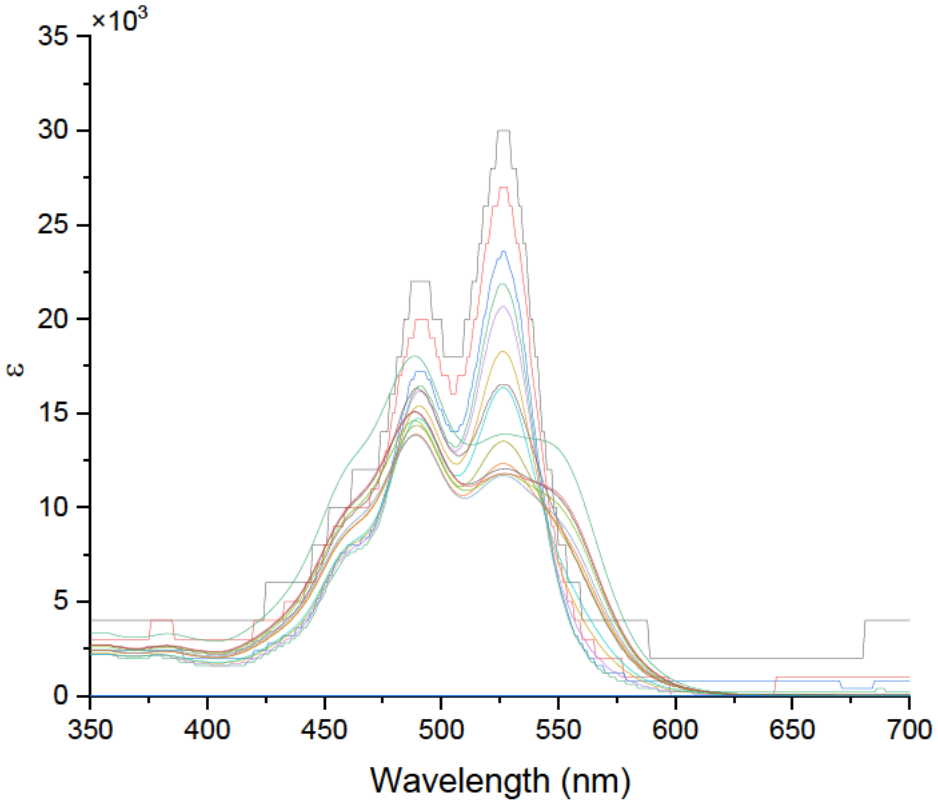

Figure 274: All UV-vis spectra between $5x10^{-8}$ and $1.5x0^{-3}$. From this the $A_{0\text{-}0}/A_{0\text{-}1}$ values were calculated for use in Figure. The $A_{0\text{-}0}/A_{0\text{-}1}$ ratio was used to define aggregation as it was thought that this was a more robust definition of aggregation state and would help minimise any error from some of the poorer data sets.

6.3 Additional NMR spectroscopy and mass spectrometry data.

Bis(C_5) PDI 1.

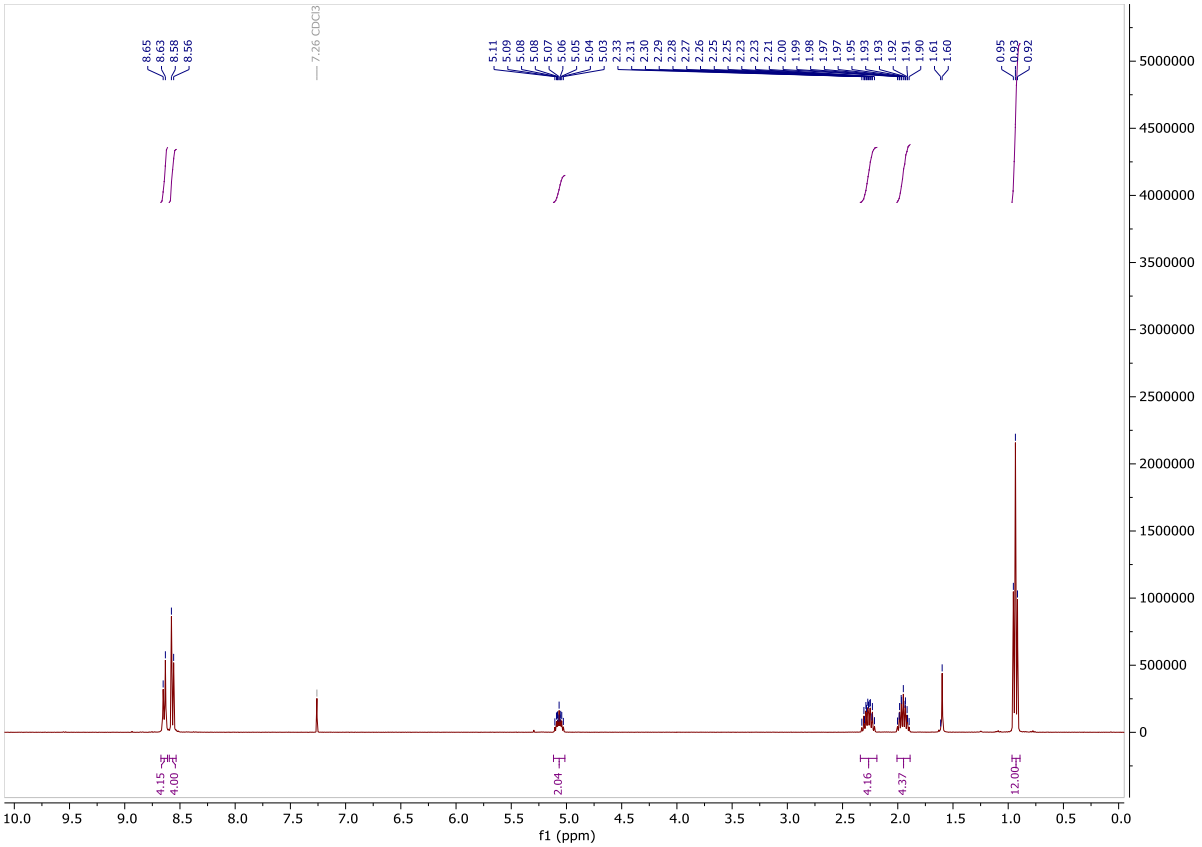

Figure 285: ^{1}H NMR spectrum of 1 in chloroform-d, 298 K, 400 MHz.

C_5 dibromo PDI 2.

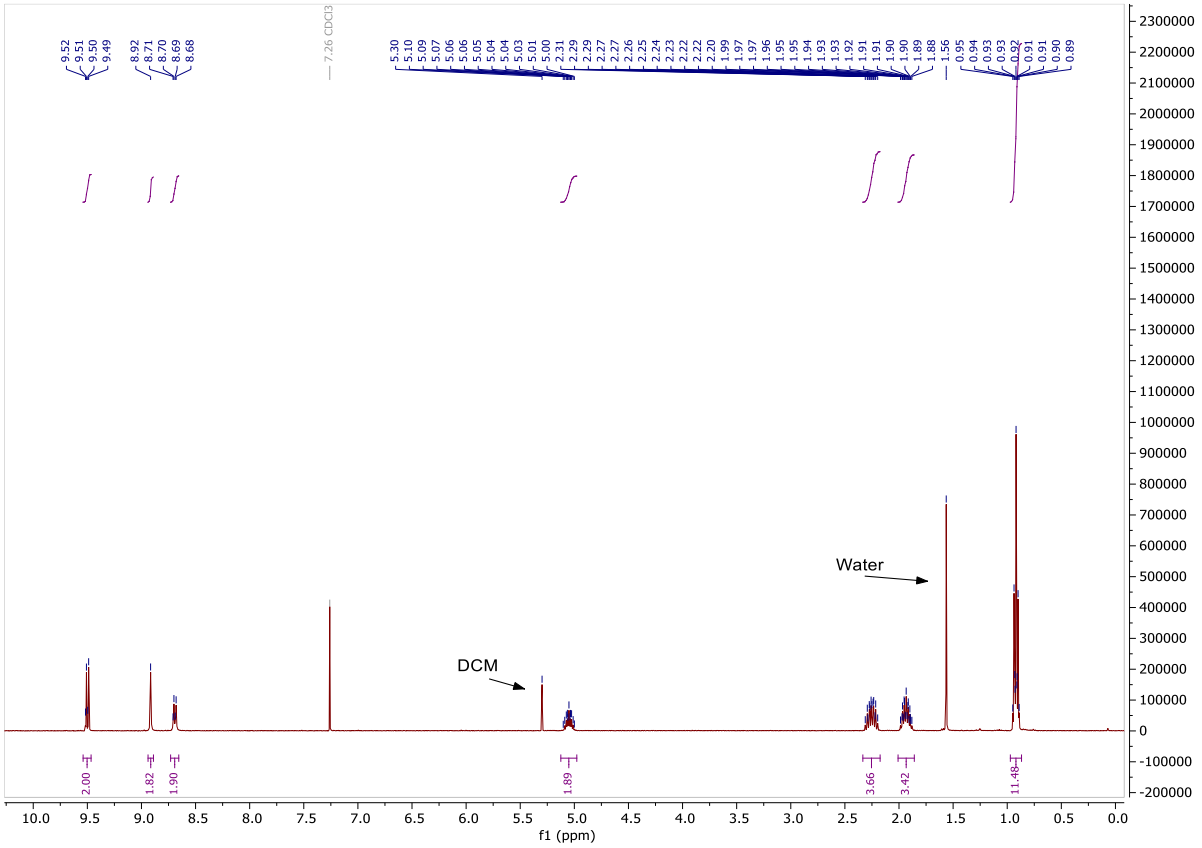

*Figure 296: ^{1}H NMR spectrum of **2** in chloroform-d, 298 K, 400 MHz.*

C_5 bis-trimethylsilyl acetylene PDI 3.

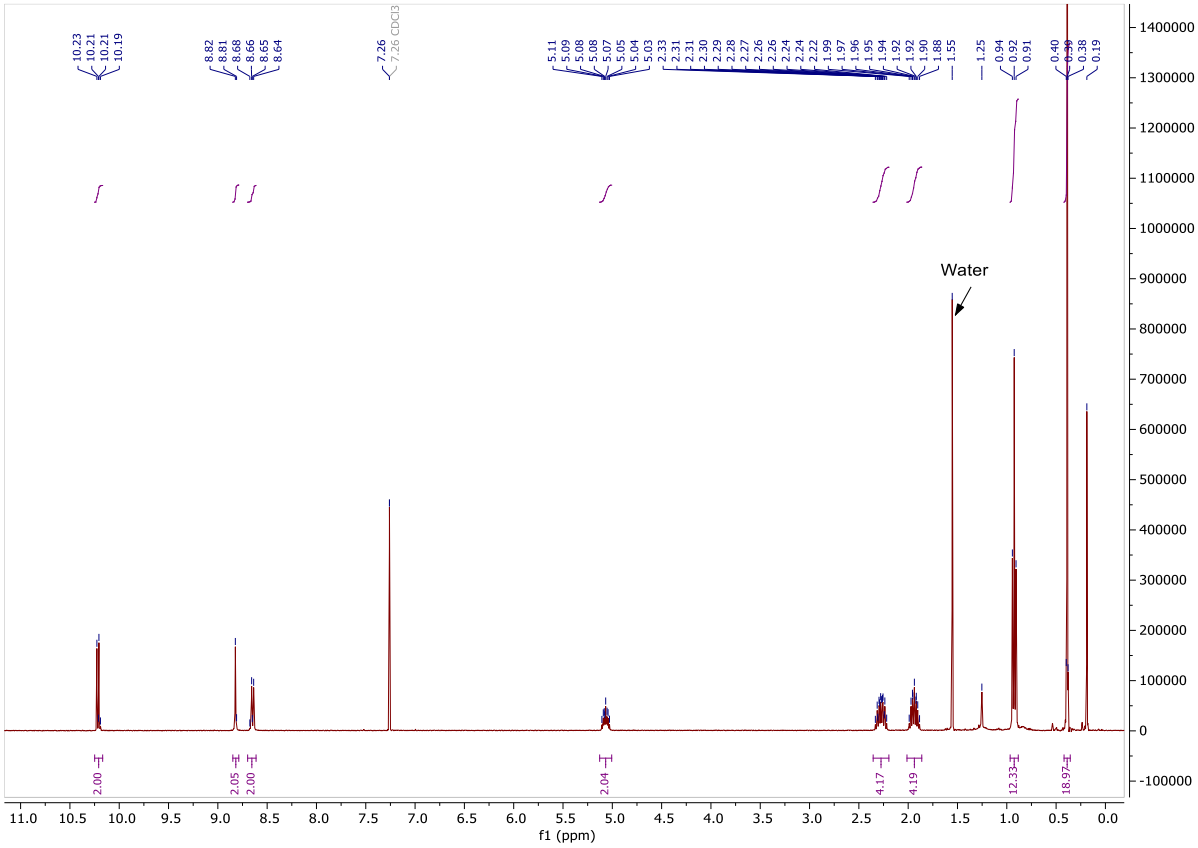

*Figure 307: ^{1}H NMR spectrum of **3** in chloroform-d, 298 K, 400 MHz.*

Octyl azide 4.

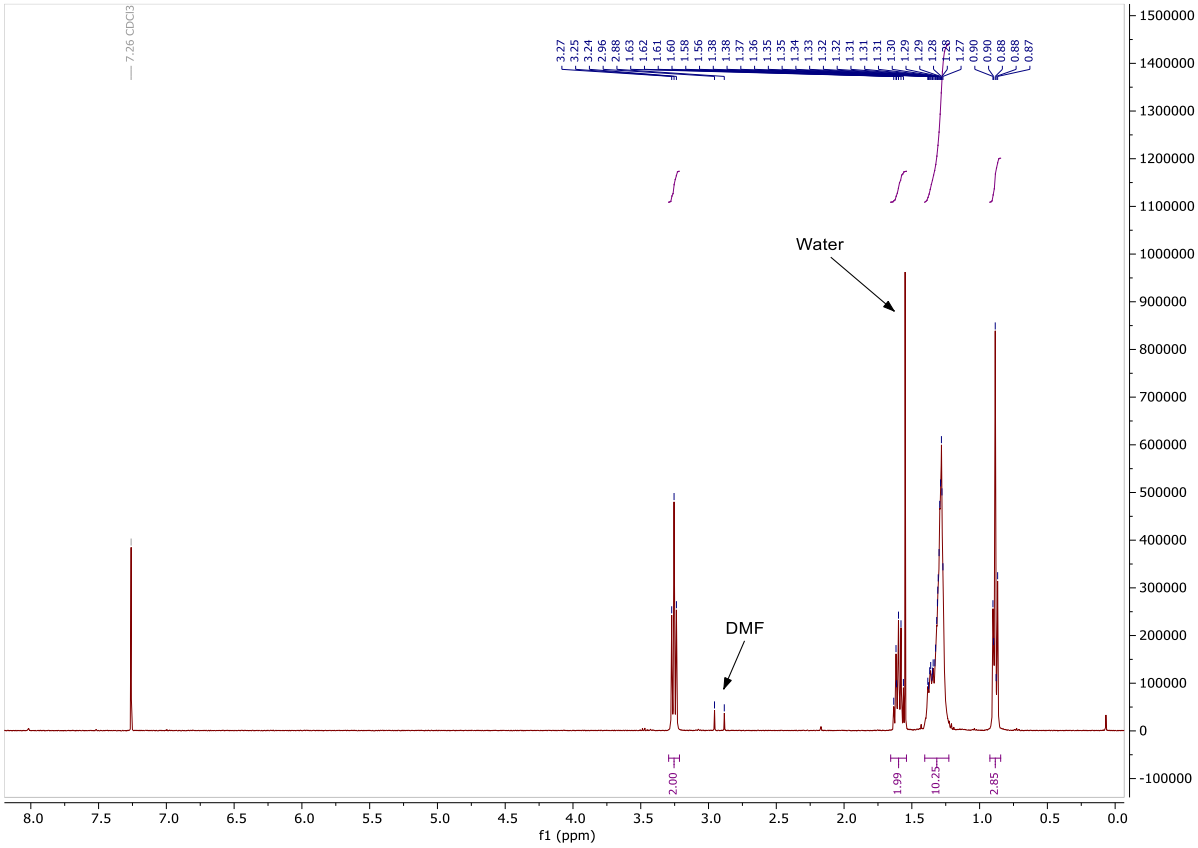

*Figure 3831: [1]H NMR spectrum of **5** in chloroform-d, 298 K, 400 MHz.*

Bis-(octyl-triazole) PDI 5.

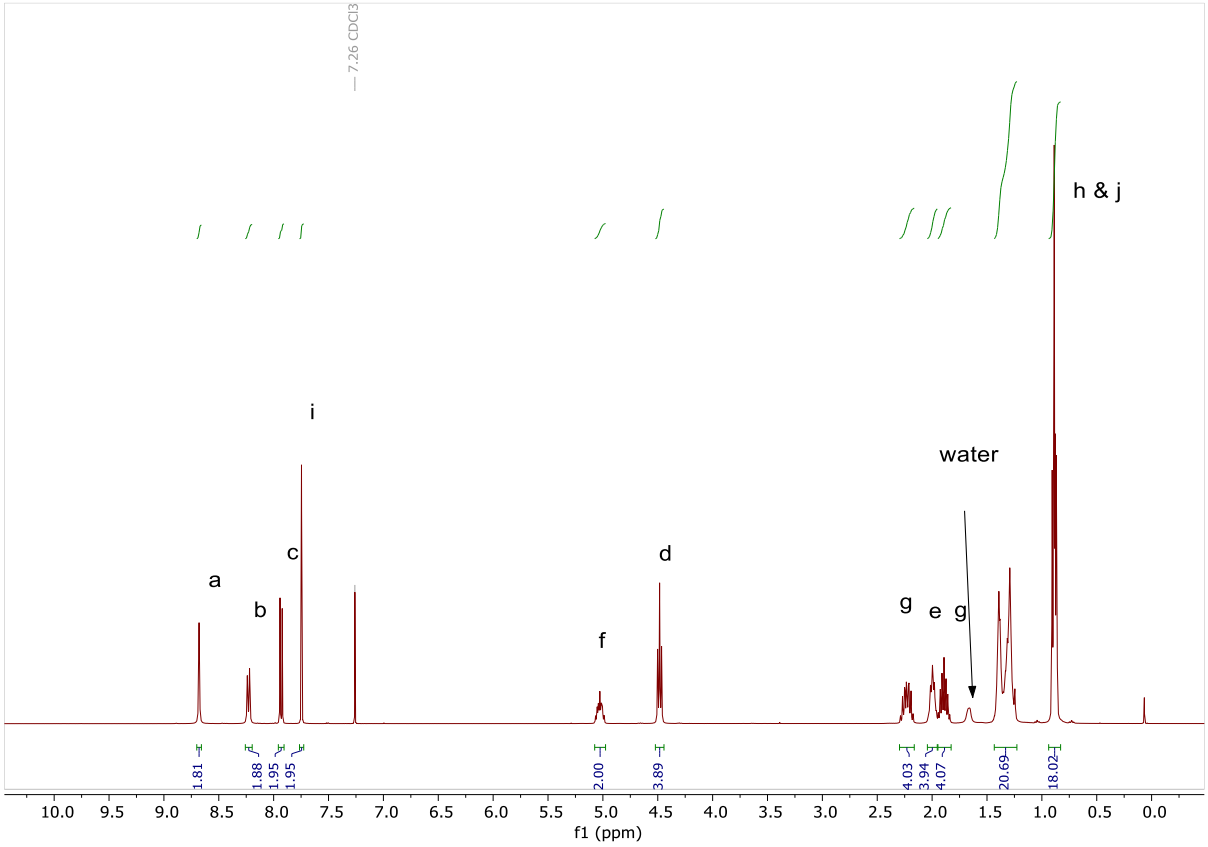

*Figure 39: ^{1}H NMR spectrum of **5** in chloroform-d, 298 K, 400 MHz.*

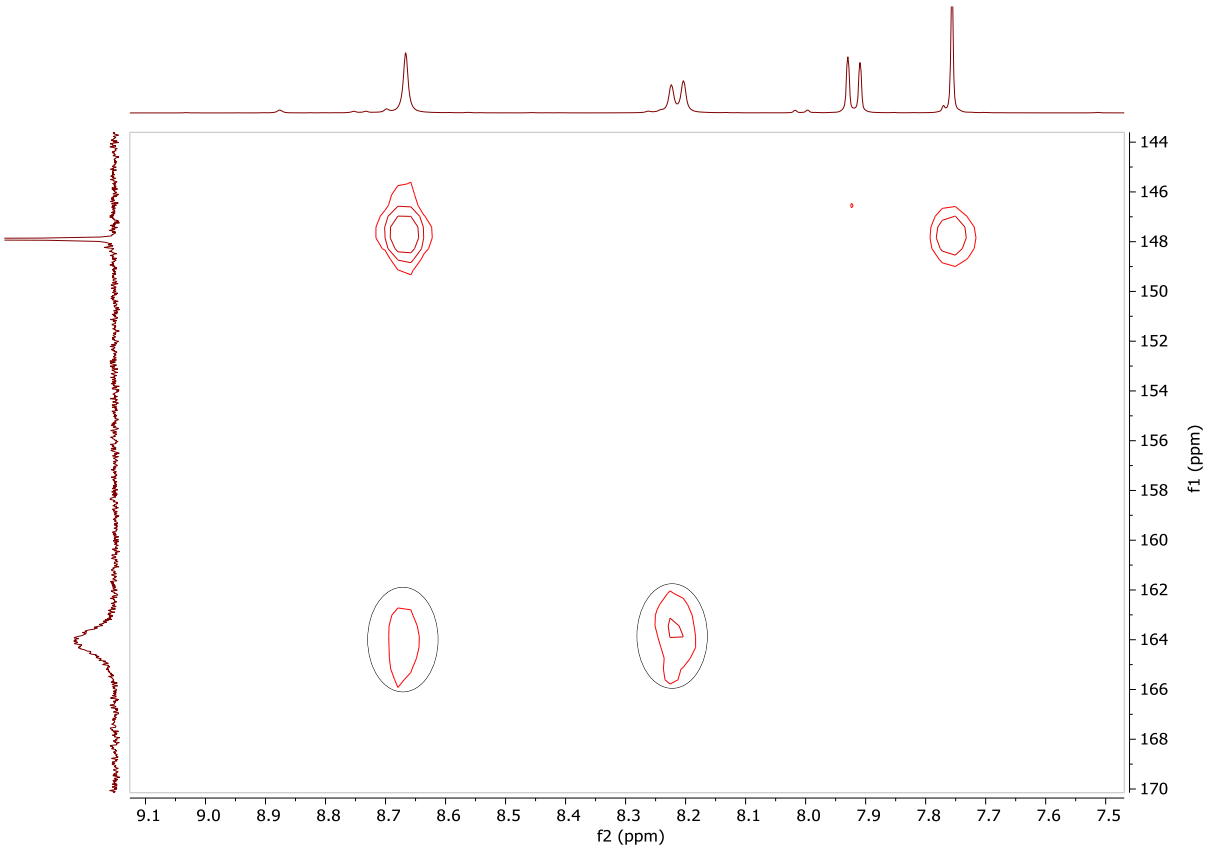

*Figure 320: HMBC NMR spectrum of **5** in chloroform-d, 298 K, 400 MHz.*

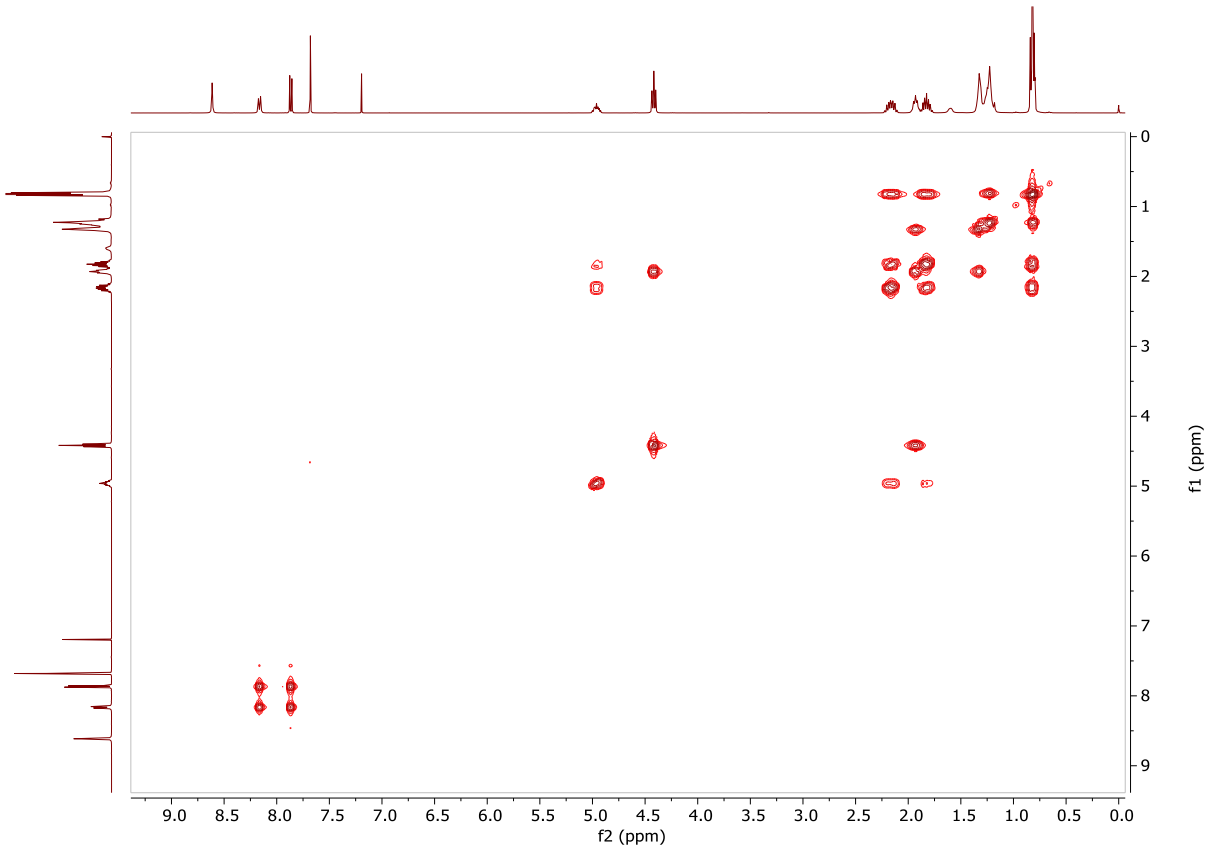

*Figure 41: COSY NMR spectrum of **5** in chloroform-d, 298 K, 400 MHz.*

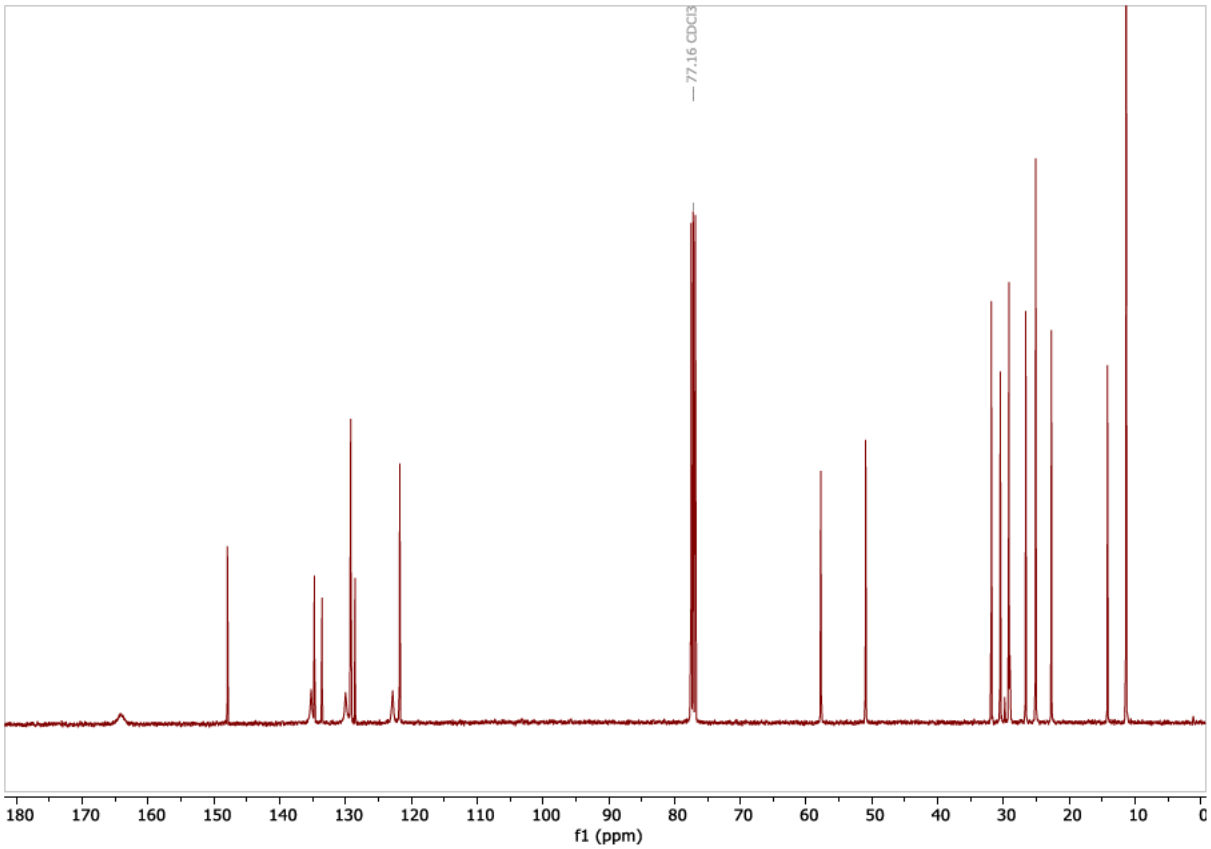

*Figure 332: ^{13}C NMR spectrum of **5** in chloroform-d, 298 K, 101 MHz.*

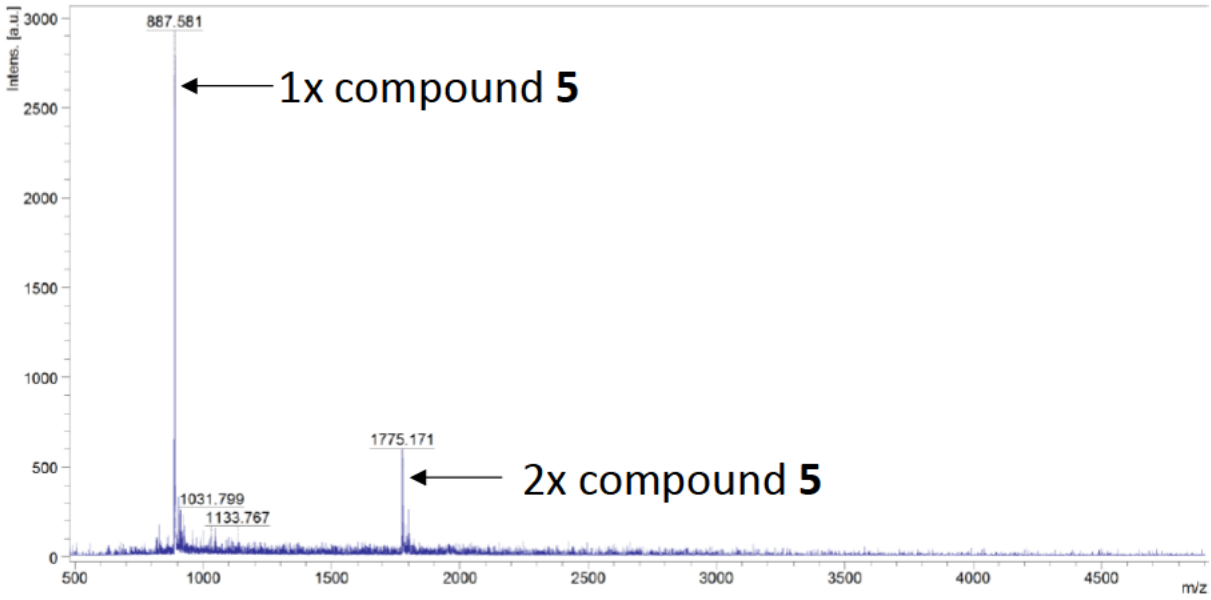

*Figure 343: MALDI-TOF MS of **5**.*

Bis(triazolium) PDI 6.$[I^-]_2$.

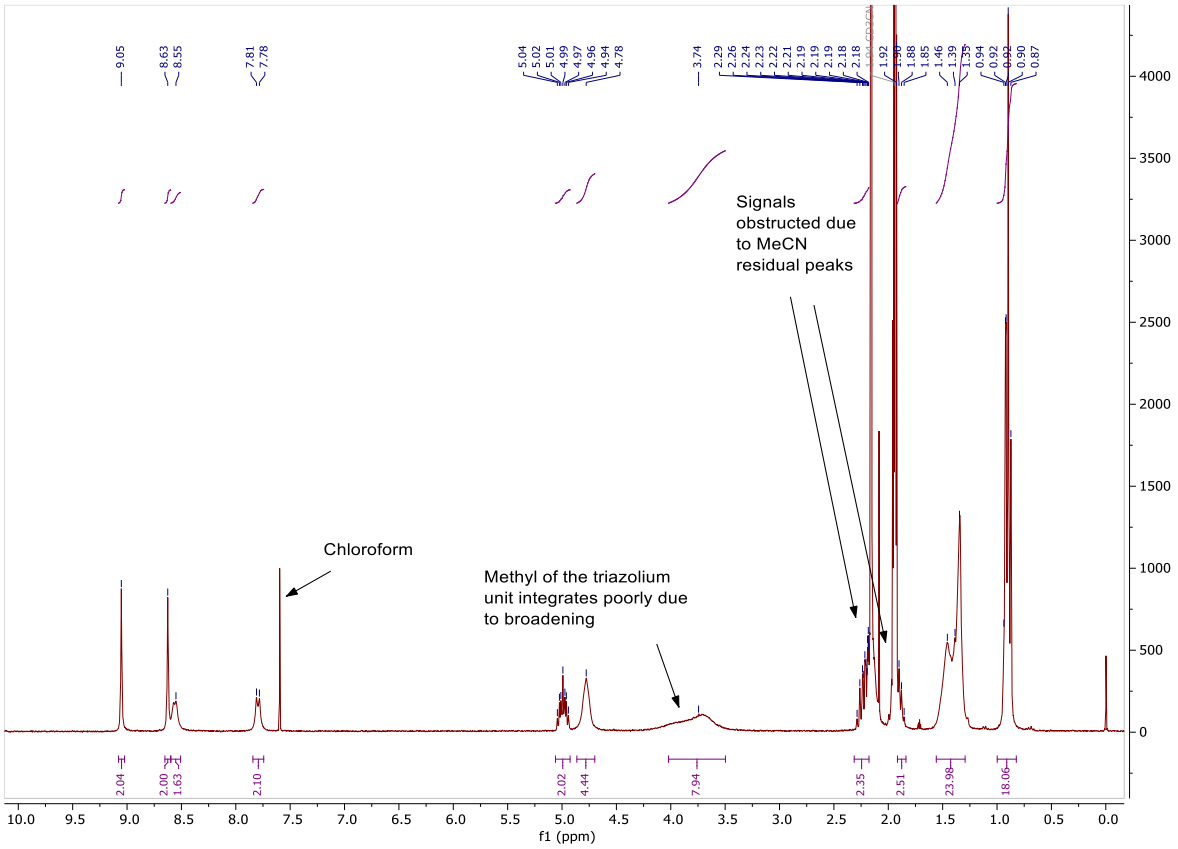

*Figure 354: ^{1}H NMR spectrum of **6.$[I^-]_2$** in acetontrile-d_3, 298 K, 300 MHz.*

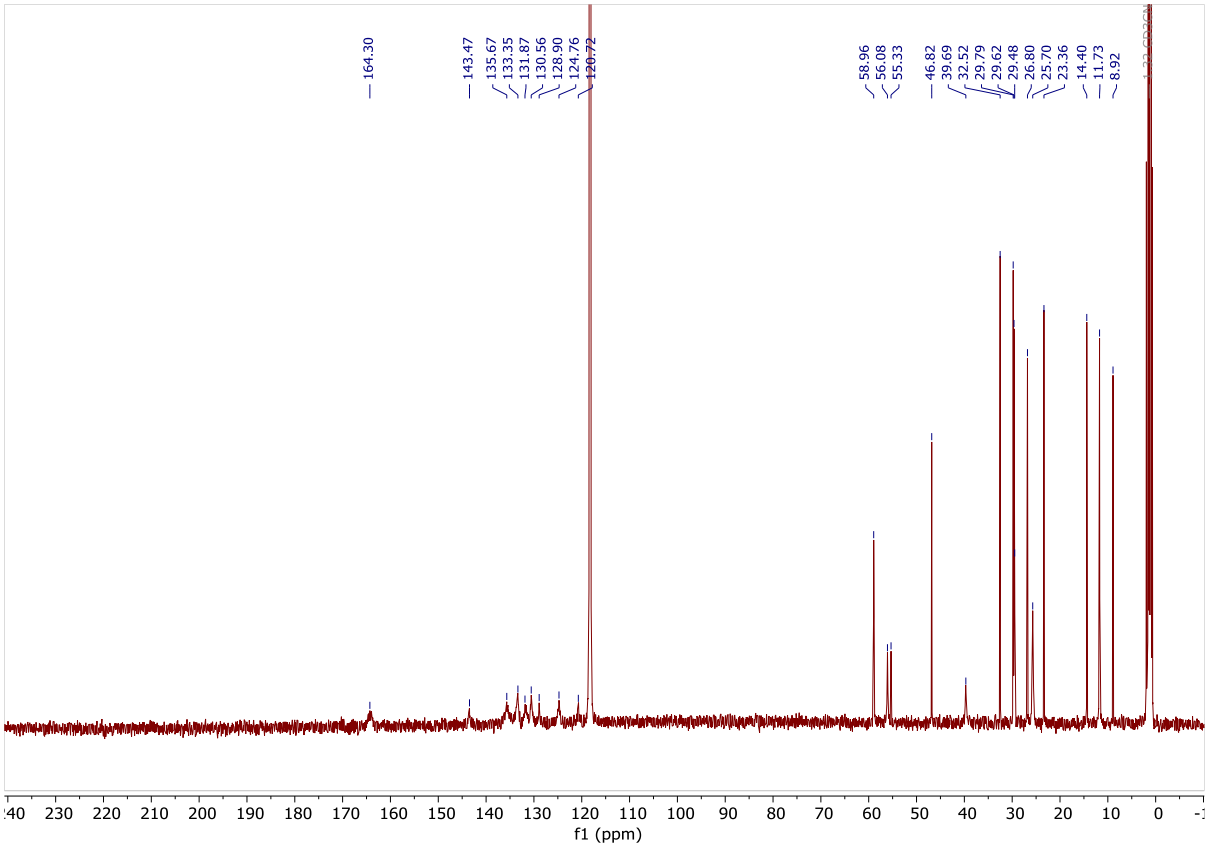

*Figure 365: ^{13}C NMR spectrum of **6.[I⁻]₂** in acetontrile-d_3, 298 K, 101 MHz.*

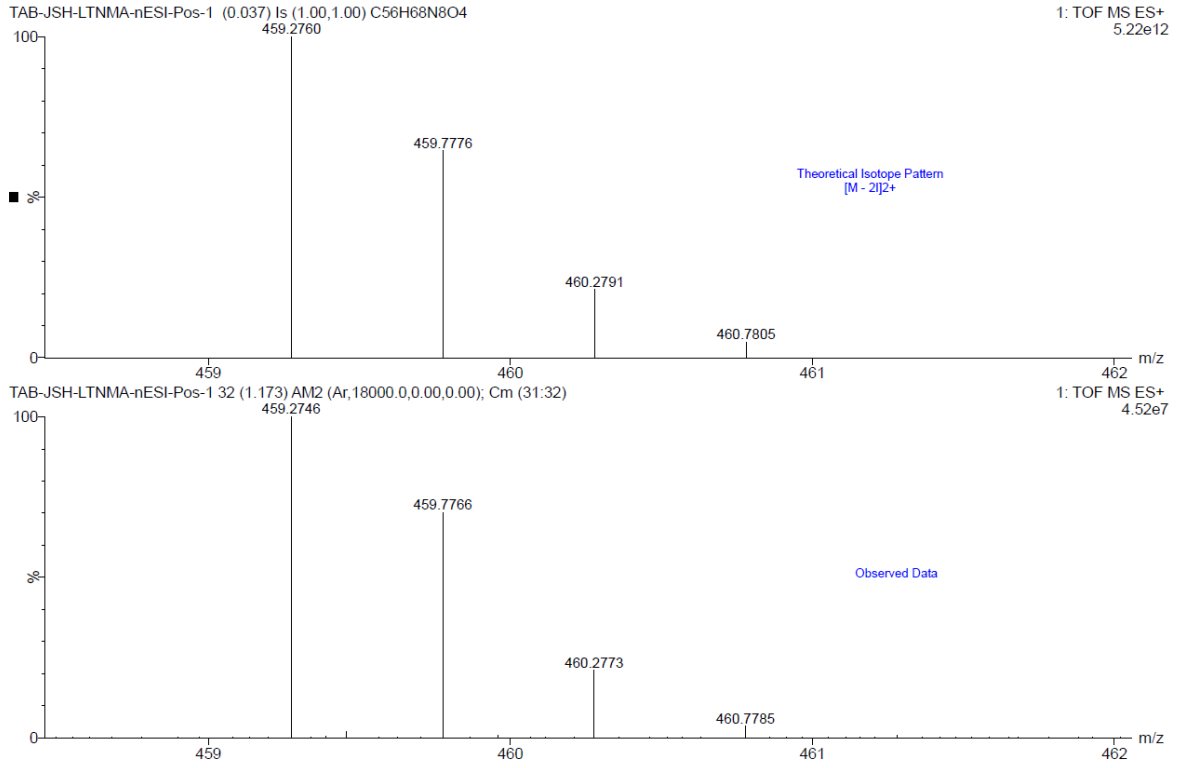

*Figure 376: Calculated (top) and observed (bottom) ESI MS, positive mode, data for compound **6.[I⁻]₂**.*

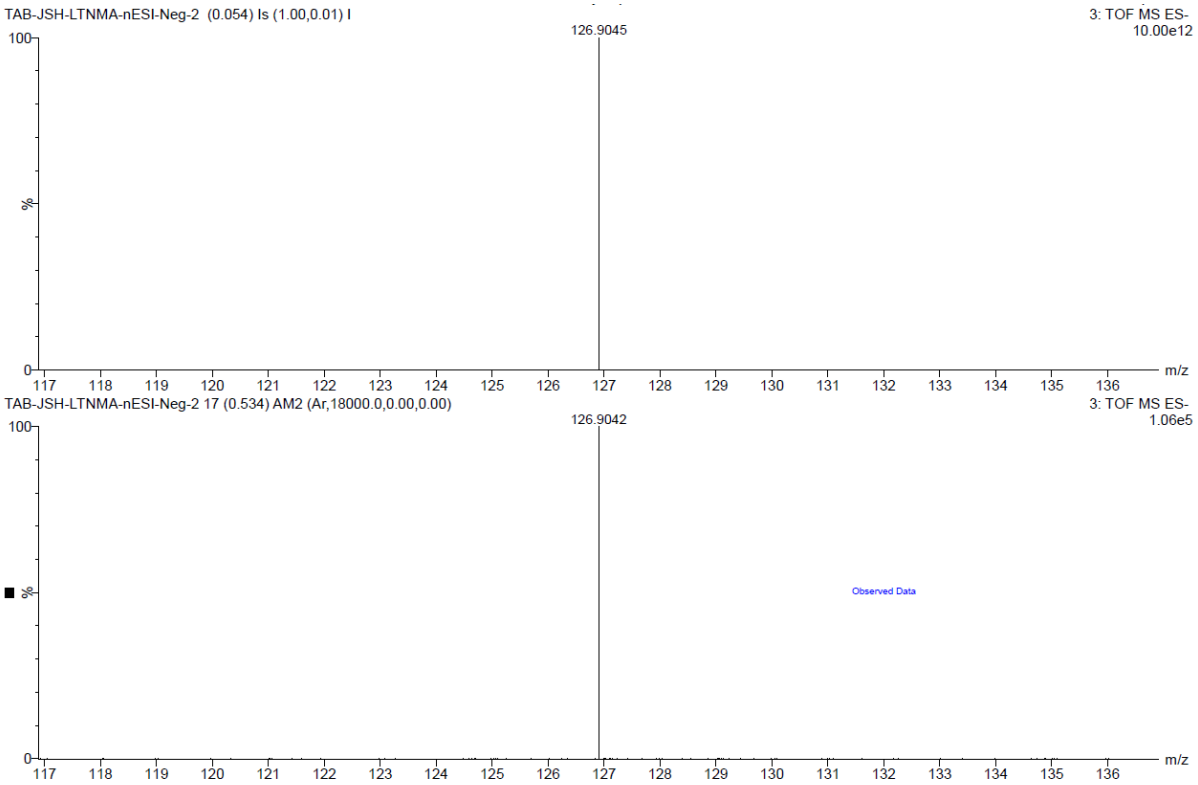

Figure 387: Calculated (top) and observed (bottom) ESI MS, negative mode, data for compound ***6.[I$^-$]$_2$.***

Bis(triazolium) PDI 6.$[PF_6^-]_2$.

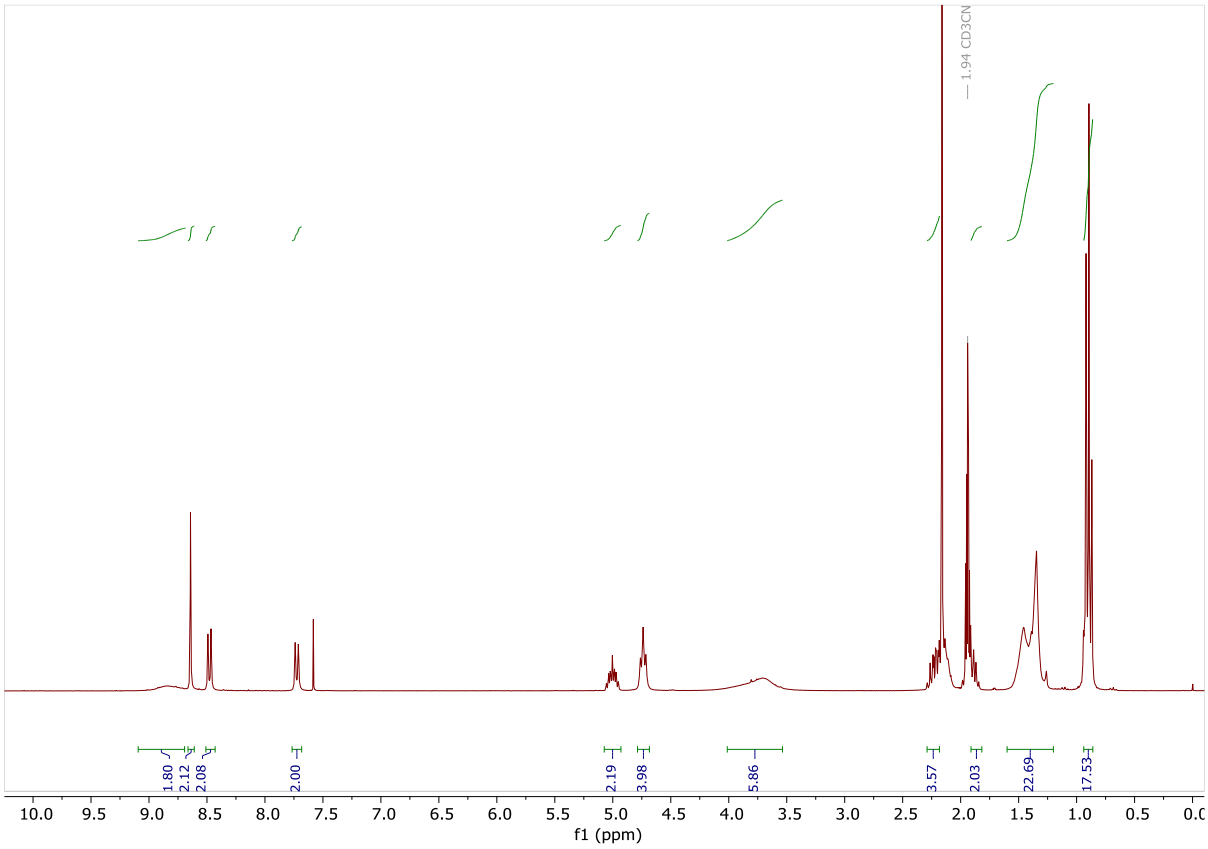

*Figure 48: ^{1}H NMR spectrum of **6.$[PF_6^-]_2$** in acetonitrile-d_3, 298 K, 400 MHz.*

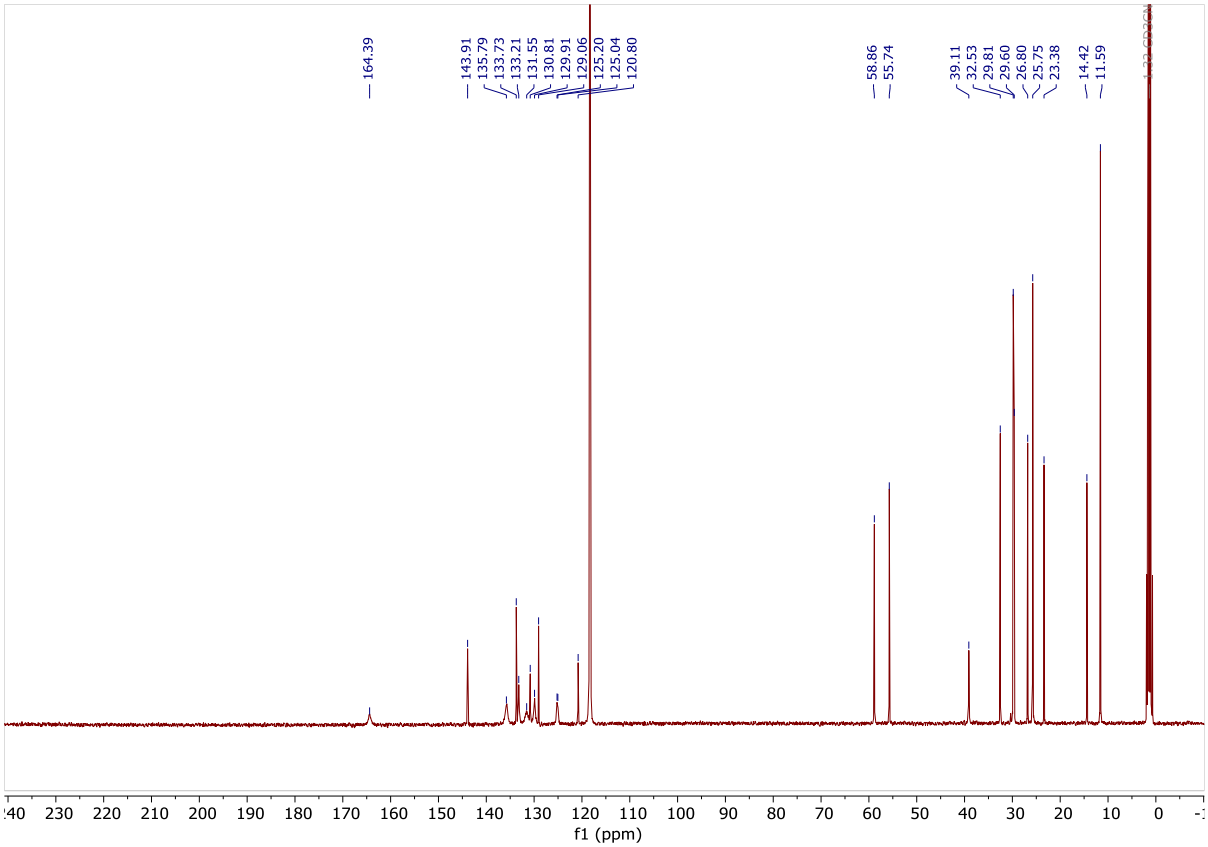

*Figure 49: ^{13}C NMR spectrum of **6.[PF_6^-]$_2$** in acetonitrile-d_3, 298 K, 101 MHz.*

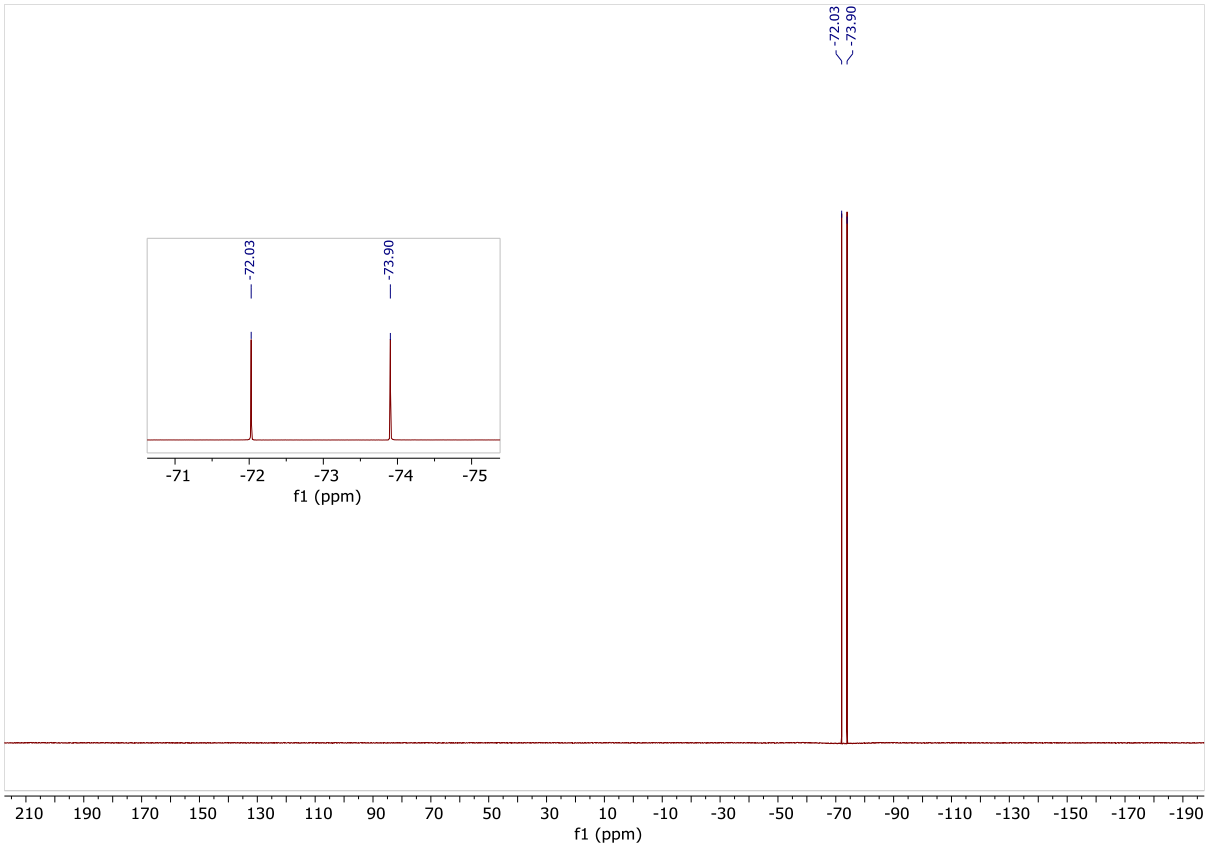

*Figure 390: ^{19}F NMR spectrum of **6.[PF_6^-]$_2$** in acetonitrile-d_3, 298 K, 377 MHz.*

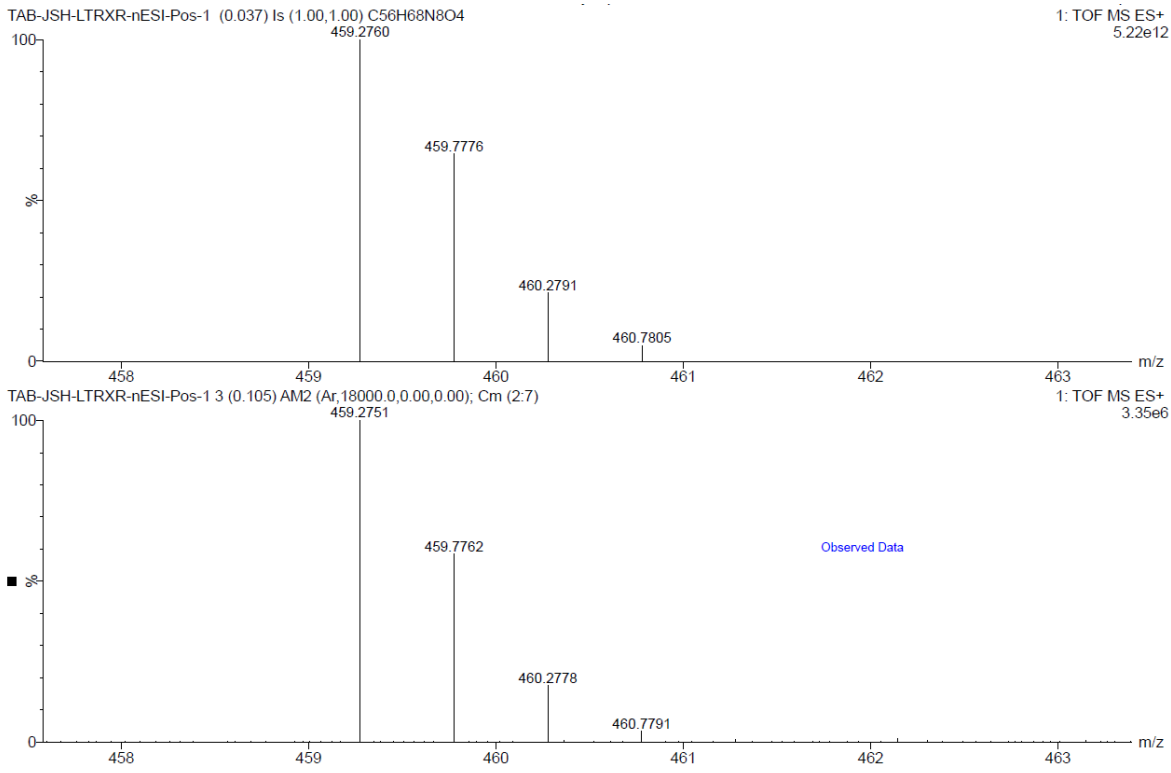

*Figure 401: Calculated (top) and observed (bottom) ESI MS, positive mode, data for compound **6.[PF_6^-]$_2$**.*

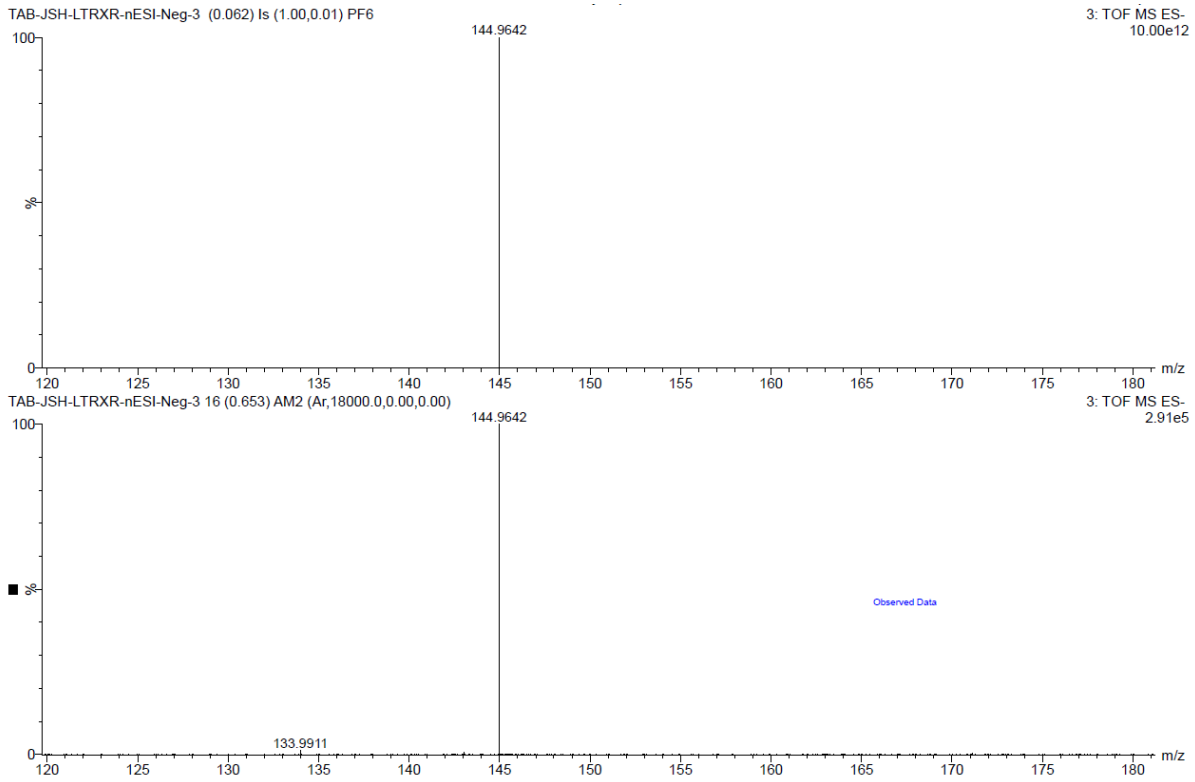

Figure 412: Calculated (top) and observed (bottom) ESI MS, negative mode, data for compound ***6.[PF_6^-]$_2$.***

7. References.

1. F. Würthner, *Chem. Commun.*, 2004, 1564–1579.
2. C. Huang, S. Barlow and S. R. Marder, *J. Org. Chem.*, 2011, **76**, 2386–2407.
3. F. Würthner, C. R. Saha-Möller, B. Fimmel, S. Ogi, P. Leowanawat and D. Schmidt, *Chem. Rev.*, 2016, **116**, 962–1052.
4. H. Langhals, A. Walter, E. Rosenbaum and L. B.-Å. Johansson, *Phys. Chem. Chem. Phys.*, 2011, **13**, 11055–11059.
5. Y. Nagao, *Prog. Org. Coat.*, 1997, **31**, 43–49.
6. F. C. Spano, *Acc. Chem. Res.*, 2010, **43**, 429–439.
7. M. Más-Montoya and R. A. J. Janssen, *Adv. Funct. Mater.*, 2017, **27**, 1605779.
8. M. Bayda, F. Dumoulin, G. L. Hug, J. Koput, R. Gorniak and A. Wojcik, *Dalton Trans.*, 2017, **46**, 1914–1926.
9. D. A. Hinton, J. D. Ng, J. Sun, S. Lee, S. K. Saikin, J. Logsdon, D. S. White, A. N. Marquard, A. C. Cavell, V. K. Krasecki, K. A. Knapper, K. M. Lupo, M. R. Wasielewski, A. Aspuru-Guzik, J. S. Biteen, P. Gopalan and R. H. Goldsmith, *J. Am. Chem. Soc.*, 2018, **140**, 15827–15841.
10. M. Son, K. H. Park, C. Shao, F. Würthner and D. Kim, *J. Phys. Chem. Lett.*, 2014, **5**, 3601–3607.
11. F. Würthner, T. E. Kaiser and C. R. Saha-Möller, *Angew. Chem. Int. Ed.*, 2011, **50**, 3376–3410.
12. H. Fidder, J. Knoester and D. A. Wiersma, *Chem. Phys. Lett.*, 1990, **171**, 529–536.
13. P. Erk, H. Hengelsberg, M. F. Haddow and R. van Gelder, *CrystEngComm*, 2004, **6**, 475–483.
14. D. Bialas, E. Kirchner, M. I. S. Röhr and F. Würthner, *J. Am. Chem. Soc.*, 2021, **143**, 4500–4518.
15. Z. Chen, A. Lohr, C. R. Saha-Möller and F. Würthner, *Chem. Soc. Rev.*, 2009, **38**, 564–584.
16. F. Würthner, V. Stepanenko, Z. Chen, C. R. Saha-Möller, N. Kocher and D. Stalke, *J. Org. Chem.*, 2004, **69**, 7933–7939.
17. H. Langhals, R. Ismael and O. Yürük, *Tetrahedron*, 2000, **56**, 5435–5441.
18. P. Rajasingh, R. Cohen, E. Shirman, L. J. W. Shimon and B. Rybtchinski, *J. Org. Chem.*, 2007, **72**, 5973–5979.
19. F. Würthner, Z. Chen, V. Dehm and V. Stepanenko, *Chem. Commun.*, 2006, 1188–1190.
20. Z. Chen, V. Stepanenko, V. Dehm, P. Prins, L. D. A. Siebbeles, J. Seibt, P. Marquetand, V. Engel and F. Würthner, *Chem. – Eur. J.*, 2007, **13**, 436–449.
21. S. Ghosh, X.-Q. Li, V. Stepanenko and F. Würthner, *Chem. – Eur. J.*, 2008, **14**, 11343–11357.
22. M. Hecht and F. Würthner, *Acc. Chem. Res.*, 2021, **54**, 642–653.
23. T. E. Kaiser, V. Stepanenko and F. Würthner, *J. Am. Chem. Soc.*, 2009, **131**, 6719–6732.
24. Z. Chen, U. Baumeister, C. Tschierske and F. Würthner, *Chem. – Eur. J.*, 2007, **13**, 450–465.
25. S. M. Rowe, S. Miller and E. J. Sorscher, *N. Engl. J. Med.*, 2005, **352**, 1992–2001.
26. S. G. Chang, D. Littlejohn and K. Y. Hu, *Science*, 1987, **237**, 756–758.
27. N. H. Evans and P. D. Beer, *Angew. Chem. Int. Ed.*, 2014, **53**, 11716–11754.
28. M. J. Langton, C. J. Serpell and P. D. Beer, *Angew. Chem. Int. Ed.*, 2016, **55**, 1974–1987.
29. P. A. Gale and C. Caltagirone, *Chem. Soc. Rev.*, 2015, **44**, 4212–4227.
30. X. Zhang, J. Yin and J. Yoon, *Chem. Rev.*, 2014, **114**, 4918–4959.
31. D. T. Quang and J. S. Kim, *Chem. Rev.*, 2010, **110**, 6280–6301.
32. N. Busschaert, C. Caltagirone, W. Van Rossom and P. A. Gale, *Chem. Rev.*, 2015, **115**, 8038–8155.
33. J. R. Askim, M. Mahmoudi and K. S. Suslick, *Chem. Soc. Rev.*, 2013, **42**, 8649–8682.
34. Z. Li, J. R. Askim and K. S. Suslick, *Chem. Rev.*, 2019, **119**, 231–292.
35. L. J. Karas, C.-H. Wu, R. Das and J. I.-C. Wu, *WIREs Comput. Mol. Sci.*, 2020, **10**, e1477.
36. E. Sandoz-Rosado, T. D. Beaudet, J. W. Andzelm and E. D. Wetzel, *Sci. Rep.*, 2018, **8**, 3708.
37. E. Arunan, G. R. Desiraju, R. A. Klein, J. Sadlej, S. Scheiner, I. Alkorta, D. C. Clary, R. H. Crabtree, J. J. Dannenberg, P. Hobza, H. G. Kjaergaard, A. C. Legon, B. Mennucci and D. J. Nesbitt, *Pure Appl. Chem.*, 2011, **83**, 1637–1641.
38. Y. Hua and A. H. Flood, *Chem. Soc. Rev.*, 2010, **39**, 1262–1271.
39. F. Zapata, L. Gonzalez, A. Caballero, I. Alkorta, J. Elguero and P. Molina, *Chem. – Eur. J.*, 2015, **21**, 9797–9808.
40. A. Kumar and P. S. Pandey, *Org. Lett.*, 2008, **10**, 165–168.

41. S. E. Penty, M. A. Zwijnenburg, G. R. F. Orton, P. Stachelek, R. Pal, Y. Xie, S. L. Griffin and T. A. Barendt, *J. Am. Chem. Soc.*, 2022, **144**, 12290–12298.
42. F. D'Anna, S. Marullo, G. Lazzara, P. Vitale and R. Noto, *Chem. – Eur. J.*, 2015, **21**, 14780–14790.
43. C. R. Martinez and B. L. Iverson, *Chem. Sci.*, 2012, **3**, 2191–2201.
44. S. Grimme, *Angew. Chem. Int. Ed.*, 2008, **47**, 3430–3434.
45. R. F. Fink, J. Seibt, V. Engel, M. Renz, M. Kaupp, S. Lochbrunner, H.-M. Zhao, J. Pfister, F. Würthner and B. Engels, *J. Am. Chem. Soc.*, 2008, **130**, 12858–12859.
46. Z. Chen, B. Fimmel and F. Würthner, *Org. Biomol. Chem.*, 2012, **10**, 5845–5855.
47. X. Feng, Y. An, Z. Yao, C. Li and G. Shi, *ACS Appl. Mater. Interfaces*, 2012, **4**, 614–618.
48. Y. Wang, J. Chen, H. Jiao, Y. Chen, W. Li, Q. Zhang and C. Yu, *Chem. – Eur. J.*, 2013, **19**, 12846–12852.
49. A. Pal, M. Karmakar, S. R. Bhatta and A. Thakur, *Coord. Chem. Rev.*, 2021, **448**, 214167.
50. Y. Lou, Y. Zhao and J.-J. Zhu, *Nanoscale Horiz.*, 2016, **1**, 125–134.
51. A. Ghosh, B. Ganguly and A. Das, *Inorg. Chem.*, 2007, **46**, 9912–9918.
52. A. Juris, V. Balzani, F. Barigelletti, S. Campagna, P. Belser and A. von Zelewsky, *Coord. Chem. Rev.*, 1988, **84**, 85–277.
53. C. W. Rogers and M. O. Wolf, *Coord. Chem. Rev.*, 2002, **233–234**, 341–350.
54. C. M. R. Almeida, J. M. C. S. Magalhães, M. F. Barroso and L. Durães, *J. Mater. Chem. C*, 2022, **10**, 15263–15276.
55. R. M. Meudtner and S. Hecht, *Angew. Chem. Int. Ed.*, 2008, **47**, 4926–4930.
56. T. R. Chan, R. Hilgraf, K. B. Sharpless and V. V. Fokin, *Org. Lett.*, 2004, **6**, 2853–2855.
57. H. C. Kolb, M. G. Finn and K. B. Sharpless, *Angew. Chem. Int. Ed.*, 2001, **40**, 2004–2021.
58. F. Kaspar, *ChemBioChem*, 2023, **24**, e202200744.
59. R. Ferrazza, B. Rossi and G. Guella, *J. Phys. Chem. B*, 2014, **118**, 7147–7155.
60. E. Sebastian and M. Hariharan, *J. Am. Chem. Soc.*, 2021, **143**, 13769–13781.
61. M. H. Ngai, P.-Y. Yang, K. Liu, Y. Shen, M. R. Wenk, S. Q. Yao and M. J. Lear, *Chem. Commun.*, 2010, **46**, 8335–8337.
62. 1 K. Liu, Z. Xu and M. Yin, *Prog. Polym. Sci.*, 2015, **46**, 25–54.